

THE UNIVERSITY OF MICHIGAN
INDUSTRY PROGRAM OF THE COLLEGE OF ENGINEERING

HEAT TRANSFER IN FALLING-FILM
LTV EVAPORATORS

Joachim R Sinek

A dissertation submitted in partial fulfillment
of the requirements for the degree of
Doctor of Philosophy in The
University of Michigan
Department of Chemical and Metallurgical Engineering
1961

September, 1961

IP-534

ACKNOWLEDGEMENTS

The author wishes to express his acknowledgements to:

the late W. L. Badger, prime mover behind the Wrightsville Beach pilot plant, who suggested the thesis topic, and to whose memory we respectfully dedicate this work;

the engineers and operators of W. L. Badger Associates, Inc., for their unfailing encouragement, friendship and assistance;

the U. S. Department of the Interior, Office of Saline Water, for permission to use the experimental data in this dissertation;

the members of the author's doctoral committee

Professor Edwin H. Young, Chairman
Professor John A. Clark
Associate Professor Kenneth F. Gordon
Mr. Ferris C. Standiford
Professor Brymer Williams

TABLE OF CONTENTS

	<u>Page</u>
ACKNOWLEDGEMENTS.....	ii
ABSTRACT.....	vii
LIST OF SYMBOLS AND ABBREVIATIONS.....	viii
 SECTIONS	
I EXPERIMENTAL WORK.....	1
EQUIPMENT.....	4
INSTRUMENTATION.....	4
TUBES.....	6
FEED DISTRIBUTION.....	7
NATURE OF HEATING SURFACE.....	7
READINGS, OBSERVATIONS AND RECORDS.....	8
CHEMICAL ANALYSIS OF BRINE CONCENTRATION.....	8
PHYSICAL PROPERTIES OF SEA WATER BRINES.....	9
CALCULATIONS.....	9
Calculation Procedure.....	9
Steam.....	9
Heat Transfer and Pressure Drop.....	12
Condenser Water.....	13
Blowdown.....	15
Feed.....	16
Mass Balance.....	17
Energy Balance.....	17
SUMMARY OF CALCULATION PROCEDURE.....	18
a) Calculation of Mass Balance.....	18
b) Calculation of Steam Enthalpy and Heat Load.....	18
c) Calculation of Feed, Blowdown and Vapor Enthalpies.....	19
d) Calculation of Enthalpy Balance.....	19
e) Calculation of Overall Heat Transfer Coeffi- cients.....	20
f) Calculation of Pressure Drop.....	20
RANGE OF PROCESS VARIABLES.....	21
OPERATING PROCEDURE.....	21
 II THEORY OF FALLING-FILM FLOW.....	 23
A. FUNDAMENTALS.....	23
B. LITERATURE RESEARCH: FLUID MECHANICS.....	26
C. LITERATURE RESEARCH: HEAT TRANSFER (NON-BOILING).....	46

TABLE OF CONTENTS (CONT'D.)

	<u>Page</u>
III LITERATURE RESEARCH ON NUCLEATE BOILING FUNDAMENTALS	57
RATE OF HEAT TRANSFER IN NUCLEATE BOILING.	57
BUBBLE FORMATION	61
BUBBLE GROWTH.	65
BUBBLE BEHAVIOR.	67
SUGGESTED HEAT TRANSFER MECHANISMS IN NUCLEATE BOILING . . .	68
IV LITERATURE RESEARCH ON GAS-LIQUID FLOW	71
V LITERATURE RESEARCH ON PERTINENT EVAPORATOR STUDIES.	77
A. CLIMBING-FILM LTV'S	77
B. WIPED-SURFACE EVAPORATORS	78
C. FALLING-FILM LTV'S.	78
VI DESIGN AND RESULTS OF EXPERIMENTS.	82
A. RUNS LWCI-1 TO LWCI-32.	83
Design of Experiment	83
Accuracy of Results.	85
Experimental Results	87
B. RUNS LWCJ-1 TO LWCJ-16 AND	
C. RUNS LWCK-10 TO LWCK-29	89
D. RUNS LWDA-2 TO LWDA-38.	92
VII THEORETICAL MODEL OF FALLING-FILM EVAPORATIVE HEAT TRANSFER MECHANISM.	96
FUNDAMENTAL MODEL.	96
BOILING POINT ELEVATION.	98
LONGITUDINAL PRESSURE-DROP MODEL	102
CALCULATION OF TUBE-SIDE HEAT TRANSFER FILM COEFFICIENT FROM THEORETICAL MODEL.	108

TABLE OF CONTENTS (CONT'D.)

	<u>Page</u>
VIII PREDICTION OF OVERALL HEAT TRANSFER COEFFICIENTS FOR RUNS WITH ZERO FEED SUPERHEAT FROM THEORETICAL MODEL.....	109e
CALCULATION OF STEAM-SIDE TEMPERATURE DROP.....	110
CALCULATION OF TUBE-WALL TEMPERATURE DROP.....	111
CALCULATION OF OVERALL HEAT TRANSFER COEFFICIENT.....	113
COMPARISON OF THEORETICAL MODEL WITH EXPERIMENTAL RESULTS.....	113
IX THEORETICAL ANALYSIS OF RESULTS FOR TESTS WITH 20°F FEED SUPERHEAT.....	118
APPENDICES	
A. EXPERIMENTAL DATA AND CALCULATIONS RUNS LWCI-1 TO LWCI-32.....	121
B. EXPERIMENTAL DATA AND CALCULATIONS RUNS LWCJ-1 TO LWCJ-16.....	124
C. EXPERIMENTAL DATA AND CALCULATIONS RUNS LWCK-10 TO LWCK-29.....	127
D. EXPERIMENTAL DATA AND CALCULATIONS RUNS LWDA-2 TO LWDA-38.....	130
E. GRAPHS USED TO CORRELATE EXPERIMENTAL DATA.....	133
F. DISCUSSION OF ACCURACY AND EVENTUAL MODIFICATION OF THEORETICAL CORRELATION OF HEAT TRANSFER COEFFICIENTS.....	143
a) Effect of Scatter in h_{stm}	144
b) Effect of Using Feed Chlorosity to Calculate U_{VH}	145
c) Effect of Neglecting Bubble Superheat.....	147
BIBLIOGRAPHIES	
BIBLIOGRAPHY ON FALLING-FILM FLUID FLOW AND (NON-BOILING) HEAT TRANSFER.....	151
BIBLIOGRAPHY ON NUCLEATE BOILING FUNDAMENTALS.....	154

TABLE OF CONTENTS (CONT'D)

	<u>Page</u>
BIBLIOGRAPHY ON GAS-LIQUID FLOW.....	157
BIBLIOGRAPHY ON EVAPORATOR STUDIES.....	160
ADDITIONAL BIBLIOGRAPHY USED IN DESIGN, RESULTS AND ANALYSIS. OF EXPERIMENTS.....	162

ABSTRACT

A procedure is presented for predicting liquid-side and overall heat transfer coefficients in falling-film evaporators. A model is developed for the heat transfer mechanism in falling-film evaporation, according to which the temperature difference across the falling film obeys the same law during evaporation as in the transfer of sensible heat and as in condensation. The temperature difference across the falling film is therefore calculated as the quotient of the heat flux and a heat transfer coefficient. For this heat transfer coefficient the correlation by Dukler is used. It consists of numerical values obtained by directly computer-integrating the basic heat and momentum transfer equations, and has been shown to correlate successfully experimental data on falling-film heaters and falling-film condensers.

In order to make a comparison with experimental data it is necessary to know the temperature difference between wall and vapor-head rather than the temperature drop across the falling film. The calculated temperature drop is therefore corrected for the longitudinal pressure drop, the boiling point rise due to solutes, and the boiling point rise due to the presence of bubbles. The latter is calculated by postulating bubbles of the same size as the film thickness, and by applying the Gibbs equation connecting bubble superheat with surface tension and bubble size.

Overall heat transfer coefficients are calculated by using the theoretical model for the liquid-side heat transfer; steam-side coefficients are estimated as 1.28 times the Nusselt correlation, on basis of the experiments of Baker, Kazmark and Stroebe, and the recommendation of McAdams; it is shown that the overall coefficient is fairly insensitive to changes in the steam-side coefficient.

The experimental work consisted of measuring overall heat transfer coefficients in a 7-tube falling-film LTV evaporator for a wide range of operating variables. The tubes employed were 1-in. and 2-in. tubes, 24 ft long. The test liquids were sea water and sea water concentrates. Boiling temperature ranged from 100 to 230°F, heat flux from 3,200 to 6,500 Btu/(hr)(sq ft), film Reynolds number from 1,000 to 11,000, film Prandtl number from 1.6 to 4.5. In roughly half the runs, the feed temperature was equal to the vapor-head saturation temperature; in the others, the feed temperature was 20°F higher. A total of 105 runs were made, each at a different combination of tube diameter, vapor-head saturation temperature, feed temperature, feed salinity, feed rate, and steam rate. For runs with feed temperature equal to the vapor-head temperature, the measured overall coefficients agreed within 10% with the calculated coefficients. For runs with feed temperature 20°F higher than the vapor-head temperature, overall coefficients were consistently 10% lower, apparently due to flashing at the tube entrance.

It is shown that the correction for boiling-point rise due to bubbles is an essential part of the correlation.

LIST OF SYMBOLS AND ABBREVIATIONS

- A Heat transfer surface area; sq ft
- b Wetted perimeter; ft
- B Falling liquid film thickness; B_p at wave peak; B_t at wave trough; B_L at tube length L ; ft
- B^+ Value of y^+ at $y = B$
- (BPR) Boiling-point rise due to presence of solute; $^{\circ}\text{F}$
- c Specific heat; c_p at constant pressure; c_l of liquid phase; $\text{Btu}/(\text{lb})(^{\circ}\text{F})$
- C, C_b, C_{sf} Dimensionless numerical constants
- (Cl) Chlorosity; grams per liter
- D Diameter; ft.; D_e equivalent diameter, in.
- E_M Momentum transfer eddy viscosity; E_H heat transfer eddy viscosity; ft^2/hr
- f Dimensionless friction factor
- $f()$ Function of; more specifically, the steam saturation temperature as function of pressure; as in: 212°F $f(29.922 \text{ in. Hg abs.})$
- (Fr) Froude number
- g Acceleration of gravity; $\text{ft}/(\text{sec})^2$ or $\text{ft}/(\text{hr})^2$

g_c	Unit conversion factor, equal to 32.17 poundals/lb _f
G	Mass flowrate per unit cross-section; G_T at the terminal tube length; lb/(hr)(sq ft)
h	Local film heat transfer coefficient; Btu/(hr)(sq ft)(°F)
h_m	Mean value of h with respect to entire heat transfer surface; h_{stm} for steam-side heat transfer; h_f for heat transferred through falling liquid film; h_{vH} for heat transferred through falling liquid film, assuming film to be at the BPR-corrected VH saturation temperature; Btu/(hr)(sq ft)(°F)
H	Enthalpy flow; Btu/hr
ΔH_{vap}	Heat of vaporization; Btu/lb
J	Mechanical equivalent of heat; 778.16 ft-lb _f /Btu
k	Conductivity; Btu/(hr)(sq ft)(°F/ft)
K_F, K_V	Dimensionless variables in Brauer's correlation
L	Tube length; L_0 reference tube length; L_T terminal tube length; ft
n	Dimensionless numerical factor in Deissler's correlation
(Nu)	Nusselt number; $(Nu)_m$ mean value of (Nu) for entire heat transfer surface
p	Pressure; p_l in liquid phase; p_v in vapor phase; P pressure drop; lb /sq ft or in. Hg

(Pr)	Prandtl number; $(Pr)_l$ liquid phase Prandtl number
q	Heat flux; Btu/(hr)(sq ft)
Q	Rate of heat transfer; Btu/hr
r	Bubble radius; r_1, r_2 , principal bubble radii; ft
r_h	Hydraulic radius; ft
R_g	Gas-phase holdup fraction; R_l liquid-phase hold-up fraction
(Re)	Reynolds number; $(Re)_{crit}$ critical Reynolds number; $(Re)_{w1}$ Reynolds number of first wave appearance; $(Re)_i, (Re)_{wi}, (Re)_c$ characteristic film Reynolds numbers in Brauer's correlation
t	Temperature; t_l in liquid phase; t_v in vapor phase; t_w at tube wall; t_{sat} saturation temperature; t_{stm} steam condensation temperature; t_{tr} transition temperature; °F
t^+	Dimensionless temperature in Deissler's correlation
Δt	Finite temperature difference; Δt_{sat} between t_w and t_{sat} ; Δt_{sub} between t_{sat} and t_l ; Δt_{stm} across steam-side condensate layer; Δt_w across metal tube wall; Δt_f across falling liquid film; Δt_{app} between t_w and the VH saturation temperature; Δt_{OAapp} between t_{stm} and the VH sat. temp.; Δt_{OAcorr} between t_{stm} and the BPR-corrected VH sat. temp.; Δt_{corr} between t_w and the BPR-corrected VH sat. temp.; °F
u	Local velocity; u_i at interface; u' at $y = \epsilon$; ft/sec

u^*	Dimensionless friction velocity
u^+	Dimensionless velocity
U_{VH}	Overall heat transfer coefficient, assuming film to be at the BPR-corrected VH sat. temp.
v	Specific volume; cu ft/lb
V	Average velocity with respect to entire flow cross-section; ft/sec
w	Mass flowrate; lb/hr
(We)	Weber number
x	Distance parallel to flow direction; ft
y	Distance normal to flow direction; ft
y^+	Dimensionless distance normal to flow direction
α	Dimensionless number expressing variation of kinetic energy with radius for fluid flow through a pipe
β	Dimensionless variable in Dukler's correlation
β'	Bubble contact angle
ϵ	Characteristic film thickness in Brauer's correlation; ft
θ	Angle of inclination with respect to horizontal
κ	Dimensionless constant in von Kármán's correlation

μ	Viscosity; lb/ (hr) (ft)
ν	Kinematic viscosity; ft ² /hr
ρ	Density; ρ_g gas density; ρ_l liquid density; lb/cu ft
σ	Surface tension; σ_{H_2O} surface tension of water; lb _f /ft
τ	Shear; τ_i interfacial shear; τ_w wall shear; lb _f /sq ft
ϕ	Characteristic heat transfer coefficient in Nusselt's correlation; Btu/(hr)(sq ft)(°F)
ψ	Dimensionless magnitude in Nusselt's correlation
λ	Characteristic bubble superheat magnitude; in. Hg
Γ	Mass flowrate per unit perimeter; lb/(hr)(ft)
Φ_l, Φ_g, X	Dimensionless ratios in Lockhart-Martinelli correlation

Abbreviations and Terminology

app	apparent; designates temperature drops when it is assumed that the evaporating liquid is at the vapor-head saturation temperature
corr	corrected; designates temperature drops when it is assumed that the evaporating liquid is at the vapor-head temperature corrected for BPR
gpl	grams per liter
OA	overall
VH	vapor-head

INTRODUCTION

Falling-film long-tube vertical evaporators are finding increasing application in the evaporation of sea water and of heat-sensitive liquids. This is mainly because these evaporators have high heat transfer coefficients at low temperature differences, and because of their small hold-up. However, the technical literature is almost completely devoid of experimental data or theoretical analyses of falling-film evaporation. This dissertation is presented in the hope that it may contribute to engineering knowledge by filling this long-felt need.

The author was fortunate in having at his disposal a well-equipped pilot plant, including a 24-ft falling-film LTV evaporator. This pilot plant was the sea water evaporator test station of the U. S. Department of the Interior, Office of Saline Water, located on the premises of the International Nickel Co. laboratory, Wrightsville Beach, N. C. It was designed, erected and operated for the Government by the author's employers, W. L. Badger Associates, Inc., Consulting Engineers, Ann Arbor; the author was in charge of the erection (1957) and subsequent operation (1957-60). - The purpose of the test station was mainly to investigate and demonstrate the application of falling-film evaporators to sea water conversion, with particular emphasis on scale prevention. Part of the time was devoted to heat transfer work: a systematic series of experiments was performed to measure heat transfer coefficients for a wide range of operating conditions. The author secured permission to use these data for his dissertation.

A model for falling-film evaporative heat transfer was developed by the author. Heat transfer coefficients calculated from this model were found to be in good agreement with the Wrightsville Beach test data, and should permit a more precise design of falling-film LTV evaporators. The model should also contribute to a better understanding of the physical nature of falling-film evaporation.

SECTION I

EXPERIMENTAL WORK

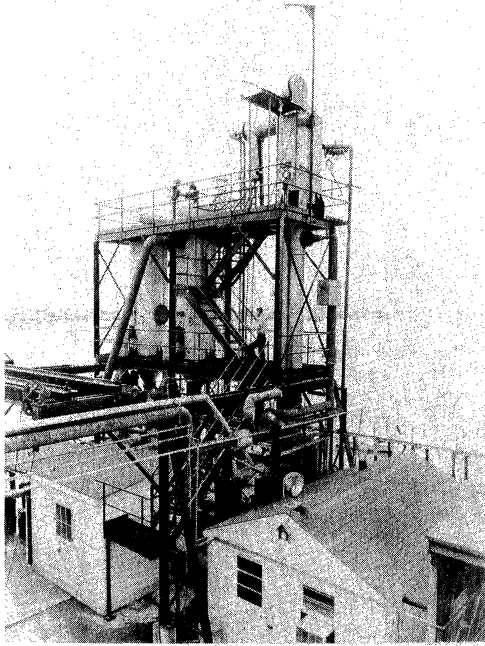
INTRODUCTION

The experimental work consisted of a series of runs in which a falling-film LTV evaporator was used to evaporate sea water brines, and in which the overall heat transfer coefficients were measured. These runs were performed over a wide range of operating conditions: feed rate, steam rate, vapor-head temperature, feed temperature, feed salinity, and tube diameter.

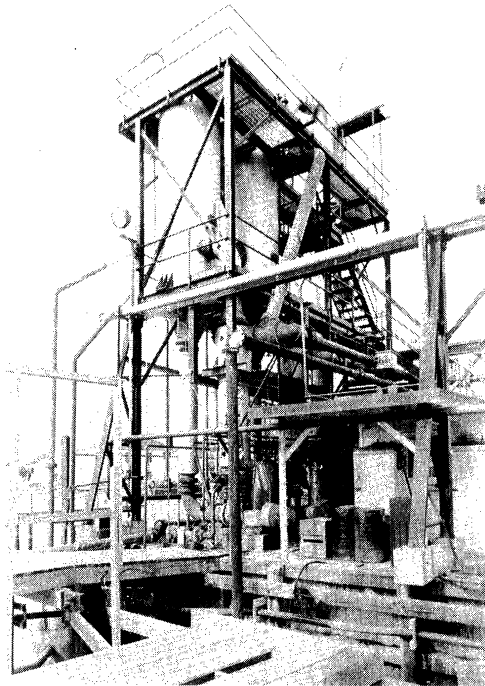
Boiling temperature ranged from 100 to 230°F, heat flux from 3,200 to 6,500 Btu/(hr)(sq ft), film Reynolds number from 1,000 to 11,000, film Prandtl number from 1.6 to 4.5, feed superheat from 0 to 20°F.

The purpose of the experimental work was the accumulation of sufficient data to enable a reasonably accurate prediction of the heat transfer coefficient to be made for a given set of operating conditions. The experimental work was necessary because, to the best of our knowledge, no such information on falling-film LTV evaporators exists in the literature.

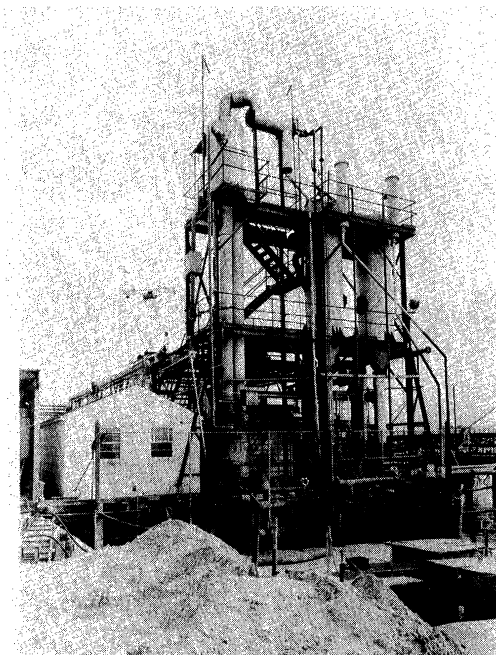
The results of the experimental work were also used in order to compare them with those predicted from the theoretical model (Sections VIII and IX).



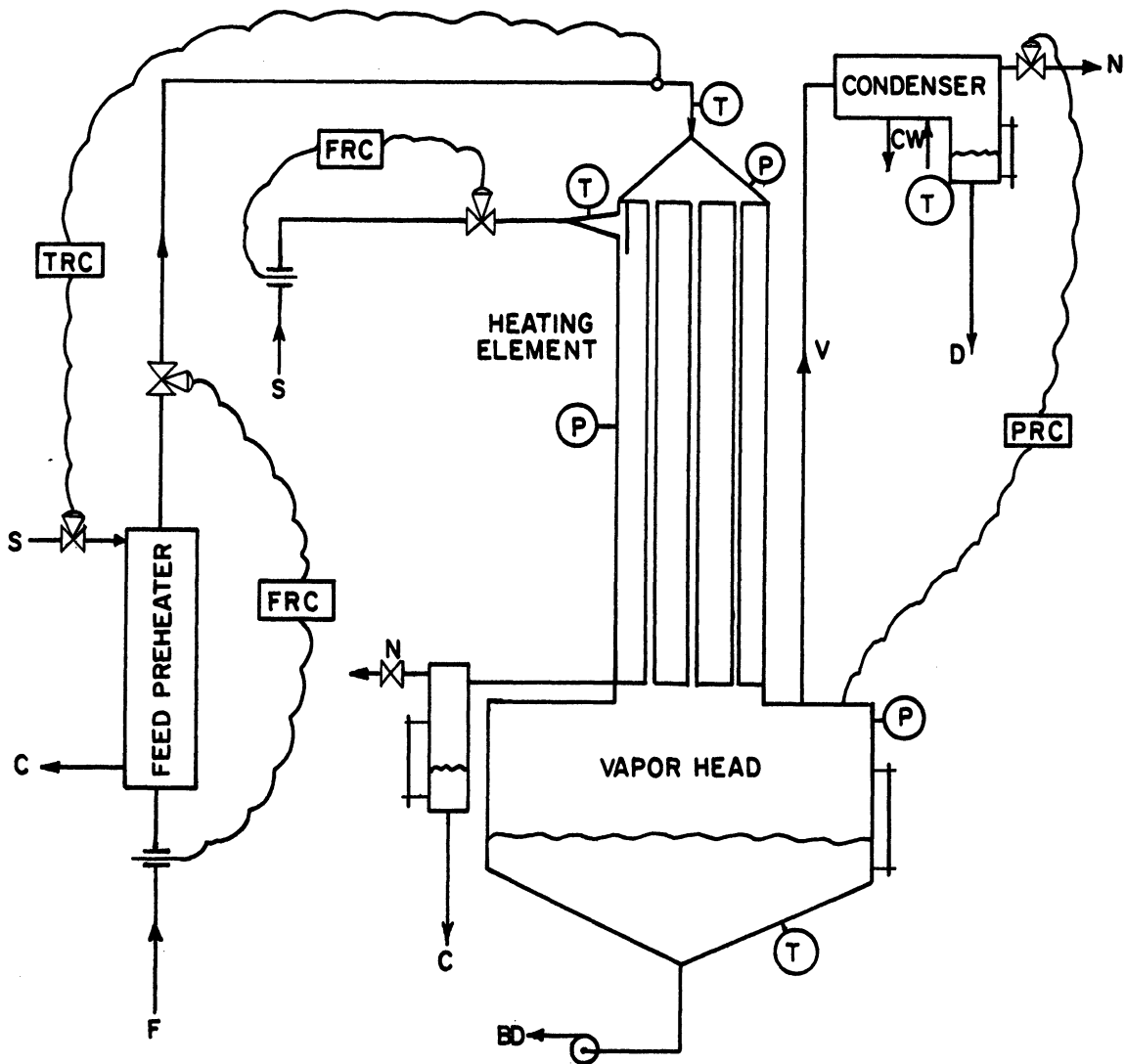
General View Looking Southeast
Control House, Left Foreground, LTV
Evaporator, Right Center. FC
Evaporators, Left Center



General View Looking Southwest
FC Evaporators, Center



General View Looking North
LTV Evaporator, Left Center FC
Evaporators, Right



F Feed
 BD Blowdown
 S Steam
 C Steam condensate
 V Vapor
 D Distillate
 CW Cooling water
 N Non-condensibles

FRC Flowrate recorder-controller
PRC Pressure recorder-controller
TRC Temperature recorder-controller
 (P) Pressure gage or manometer
 (T) Thermometer


 Sightglass on volumetric drip tank

Figure 1

EQUIPMENT

The experimental equipment was part of the sea water evaporation pilot plant on Harbor Island, on the North Carolina coast. This plant is an open-air installation and is located a few feet from the ocean's edge, on the premises of the corrosion test station of the International Nickel Co., Inc., Wrightsville Beach, N.C.

The test evaporator was a falling-film LTV (Figure 1). The heating element was essentially a 24-ft vertical single-pass heat exchanger. Feed entered the tubes at the top, and flowed down through the tubes while receiving heat from the steam, which condensed on the shell-side. A mixture of vapor and concentrate ("blowdown") came out of the bottom tube ends and into a wide separating tank ("vapor-head"). Vapor was led from the top of the vapor-head to a surface condenser; blowdown was pumped out of the bottom.

Auxiliary equipment included a small steam-heated feed pre-heater; a surface condenser; a two-stage Nash vacuum pump with an additional steam-jet air ejector; two plant-size forced-circulation evaporators (FC's) operating independently of the LTV. Steam was supplied by two nearby boilers at ca. 105 psi, and reduced to 15-30 psi prior to entering the system. - The entire equipment was provided with heavy thermal insulation.

INSTRUMENTATION

Two sets of instrumentation were provided, for the following two purposes:

- 1) Process control, in order to maintain the operating variables at steady predetermined values.
- 2) Measurement, to calibrate the process control instruments, and for the accurate determination of all variables necessary for a mass balance, an enthalpy balance, and a calculation of the overall heat transfer coefficient.

Process control of feed flowrate, feed temperature, steam flowrate, and vapor head pressure was carried out by means of pneumatic recorder-controllers, panel-mounted in a separate control shack. It should be pointed out here that the heat load was controlled by an orifice-type steam flowrate controller in the steam line, not by a steam-pressure controller in the steam chest; steam-side pressure was, therefore, a dependent variable, not an operating variable.

Measurement of blowdown flowrate, distillate flowrate and steam condensate flowrate was carried out in volumetric drip-pots provided with sight-glasses; the rate of rise in the tanks was timed with a stopwatch. These volumetric drip-pots were previously calibrated with weighed amounts of water. (The vapor-head acted as volumetric drip-pot for the blowdown rate.) All three drip-pots had calibrated thermometers. In addition, blowdown concentration was determined by chemical analysis, since the density of brines is a function of concentration as well as of temperature. - Measurement of feed temperature was carried out with a calibrated thermometer located close to the feed cone. - Measurement of steam temperature was similarly taken on a thermometer located close to the steam entrance cone. - Measurements of feed pressure, steam pressure

and vapor-head pressure were performed with mercury manometers (vacuum operation) or with sensitive Bourdon gages, previously calibrated against mercury manometers (pressure operation).

An instrument that was used neither for control nor for measurement, but which gave an excellent picture of the steadiness of the process, was an automatic temperature-difference recorder. It showed the time-dependence of the temperature difference between the condensing steam and the vapor in the vapor-head. It consisted of a resistance bulb in the steam-chest and a similar resistance bulb in the top part of the vapor-head, electrically connected to a panel-mounted indicator.

TUBES

The test evaporator was a 7-tube LTV; one tube was mounted in the center of the circular tube-sheets, the other six around it on a triangular pitch. The LTV was built for 24-ft tubes. The tube sheets were fashioned in such a way that the tubes were not rolled in but grommetted in. Three neoprene grommets per tube end were used, and proved satisfactory.

Tests were carried out with 24-ft tubes; 2-in. 12 ga. tubes were used for all operating conditions, and a similar series of runs was then repeated with 1-in. 16 ga. tubes.

Mixed tube bundles were used, with respect to tube materials, since other tubes were not available. The 2-in. tube bundle consisted of 2 copper, 2 aluminum brass, 1 arsenical admiralty, 1 Ampco grade 8, and 1 90/10 cupronickel tube. The 1-in. tube bundle had 2 copper, 3 aluminum

brass, 1 arsenical admiralty and 1 90/10 cupronickel tube. Although mixed tube bundles are generally not desirable, the difference in conductivity of the metals was not enough to cause an appreciable maldistribution of heat load.

FEED DISTRIBUTION

Even feed distribution among the 7 tubes presented a problem due to the absence or near-absence of a longitudinal pressure drop through the tubes. (This problem is not encountered in bottom-fed LTV's.) Careful levelling of the upper tube ends proved unsuccessful. The final solution was the use of inserts fitted on the upper tube ends. These inserts contained a horizontal orifice-plate or a nozzle, through which the feed had to flow to reach the tube itself, and which caused a pressure drop high enough to equalize the feed distribution. A horizontal splash plate only a little smaller than the tube I. D. and mounted under the orifice converted the jet into falling-film flow; this was visually verified on glass tubes.

The performance of a feed distribution device was measured by timing the flowrate of each individual tube with beaker and stopwatch.

The disadvantage of having to use inserts was the impossibility of measuring longitudinal pressure drops directly. This problem will be referred to in more detail.

NATURE OF HEATING SURFACE

The heating surface was inspected by opening up the LTV, removing

the inserts, and looking through each tube against a light. No fouling, salting or scaling was ever observed. Scale was prevented by controlling the feed pH with sulfuric acid; this was checked by hourly pH-meter readings.

No time-dependence of heat transfer rate over a period of many weeks could be observed.

READINGS, OBSERVATIONS AND RECORDS

Test work was carried out on a 24-hour day basis. Each shift was manned by an engineer and an operator. Each hour all instrument readings were taken and written down on specially prepared data sheets. Every three hours, or whenever deemed necessary, the drip-pot readings were taken in addition to the other readings; also, samples of feed and blowdown were taken and the concentrations determined by chemical analysis. Hourly observation of a descriptive nature were also written on log sheets facing the data sheets.

CHEMICAL ANALYSIS OF BRINE CONCENTRATION

Analyses were carried out in a chemical laboratory close at hand. Brine chlorosity was determined directly by titration with standardized silver nitrate. Chlorosity is defined as the grams per liter (20°C) of total halide expressed as chloride. Concentration can also be expressed by concentration factor, which is the ratio of salinity to the salinity of "normal" sea water*; sea water generally has a concentration factor

* A universal standard; see Sverdrup, H. V., et al. "The Oceans", Prentice-Hall, 1st Ed., 1942.

close to 1.0. Concentration factor is a unique function of chlorosity, and has been tabulated.

PHYSICAL PROPERTIES OF SEA WATER BRINES

Charts were used in which density, concentration factor, specific heat and boiling point rise are given as functions of chlorosity and temperature. These charts were compiled for the Office of Saline Water by W.L. Badger Associates, Inc.

CALCULATIONS

Calculations were performed on specially prepared calculation sheets (see sample calculation sheet).

Calculation Procedure

The calculation procedure used for these tests is described herein in considerable detail to help clarify any questions that might arise. A sample calculation form, numbered to correspond to the following description, is shown on page 10.

Steam

1. Pressure measured by bourdon tube gage (if used) on heating element.
2. Correction as determined by gage calibration.
3. Corrected pressure, or actual vacuum reading if measured by mercury manometer.
4. Barometric pressure as obtained from aneroid barometer,

CALCULATION FORM FOR TEST L.T.V. EVAPORATOR

Test No. (1) Start-up date, time: _____ Op: _____ Date, time: _____
 LTV effect No. _____ Flowsheet: _____
 Calculated by: _____ Recorded in book: _____ Date, time: _____
 air temp., °F _____

Steam:

cond. press., in. Hg read (1)
 Corr. (2), corr'd. (3)
 Corrected barom. press. (4)
 cond. press., in. Hg abs. (5)
 saturation temperature, °F (6)
 actual temperature, °F (7)
 steam enthalpy, Btu/lb (8)
 drip temperature, °F (9)
 drip enthalpy, Btu/lb (10)
 heat input, Btu/lb (11)
 drip pot interval, sec. (12)
 drip pot combined factor (13)
 drip pot reading, mm. (14)
 flow rate, lb/hr (15)
 Flowmeter reading (16)
 Flowmeter factor (17)
 total heat input, Btu/hr (18)
 heat to atmosphere, Btu/hr (19)
 heat to vapor side, Btu/hr (20)

Heat Transfer and Pressure Drop:

heat transfer area, sq. ft. (21)
 V.H. press., in. Hg read (22)
 Corr. (23), corr'd. (24)
 V.H. press., in. Hg abs. (25)
 V.H. satur. temp., °F (26)
 PP overall Δt , °F (27)
 PP overall heat tr. coeff. (28)
 V.H. temperature, °F read (29)
 Corr. _____, corr'd. (30)
 PT overall Δt , °F (31)
 PT overall heat tr. coeff. (32)
 Feed press., in. Hg read (33)
 Corr. _____, corr'd. (34)
 Feed press., in. Hg abs. (35)
 Overall ΔP , in. Hg (36)

Condenser Water:

rotameter reading (37)
 rotameter combined factor (38)
 flow rate, lb/hr (39)
 temp. out....corr _____ c'd, °F (40)
 temp. incorr _____ c'd, °F (41)
 temperature rise, °F (42)
 heat gain, Btu/hr (43)

Distillate:

latent heat. Btu/lb. (44)
 sensible ht. above feed T., Btu/lb (45)
 heat from evap., Btu/lb. (46)
 drip temp (47) °F; Feed-drip, Btu/lb (48)
 heat to cond., Btu/lb. (49)
 drip pot interval, sec. (50)
 drip pot combined factor (51)
 drip pot reading, mm. (52)
 evaporation rate, lb/hr (53)
 total heat from evap., Btu/hr (54)
 total heat to cond., Btu/hr (55)
 Condenser ht. bal. error ((57)%) (56)

Blowdown:

temp....., Corr. _____, c'd. °F (58)
 sp. gr (59) at (60) °F, c'd (61)
 chloride, gpl (62)
 concentration factor (63)
 specific heat, Btu/lb. (64)
 enthalpy above feed T. Btu/lb (65)
 drip pot interval, sec. (66)
 drip pot combined factor (67)
 drip pot reading, mm. (68)
 flow rate, lb/hr (69)
 enthalpy flow, Btu/hr (70)
 BFR (71), corr. Δt (72), corr. coeff. (73)

Feed:

temp.....Corr. _____, c'd. °F (74)
 sp. gr (75) at (76) °F, c'd. (77)
 chloride, gpl (78)
 concentration factor (79)
 flowmeter reading (80)
 flowmeter factor (81)
 flow rate, lb/hr (82)
 flow based on conc'n. ratio, lb/hr (83)
 feed/evaporation ratio (84)

Mass Balance:

Evaporation rate, lb/hr (85)
 Blowdown rate, lb/hr (86)
 Total output, lb/hr (87)
 Feed rate, meas. lb/hr (88)
 Error ((90)%) lb/hr (89)
 Feed rate, analyt, lb/hr (91)
 Error ((93)%) lb/hr (92)

Energy Balance(enthalpies above feed temp.)

Blowdown enthalpy, Btu/hr (94)
 Vapor enthalpy, Btu/hr (95)
 Loss to atmosphere, Btu/hr (96)
 Total output, Btu/hr (97)
 Heat to vapor side, Btu/hr (98)
 Error ((100)%) Btu/hr (99)

checked frequently with local airport.

5. Item (4) plus (if under pressure) or minus (if vacuum) item (3).

6. Saturation temperature from Keenan and Keyes' Steam Tables at absolute pressure indicated by item (5).

7. Actual steam temperature measured at inlet to heating element. This thermometer usually indicated some superheat. The piping was arranged to minimize the possibility of moisture entrainment in the steam.

8. From Steam Tables at pressure (5) and temperature (7). If temperature (7) was below 200°F., enthalpy of saturated vapor at pressure (5) was used.

9. Actual temperature of steam condensate. This was usually close to item (6), but accuracy was doubtful.

10. Enthalpy of water at temperature (6), from Steam Tables.

11. Item (8) minus item (10) gives heat available per pound of steam.

12. Time, measured by stopwatch, for condensate level to rise a fixed distance (14) in the gage glass on the volumetric condensate measuring tank when the discharge pump was stopped and the discharge valve closed.

13. Calibration factor of volumetric tank--a function of the effect of temperature on the density of water and the measuring distance. Determined originally by adding known weights of water and measuring the rise in level.

14. Distance level rose in time (12) -- 5 inches in these tests.

15. Item (13) divided by item (12) gives pounds per hour of steam used.

16. Actual reading of recording flow controller.

17. Item (15) divided by item (16)--used only to aid in subsequent adjustments of flow controller to get desired steam flow rates.

18. Item (15) times item (11) gives total heat given up by steam in Btu per hour.

19. Heat loss from steam side of heating element--as determined by test as a function of item (6) minus the outside air temperature.

20. Item (18) minus item (19) gives the rate of heat transfer through the heating surface.

Heat Transfer and Pressure Drop

21. Area based on inside diameter of the 7 tubes--78.3 square feet for 2-in. tubes, 38.3 square feet for 1-in. tubes.

22. Not used since all vacuum and pressure readings obtained by mercury manometer.

23. Ditto.

24. Actual vacuum in vapor head, as measured by mercury manometer.

25. Item (4) minus item (24).

26. Saturation temperature at pressure (25), from Steam Tables.

27. Item (6) minus item (26)--the apparent temperature difference across the heating surface, assuming that the sea water had no boiling point elevation.

28. Item (20) divided by (item (21) times item (27))--the overall heat transfer coefficient before correction for boiling point elevation.

29. Actual temperature read on thermometer in bottom vapor head. This thermometer should read approximate saturated vapor temperature.

30. Item (29), corrected for thermometer calibration error. This temperature was used primarily as rough check of item (26).

31., 32. Not used, except as rough or quick check, and as a guide in adjusting the vacuum controller.

33. Actual reading of pressure gage or mercury manometer connected to feed cone at inlet to evaporator tubes.

34. Item (33) corrected for gage calibration error, or actual manometer reading when such was used.

35. Item (4) minus item (34).

36. Item (35) minus item (25)--pressure drop from orifice to outlet of tubes, due to friction, hydrostatic head, acceleration effects, and orifice pressure-drop.

Condenser Water

37. Actual reading of rotameter in sea water line to surface condenser used to condense distillate from LTV.

38. Combined factor equal to calibration factor determined by test of rotameter times the specific heat of sea water (0.955 Btu/lb.-°F.).

39. Item (37) times item (38), = lb/hr. sea water times 0.955.

40. Temperature of sea water leaving condenser, corrected for calibration error.

41. Temperature of sea water entering condenser, corrected for calibration error.

42. Item (40) minus item (41).

43. Item (39) times item (42)--heat picked up by sea water in condensing distillate.

Distillate

44. Latent heat of water at temperature (26), from Steam Tables.

45. Item (26) minus item (74)--heat required to raise one pound water from feed temperature to distillation temperature (specific heat--1.0).

46. Item (45) plus item (44)--enthalpy of vapor above feed temperature.

47. Actual temperature of condensate in measuring tank.

48. Item (74) minus item (47)--heat given up in sub-cooling condensate.

49. Item (46) plus item (48)--heat given up in condensing one pound of distillate and subcooling it to temperature (47).

50. Time, measured by stopwatch, for distillate level to rise a fixed distance in calibrated measuring tank.

51. Calibration factor of volumetric tank--similar to item (13).

52. Distance level rose in time (50)--5 inches in these tests.

53. Item (51) divided by item (50) gives pounds per hour of distillate.

54. Item (53) times item (46) gives Btu per hour heat leaving the evaporator with the distillate (taking liquid at the feed temperature as 0).

55. Item (53) times item (49) gives Btu per hour given up to the condenser water in condensing and subcooling the distillate.

56. Item (43) minus item (55)--heat actually picked up by condenser water less heat that should have been given up to the condenser water.

57. Item (56) divided by item (55). This is a secondary check of the overall heat balance. It is only used to indicate the probable source of error if item (100) is relatively large.

Blowdown

58. Same as item (30).

59. Specific gravity measured by hydrometer.

60. Temperature of gravity measurement.

61. Specific gravity at flowing temperature (58). Obtained from physical property charts, either from items (59) and (60) or from item (62).

62. Chlorosity--established by titration.

63. Concentration factor based on standard sea water of 19.262 chlorosity. Determined from physical property charts.

64. Specific heat at chlorosity (62) and temperature (58)--from physical property charts.

65. Item (64) times (item (58) minus item (74))--heat required to raise one pound of blowdown from feed to discharge temperature.

66. Similar to items (12) and (50).

67. Similar to items (13) and (51)--a function of measuring distance (68) and specific gravity (61).

68. Measuring distance--7 inches in these tests.

69. Item (67) divided by item (66).

70. Item (65) times item (69).

71. Boiling point rise from physical property charts at chlorosity (62) and temperature (58).

72. Item (27) minus item (71)--overall temperature difference corrected for boiling point rise. This is temperature difference used in correlating all data.

73. Overall heat transfer coefficient corrected for boiling point rise--as used in correlations.

Feed

74. Actual feed temperature, as read corrected for thermometer calibration.

75. Similar to item (59), for a sample of LTV feed liquor.

76. Similar to item (60), for a sample of LTV feed liquor.

77. Similar to item (61), at temperature (74).

78. Similar to item (62).

79. Similar to item (63).

80. Actual reading of recording feed flow controller.

81. Calibration factor for flow controller obtained by comparing controller with volumetric measurements in blowdown tank.

82. Item (80) times item (81)--a function of flow rate and specific gravity (77).

83. Item (69) times item (63), divided by item (79)--due to high accuracy of chlorosity determinations, this is a more accurate measure of feed flow than item (82).

84. Item (83) divided by item (53).

Mass Balance

85. Same as item (53).
86. Same as item (69).
87. Item (85) plus item (86).
88. Same as item (82). Theoretically equal to (87).
89. Item (87) minus item (88).
90. Item (89) divided by item (87), times 100.
91. Same as item (83). Theoretically equal to (87).
92. Item (87) minus item (91).
93. Item (92) divided by item (87), times 100. This is an accurate indication of errors in flow rate measurement. Errors of 10% would usually be considered satisfactory, but the error in these tests rarely exceeded 3%.

Energy Balance

94. Same as item (70).
95. Same as item (54).
96. Heat loss from vapor side of LTV--as determined by test as a function of item (26) minus the outside air temperature.
97. Sum of items (94), (95), and (96). Total calculated heat transferred through the heating surface, on the basis of the heat carried away.
98. Same as item (20). Calculated heat transferred from the steam to the heating surface. Theoretically equal to (97).
99. Item (97) minus item (98).
100. Item (99) divided by item (97), times 100. This is a good

check of heat input and distillate production. Errors of 15% would usually be considered satisfactory. The error in these tests rarely exceeded 8%.

SUMMARY OF CALCULATION PROCEDURE

a) Calculation of Mass Balance

The evaporation rate was determined by timing the distillate drip-pot, and determining the distillate density by its temperature. The blowdown rate was similarly determined, by timing, and from blowdown temperature and concentration. Both rates were added together to give a value for the feed flowrate. - This value was compared to the blowdown rate multiplied by the ratio of ~~blowdown concentration~~ $\frac{\text{blowdown concentration}}{\text{blow feed concentration}}$ to feed concentration.

b) Calculation of Steam Enthalpy and Heat Load

The steam flowrate was determined from the steam condensate drip-pot. The steam saturation temperature was determined by measuring the absolute pressure of steam condensation and using the steam tables. The steam superheat was calculated from the saturation temperature and the temperature reading of the incoming steam. This determined the enthalpy of the condensing steam, in Btu/hr.

From this was subtracted the heat loss from steam chest to atmosphere. This heat loss was experimentally determined before the beginning of the heat transfer runs as function of the temperature difference between steam chest and atmosphere, by filling the empty steam chest

with steam and measuring the rate of condensation for various temperature differences. This calibration was repeated after the heat transfer runs, and was found to be unchanged. The heat loss was of the order of 3,000 - 13,000 Btu/hr for the heat transfer runs.

The steam-chest was continuously vented from the top of the condensate drip-pot; during vacuum operation, to the vacuum pump, and during pressure operation, to the atmosphere. Venting was always excessive to insure removal of non-condensibles.

c) Calculation of Feed, Blowdown and Vapor Enthalpies

For the purpose of this calculation, the feed was arbitrarily designed as having zero enthalpy. - The blowdown enthalpy was calculated by multiplying the blowdown rate by the blowdown specific heat and by the blowdown-minus-feed temperature difference. - The specific vapor enthalpy, Btu/lb, was calculated by adding the heat of vaporization to the vapor-minus-feed temperature difference; this was then multiplied by the vapor flowrate, lb/hr.

d) Calculation of Enthalpy Balance

Blowdown enthalpy and vapor enthalpy were added and compared to the heat load. A correction was added due to the heat losses from the vapor-side (vapor-head, vapor line) to the atmosphere. This heat loss was determined by measuring the cooling rate of circulating hot sea water in a separate heat-loss test, performed before the heat transfer runs were started.

As a check, a heat balance was also calculated around the condenser, by use of cooling water flowrate and temperature rise. This balance was only approximate, but served to point out any gross deviations.

e) Calculation of Overall Heat Transfer Coefficients

Steam-side temperature was taken as the saturation temperature corresponding to steam-chest absolute pressure. - "Apparent" vapor-side temperature was taken as the saturation temperature corresponding to vapor-head absolute pressure. - "Corrected" vapor-side temperature was taken as the "apparent" vapor-side temperature plus the boiling-point rise corresponding to the particular blowdown concentration and temperature.

In calculating the overall heat transfer coefficients, the calculated steam-side heat load and the inner tube diameters were used.* The apparent coefficient was calculated by using the apparent vapor-side temperature to calculate the overall temperature difference; the corrected overall heat transfer coefficient was similarly calculated by using the corrected vapor-side temperature to obtain the overall temperature difference.

f) Calculation of Pressure Drop

Due to the presence of tube inserts, pressure drops could not be measured directly. Vapor-head pressure was subtracted from feed pressure to give the desired pressure drop plus the orifice pressure drop. After

* 38.3 sq ft for 7 1-in. tubes, 78.3 sq ft for 7 2-in. tubes.

each run, the steam was turned off, all other operating variables remaining unchanged; the resulting pressure drop was then due to the inserts only, and was subtracted from the orifice-plus-vapor pressure drop to give the desired two-phase flow pressure drop.

RANGE OF PROCESS VARIABLES

The following is a list of the process variables and their explored range:

Tube I.D., in.:	0.870, 1.782
Vapor-head sat. temp., °F:	100, 125, 150, 175, 200, 230
Feed concentration factor:	1, 2
Feed flowrate, lb/hr:	1-in. tubes: 1,500, 3,000 2-in. tubes: 1,500, 3,000, 6,000
Steam flowrate, lb/hr:	1-in. tubes: 150, 250 2-in. tubes: 250, 450
Feed superheat*, °F:	0, 20

The test schedule consisted of the determination of heat transfer coefficients for all combinations of process variables.

OPERATING PROCEDURE

Since the equipment was run on a non-stop schedule, the beginning of a run generally coincided with the end of the previous run. The process variables were changed by setting the automatic control instruments to the desired values; this was subsequently checked from

*Feed superheat = Feed temperature - V. H. saturation temperature.

the next set of readings of the measurement instruments. - After three or four hours a complete calculation was made from the last set of readings. This was repeated every hour; generally two or three such calculations were made each run, and the results compared. If there was a change in readings, the run was continued until perfectly constant conditions were reached. Usually, however, steady-state was reached after two hours of operation, but the run continued for three or four hours more to ensure non-transient behavior.

The two FC's* were generally idle and were used as feed storage tanks, one for feed of concentration factor 1.0, the other for 2.0. Blowdown and distillate were recombined and pumped back to the respective FC. For tests with concentration factor 1.0 and cold feed (100 or 125 °F), sea water was used directly, and the blowdown and distillate pumped back to the ocean. - Feed of concentration factor 2.0 was directly prepared in one of the FC's.

* FC = forced circulation evaporator

SECTION II
THEORY OF FALLING-FILM FLOW
A. FUNDAMENTALS

For steady-state one-dimensional downward flow through a vertical round tube, a force balance on an element of downward length dL yields, for any flow regime,

$$-\frac{dp}{dL} = \frac{1}{2\alpha g_c v} \frac{d(v^2)}{dL} + \frac{\tau_w}{r_h} - \frac{g}{vg_c} \quad (1)$$

The wall shear stress τ_w is taken positive when opposed to the flow direction L .

An energy balance on this same element yields:

$$\frac{dH}{dL} = \frac{dQ}{dL} - \frac{wv}{J} \left[\frac{1}{2\alpha g_c v} \frac{d(v^2)}{dL} - \frac{g}{vg_c} \right] \quad (2)$$

The dimensionless velocity distribution factor α is due to radial variations in kinetic energy. It is 0.5 for parabolic velocity distribution, 1.0 for highly turbulent flow.

Assume isenthalpic flow, with negligible longitudinal variation in kinetic energy. From equ. (1):

$$-\frac{dp}{dL} = \frac{\tau_w}{r_h} - \frac{g}{vg_c} \quad (3)$$

Consider the effect of decreasing flowrate on a tube with initially high-speed full-pipe flow. For any type of flow to take place in the L -direction, i.e., downwards, the pressure drop $-\frac{dp}{dL}$ cannot be negative:

$$\therefore \frac{\tau_w}{r_h} \geq \frac{g}{vg_c} \quad (4)$$

This is valid for any type of flow regime.

Let τ_{wA} be the unique wall shear stress such as to cause zero pressure drop in full-pipe flow. It is, therefore, the lowest wall shear stress at which full-pipe flow can take place. For full-pipe flow, $r_h = \frac{D}{4}$:

$$\therefore \frac{4\tau_{wA}}{D} = \frac{g}{vg_c} \quad (5)$$

From equ. (4) we have, for any flow regime,

$$\frac{\tau_w}{r_h} \geq \frac{4\tau_{wA}}{D}, \text{ or } \frac{\tau_w}{\tau_{wA}} \geq \frac{r_h}{D/4} \quad (6)$$

For full-pipe flow, $r_h = \frac{D}{4}$, $\tau_w \geq \tau_{wA}$

As we decrease the flowrate and τ_w falls below τ_{wA} , it must necessarily follow from equ. (6) that r_h becomes less than $\frac{D}{4}$. If the tube wall remains wetted, annular flow must result.

In annular flow, then, the pressure drop is zero*; friction loss and eventual gain in kinetic energy occur at the expense of potential energy only.

The flowrates employed in our research never exceeded 7% of the minimum flowrate necessary to cause full-pipe flow, i.e., to cause a wall shear stress τ_{wA} .

* For the purpose of this analysis, no interfacial shear was assumed.

The hydraulic radius for a film of thickness B is:

$$r_h \equiv \frac{\frac{\pi}{4} [D^2 - (D - 2B)^2]}{\pi D} \equiv B \left(1 - \frac{B}{D}\right) \quad (7)$$

For very thin films this expression reduces to:

$$r_h = B \quad (8)$$

The Reynolds number is defined as in full-pipe flow:

$$(\text{Re}) \equiv \frac{4r_h V}{\nu} \equiv \frac{4w}{\pi D \mu} \equiv \frac{4\Gamma}{\mu} \quad (9)$$

It is, therefore, not necessary to know the film thickness in order to calculate the Reynolds number.

For films thin enough so that equ. (8) holds, equ. (9) becomes:

$$(\text{Re}) = \frac{4BV}{\nu} \quad (10)$$

B) LITERATURE RESEARCH: FLUID MECHANICS

Consider a liquid flowing down a flat plate, at an angle with the horizontal. Assume no interfacial shear, and perfectly streamline flow (Figure 2). A force balance yields:

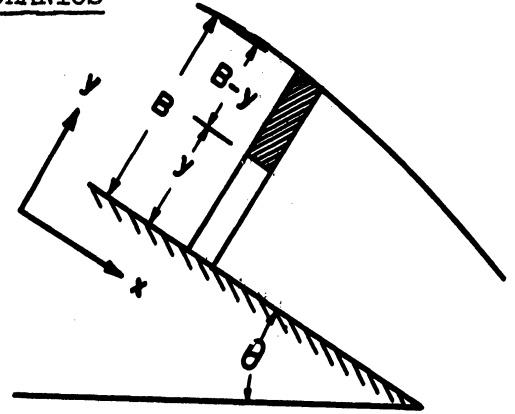


Figure 2

$$\rho g(B-y)b \, dx \sin \theta = \left(\mu \frac{du}{dy} \right) b \, dx \quad (11)$$

Postulating zero wall velocity, equ. (11) is integrated across the film:

$$u = \frac{g}{\nu} \left(By - \frac{y^2}{2} \right) \sin \theta \quad (12)$$

The mass flowrate per unit breadth is calculated as:

$$\Gamma \equiv \int_0^B u \rho \, dy = \frac{\rho g B^3}{3\nu} \sin \theta \quad (13)$$

The results of this classical analysis by Nusselt⁽³⁷⁾ in 1916 can also be expressed in the following ways:

$$B = \left(\frac{3\nu^2}{4g} \right)^{1/3} (\text{Re})^{1/3} \sin^{-1/3} \theta \quad (14)$$

$$V = \left(\frac{g\nu}{48} \right)^{1/3} (\text{Re})^{2/3} \sin^{1/3} \theta \quad (15)$$

$$\tau_w = \frac{\rho g B}{g_c} \sin \theta \quad (16)$$

TABLE I
List of Experimental Studies on Momentum Transfer and/or of
Single-Phase Heat Transfer in Falling Films

AUTHOR	YEAR	TEST LIQUID	APPARATUS	WIDTH OR DIA. (in.)	LENGTH (in.)	RANGE OF (Re)	FILM THICKNESS MEASUREMENT	REF.
Hopf	1910	water, molasses	glass trough 0.5 - 3.5° inclination	2.05	15.8	600 - 2,400	micrometer	31
Claaen	1918	water, aq. NaCl, molasses	outer wall vertical steel & brass tubes	1.97 1.57	53.1 77.1	28 - 120	holdup	14
Schoklitsch	1920	water	glass trough 0.25 - 2.0° inclination	10.0	--	88 - 180,000	----	41
Chwang	1926	water, min. oil	glass plate 0 - 13° inclination	9.84	--	3.6 - 440	micrometer	13
Cooper, Willey	1930	dil. aq. H ₂ SO ₄	inner wall vertical glass tube	0.439	25.0	1.53 - 192	holdup	18
Warden	1930	water	inner wall vertical glass & brass tubes	2.43 2.50	28.8 30.1	278 - 7,320	holdup	44
Kirbride	1934	water, min. oil	outer wall vert. - tube	--	29.9	0.16 - 8,000	micrometer	33
Fallah, Hunter, Nash	1934	water	inner wall vertical glass tubes	0.532 0.875 1.011	56.5 84.4 57.5	80 - 3,370	holdup	25
Bays, McAdams	1937	2 min. oils	inner wall vertical	1.5 2.5	49 - 73	2 - 2,000	* only	5
Sexauer	1939	water	outer wall vertical steel & brass tubes	1.18 2.36	8 - 102	3,300 - 16,500	micrometer	43
McAdams, Drew, Bays	1940	water	inner wall vertical	1.5 2.5	49 - 73	2,100 - 51,000	* only	35
Friedman, Miller	1941	water, 3 min. oils	inner wall vertical Pyrex tubes	1.00 0.62	60	0.09 - 460	holdup	26
Grinley	1945	water, CCl ₄ , CCl ₆ , aq. glycerol, aq. EtOH	-----	--	--	8 - 4,300	----	30
Pennie, Belanger	1952	5% aq. Na ₂ CO ₃	inner wall vertical copper tube	0.502	--	50 - 13,000	micrometer	39
Dukler, Bergelin	1952	water	vert. flat brass plate	24	96	480 - 3,000	film capacitance	22
Brotz	1954	water, C ₁₅ H ₃₂ , min. oil	inside wall vertical glass tubes	0.583 0.787 1.575	11.8 19.7 39.4	400 - 17,200	holdup Also *	10
Garwin, Kelly	1955	water	flat brass plate 0 - 90° inclination	8	30	2,900 - 12,800	* only	27
Brauer	1956	water, aq. glycol	outer wall vertical brass tube	1.772	70.9	0 - 4,000	photographs, * holdup. Also	6
Anderson, Moutzouranis	1960	water	inside wall vertical glass tube	0.427	50		holdup	1

* Heat transfer tests

$$f \equiv \frac{\tau_{wg}c}{\rho v^2/2} \equiv \frac{24}{(Re)} \quad (17)$$

From equ. (12) and (15) it can also be seen that the velocity u_i at the interface (free surface) is 1.5 times the average velocity.

For vertically downward flow, of course, $\sin \theta$ is equal to one in all these equations.

Hopf* (31), the earliest investigator (1910), used too narrow a trough for his data to be considered reliable except for very shallow depths because of ripple formation at the side walls. - Claassen⁽¹⁴⁾ used very thin films, of the order of several mils, on pipes of varying degrees of roughness. Unfortunately, over half of his runs were made with molasses whose viscosity he did not record. - Schoklitsch⁽⁴¹⁾ extended his tests to very high flowrates and observed the flow regimes with the classical color-band method.

Copper, Drew and McAdams⁽¹⁷⁾ correlated the results of the first six investigators of Table I. The results show fairly good agreement with Nusselt's theoretical analysis for low flowrates. The friction factors scatter ca. $\pm 30\%$ about the straight line of equ. (17) when plotted on a log-log graph, for (Re) of less than 1,000. In analogy with full-pipe flow, this was considered the streamline portion. Above a (Re) of ca. 2,000 the friction factors changed much less with (Re), and this was, therefore, considered to be the turbulent zone. Other

*See Table I.

manifestations of turbulence, such as eddies and waves, were observed in this range.

This analogy between full-pipe and falling-film flow was contradicted by Kirkbride's observation⁽³³⁾ that the first appearance of waves or ripples occurred in falling water films at a (Re) as low as 8. He noticed that the wave peaks were as much as 3.7 times the average film thickness. The (Re) of first wave appearance, $(Re)_{w1}$, decreased as more viscous liquids were used. His film thickness measurement data below $(Re)_{w1}$, i.e. for smooth films, followed the Nusselt theory, but those above, i.e., for wavy flow, did not. The latter may have been due to Kirkbride's micrometer technique, which gave maximum rather than average film thickness readings.

Fallah, Hunter and Nash⁽²⁵⁾ correlated data from the literature in a manner similar to Cooper, Drew and McAdams. Their own data were in fairly good agreement with the Nusselt theory for the entire viscous region. - Sexauer⁽⁴³⁾ ran falling-film tests at very high flowrates. He used a retracting micrometer tip and took his film thickness readings as the tip freed itself from the liquid. His readings were in poor agreement with the Nusselt theory.

Friedman and Miller⁽²⁶⁾ confirmed Kirkbride's observations regarding ripples for (Re) above 25; they also found the velocity at the interface to be much higher than predicted by Nusselt above a (Re) of 25. These velocities were measured with a dye technique. However, they found that the mean film thickness followed Nusselt's correlation up to (Re) of 1,000 - 2,000.

Grimley⁽³⁰⁾ also observed wave motion in falling-film flow at values of (Re) above 25. He obtained very clear spark photographs of these waves. By studying the behavior of test liquids with a viscosity range of 0.7 - 26.4 cp and a surface tension range of 19 - 75 dyne/cm, he derived the following dimensionless relation for the Reynolds number of incipient wave formation:

$$(\text{Re})_{w1} \approx 1.16 \left(\frac{\sigma^3 \rho}{\mu^4 g} \right)^{1/8} \quad (18)$$

For water at room temperature this turns out to be 25. - Grimley further observed from his photographs that the waves propagated in an orderly fashion up to a (Re) of 1,000 for water, and that turbulence set in at a (Re) of ca. 2,000. He found that the range of wave flow regime was not affected by moderate air velocities in either direction. - Grimley studied the velocity profile by adding a drop of dye to the surface, observing it with a modified ultramicroscope and timing the rate of fall; no further description of the method is given. The resulting velocity profile starts out from the wall at values of u that are slightly below Nusselt's theory; at a $\frac{y}{B}$ ratio of ca. 0.9, however, the velocity rises to a sudden peak as much as 3 times the value of the theoretical maximum velocity. At the interface itself the profile converges with Nusselt's.

Pennie and Belanger⁽³⁹⁾ in 1952 measured the film thickness in a falling-film heater. A sewing needle controlled by a micrometer traversed the entire tube. The needle was glyptal-coated except for the point, and was connected in series with an audio-oscillator. When passing through

the air space no sound was emitted until re-entry into the film at the opposite side. The whole needle was inclined 45° to the horizontal in order to improve accuracy. - Their values tend to be too high since they had no way of determining mean rather than maximum film thicknesses. - This research was carried out in a single tube similar to those used in their falling film heater. It is interesting to note that in the description of their heater the authors showed tube entrance orifices for flow distribution very similar to those used by us; also, their observation of the flow pattern as a falling-film liquid emerges from the bottom tube ends coincides with ours.

Dukler and Bergelin⁽²²⁾ in 1952 presented the first new theoretical treatment of falling-film flow since Nusselt. Nusselt had developed his equations for streamline flow only, since at that time little was known about turbulent flow. Dukler and Bergelin used the Nikuradze - von Karman universal velocity profile to integrate the flowrate equation through the laminar layer, the buffer layer and into the turbulent layer, thus presenting a universal correlation for any flow regime. With the usual dimensionless variables:

$$y^+ \equiv \frac{yu^*}{\nu} \quad (19)$$

$$u^+ \equiv \frac{u}{u^*} \quad (20)$$

the friction velocity $u^* \equiv \sqrt{\frac{\tau_w g_c}{\rho}}$ (21)

and with $B^+ \equiv \frac{Bu^*}{\nu} \equiv y^+(y=B)$ (22)

one can integrate the flowrate equation for thin films:

$$(\text{Re}) = 4 \int_0^{B^+} u^+ dy^+ \quad (23)$$

with a given universal velocity profile correlation.

Nikuradze's universal velocity profile and its substitution into equ. (23) are, respectively,

$$u^+ = y^+ \quad (0 < y^+ < 5) \quad , \text{ or} \quad (\text{Re}) = 2B^{+2} \quad (0 < (\text{Re}) < 60) \quad (24)$$

$$u^+ = -3.05 + 5.00 \ln y^+ \quad (5 < y^+ < 30) \quad , \text{ or} \quad (\text{Re}) = B^+ (5 \ln B^+ - 8.05) + 12.05 \quad (60 < (\text{Re}) < 1,080) \quad (25)$$

$$u^+ = 5.5 + 2.5 \ln y^+ \quad (y^+ > 30) \quad , \text{ or} \quad (\text{Re}) = B^+ (2.5 \ln B^+ + 3.0) - 64 \quad ((\text{Re}) > 1,080) \quad (26)$$

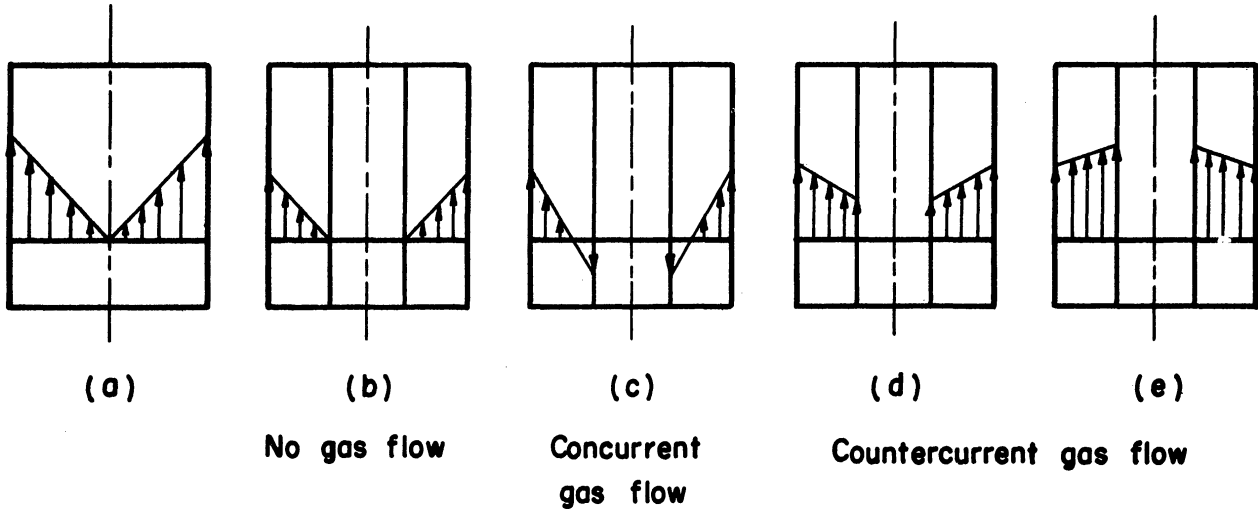
Dukler and Bergelin extended their theory to include an interfacial shear stress τ_i different from zero. In full-pipe flow (Figure 3a) the radial shear stress profile for a given hydraulic radius is given by the wall shear stress τ_w alone. In falling-film flow (Figures 3b, c, d, e) the shear profile, and hence the velocity profile, depends on τ_i as well as on τ_w and the hydraulic radius. If the film is thin enough so that the hydraulic radius is equal to the film thickness B , a force balance on an element of film gives:

$$\tau_w = \tau_i + \frac{B\rho g}{g_c} \quad (27)$$

$$\therefore u^* = \sqrt{\frac{\tau_i g_c}{\rho} + Bg} \quad (28)$$

$$\therefore B^+ = \frac{B}{\nu} \sqrt{\frac{\tau_i g_c}{\rho} + Bg} \quad (29)$$

For a given Reynolds number, B^+ is calculated from equ. (24) to (26) and substituted into equ. (29); for a known value of τ_i one can then calculate the film thickness B .



(All liquid flow in downward direction)

Figure 3

The interfacial shear stress τ_i can be derived from the general pressure drop equation of the gas core:

$$-\frac{dp}{dL} = \frac{1}{2\alpha g_c} \rho_g \frac{d(v_g^2)}{dL} + \frac{4\tau_i}{D} - \frac{\rho_g g}{g_c} \quad (30)$$

$$\therefore \tau_i = \frac{D}{4} \left(\rho_g \frac{g}{g_c} - \frac{dp}{dL} \right) \quad (31)$$

if kinetic energy changes can be neglected and the film is very thin in relation to tube diameter. - The term in parentheses in equ. (31) is the frictional gas-phase pressure drop.

Dukler and Bergelin presented experimental evidence only for the case of zero interfacial shear. Equ. (29) simplifies to:

$$B = B^+{}^{2/3} \left(\frac{\nu^2}{g} \right)^{1/3} \quad (32)$$

which below $y^+ = 30$, $(Re) = 1,080$, falls very close to the Nusselt correlation when applying equ. (24) and (25). The authors used a Reynolds number range of 480 - 3,000 and found fairly good agreement with their theory. Their experimental set-up was the flow of a thin water film down a vertical flat brass plate. The film thickness was measured indirectly by determining the electric capacitance of the film; this was done with small disc electrodes held close to the film, and gave the root-mean-square film thickness. The mean film thickness was calculated from the root-mean-square film thickness by means of a geometric correction derived from the study of the actual wave profiles on high-speed flash photographs. - Brauer⁽⁶⁾ has observed that the results of Dukler and Bergelin fell slightly above their theoretical film thickness curve, and attributed it to the size of their disc electrodes, which, although small ($1/8 \times 3/16$ in.), were probably still too large.

Dukler and Bergelin's theory depends on the Nikuradze velocity profile, which was obtained with full-pipe flow. Dukler and Bergelin justified its application to film flow by postulating that a given element of fluid does not "know" whether it is part of a liquid mass in full-pipe flow or in film flow. For zero interfacial shear, their experimental results seem to support their reasoning. For moderate values of τ_i they reasoned that Nikuradze's correlation should still be applicable within the bulk of the film for the same reason as before, and that at

the interface itself the turbulence would be so high as to make little difference.

Brötz⁽¹⁰⁾ in 1954 determined film thicknesses for flow down the inner walls of vertical glass tubes. He found Nusselt's relationship to hold up to a (Re) of 2,360; above this point he found B to be proportional to $(Re)^{1/3}$ but was unable to formulate a general correlation.

Perhaps the most painstaking experimental investigation on falling-film flow is due to Brauer⁽⁶⁾ in 1956. He investigated flow down the outside wall of a long vertical brass tube at room temperature. Reynolds numbers ranged all the way up to a highly turbulent 4,000. To determine the effect of viscosity he used water and aqueous diethylene glycol solutions, the viscosity ranging from 0.90 to 14 cp. Specific gravity was 1.0 - 1.1. The effect of surface tension was evaluated by artificially depressing water with small amounts of dodecyl sodium sulfate; surface tension ranged from 62% to 100% of normal water (74.6 dyne/cm).

Brauer determined the following variables at different Reynolds numbers: the wave peak film thickness, B_p ; the wave trough thickness, B_t ; the average film thickness, B ; the velocity at the interface, u_i ; the average velocity, V ; the friction factor, f .

Peak and trough film thicknesses were determined by using a micrometric needle-probe; an oscillograph coupled to an electronic counter was connected to the needle. The number of waves per unit time were counted for given wall-to-needle distances, and the statistical frequencies were thus determined. The frequency curves were symmetrical

about well-defined maxima which were characteristic of the flow regime, and which gave B_p and B_t .

The average film thickness was determined by taking shadow photographs of the tube without liquid and with liquid, and planimetering the difference in area.

Hold-up measurements gave the flowrates, which yielded the average velocities via the average film thicknesses. Interfacial velocities were determined by floating tiny pieces of flat plastic down the tube; for low velocities the rate of fall was visually timed, and for higher velocities a piece of plastic was photographed for a given exposure time, and the length of the streak measured.

Wall shear stress was measured indirectly. The heat transfer coefficient was experimentally determined by inserting a small, electrically heated copper surface flush into one spot on the tube, and measuring the heat input and the copper surface temperature. Brauer "calibrated" this instrument with smooth films to give τ_w as function of the heat transfer coefficient h , since for smooth films τ_w can be calculated from the film thickness via equ. (27). The instrument was then used to determine τ_w on wavy films by postulating that the analogy between heat transfer and momentum transfer was the same for wavy films as for smooth films.

Brauer clearly distinguished a turbulent region above a critical Reynolds number $(Re)_{crit}$. This is analogous to full-pipe flow. Below this critical point, however, he distinguished 5 more different flow

TABLE II

PROPERTIES OF BRAUER'S FLOW REGIMES

(Re)	f	B	B _p /B	V	u _i /V
< w ₁	24(Re) ⁻¹	$\left(\frac{3v^2}{4g}\right)^{1/3}(\text{Re})^{1/3}$	1	$\left(\frac{gv}{48}\right)^{1/3}(\text{Re})^{2/3}$	1.5
w ₁ -i	1.22(Re) ^{-1/3}		1 → 2.65		1.5 → 2.15
w ₂ -c	34(Re) ⁻¹		2.65		2.15
c-crit	72(Re) ^{-17/15}	$\left(\frac{3v^2}{4g}\right)^{1/3}(\text{Re})^{-1/5}(\text{Re})^{8/15}$	2.65 → up	$\left(\frac{gv}{48}\right)^{1/3}(\text{Re})^{1/5}(\text{Re})^{7/15}$	2.15 → 1.5
> crit	72(Re) ^{-3/5}(\text{Re})^{-8/15}}				1.5

regimes, separated by 4 characteristic Reynolds numbers denominated $(Re)_{w_1}$, $(Re)_i$, $(Re)_{w_2}$ and $(Re)_c$.

The visual aspects of the different flow regimes were described as follows. Starting with a very low flow rate, the film was perfectly smooth up to $(Re)_{w_1}$, the point of first wave formation (16 for water). Above this point small sine waves flowed smoothly all the way down the tube in closed rings. These waves formed roughly 4 in. below the feed point. At $(Re)_i$, the point of instability (36 for water), the waves broke up after 5 - 6 in. of travel. These partial waves then proceeded further down the tube at different velocities, overtaking one another to form new waves. The location below the feed point where waves first formed also wandered up and down, but always about its original mean position. At $(Re)_{w_2}$ (60 for water) no further change took place with increasing flowrate. In the neighborhood of the critical point $(Re)_{crit}$ (1,600 for water), the wave surface changed from smooth to rough due to the formation of capillary waves. Turbulent spots formed on the interface, and at Reynolds numbers above 2,400 very large ring waves formed that seemed to fall rather than to flow down the tube. - No visual effects were seen to change as $(Re)_c$ was passed (320 for water). - See Table II for a quantitative description of Brauer's flow regimes.

In full-pipe flow, the transition from laminar to turbulent flow occurs at a Reynolds number having a fixed value independent of the fluid's physical properties. Brauer found that for film flow, all 5 characteristic Reynolds number depend on physical properties. Brauer expressed them in terms of the same dimensionless variable

$$\frac{\sigma^3 \rho}{\mu^4 g}$$

used by Grimley. This number, called K_F by Brauer, is the only combination of the Reynolds, Froude and Weber numbers that does not include inertial forces, i.e., velocity and film thickness:

$$K_F \equiv \frac{\sigma 3\rho}{\mu^4 g} \equiv \frac{(Re)^4 (Fr)}{(We)^3} \quad (33)$$

It is, therefore, the dimensionless variable that relates gravity forces, viscous forces and surface forces. See Table III.

Table III

	General Value	Value for Water at Room Temperature
$(Re)_{w1}$	$1.224 K_F^{1/10}$	16
$(Re)_i$	$2.88 K_F^{1/10}$	36
$(Re)_{w2}$	$5.40 K_F^{1/10}$	60
$(Re)_c$	$0.0724 K_F^{1/3}$	320
$(Re)_{crit}$	$140 K_F^{1/10}$	1,600

For flow to be fully developed, i.e., constant $\frac{B_p}{B}$ ratio, Brauer found experimentally that the entrance length was equal to $892 B$, or $892 \left(\frac{3\nu^2}{4g}\right)^{1/3} (Re)^{1/3}$.

In this expression, the non-turbulent value for B is used because the film, though fully developed, was found to observe a non-turbulent behavior for a short distance after constant $\frac{B_p}{B}$ was attained.

The effect of a trip wire was studied by Brauer. He found that it only had local effect, and that the disturbance smoothed out quickly. - He also measured the interfacial surface area on his shadow photographs. He found that the increase in area due to waves was negligibly small even for turbulent flow. - The only effect due to a change of surface tension, according to Brauer, is a shift in the values of the characteristic Reynolds numbers, especially $(Re)_{crit}$; no other effect could be detected.

On comparing Brauer's results for average film thickness with those of Dukler and Bergelin, the two correlations are seen to check very closely in the turbulent as well as in the sub-critical range, although the two correlations were derived in quite different ways. His results also check with those of Friedman and Miller. - Brauer's friction factor plot departs from Nusselt's above $(Re)_{w1}$, but comes so close to it as to fall well within the scatter of the data summary of Cooper, Drew and McAdams. - His observations on wave formation and on the dependence of $(Re)_{w1}$ on physical properties check with Kirkbride, Friedman and Miller, and Grimley.

Brauer's results present two curious features. One is the value of $\frac{u_i}{V}$, which even for highly turbulent flow was observed to be 1.5. The other is, that his friction factors do not satisfy the force balance from equ. (27), $\tau_w g_c = E \rho g$, except for smooth films. Brauer mentioned these two points but only explained them as resulting from wave action.

Dukler⁽²³⁾ in 1960 questioned the existence of a laminar sublayer in turbulent falling-film flow. - It has long been known that for full-pipe flow the laminar sublayer is a useful approximation only. In 1932 Fage and Townend⁽²⁴⁾ had detected dampened radial pulsations very close to the tube wall; even at 0.5μ from the wall they were unable to find rectilinear motion if the core of the liquid flowing through the pipe was turbulent.* The increase of turbulence with distance from the wall is gradual, not stepwise; since for full-pipe flow the region near the wall is only a small part of the entire flow cross-section, the inaccuracy involved in assuming the existence of a purely laminar sublayer is negligibly small. - Dukler reasoned that for falling-film flow the inaccuracy would be excessive, and that both laminar and turbulent transfer mechanisms had to be considered at all points of the film. The general shear stress equation, to be integrated across the entire film, is therefore:

$$\tau = \frac{1}{g_c} \left(\mu + \rho E_M \right) \frac{du}{dy} \quad (34)$$

or, in dimensionless form:

$$\frac{\tau}{\tau_w} = \left(1 + \frac{E_M}{\nu} \right) \frac{du^+}{dy^+} \quad (35)$$

Dukler used the Deissler correlation (19), (20) for the eddy diffusivity E_M near the wall:

* They used an ultramicroscope to observe the flow of tap water through a horizontal glass tube. When intensely illuminated, the water was found to contain sufficient particles to act as bright points of light when viewed against a dark background.

$$E_M = n^2 u y \left(1 - e^{-\frac{n^2 u y}{\nu}} \right) = \nu n^2 u^+ y^+ \left(1 - e^{-n^2 u^+ y^+} \right) \quad (0 \leq y^+ < 20) \quad (36)$$

and the von Kármán correlation for highly developed turbulent flow at a region further removed from the wall:

$$E_M = \kappa^2 \frac{(du/dy)^3}{(d^2u/dy^2)^2} = \kappa^2 \nu \frac{(du^+/dy^+)^3}{(d^2u^+/dy^{+2})^2} \quad (y^+ \geq 20) \quad (37)$$

The dimensionless shear stress equation, (35), thus becomes:

$$\frac{\tau}{\tau_w} = \left[1 + n^2 u^+ y^+ (1 - e^{-n^2 u^+ y^+}) \right] \frac{du^+}{dy^+} \quad (0 \leq y^+ < 20) \quad (38)$$

and

$$\frac{\tau}{\tau_w} = \kappa^2 \frac{(du^+/dy^+)^4}{(d^2u^+/dy^{+2})^2} \quad (y^+ \geq 20) \quad (39)$$

The Deissler correlation is semi-empirical, and has been substantiated by full-pipe tests with air, water, glycol, and sodium hydroxide. Tests were run at wall-distance parameters as low as $y^+ = 2$. The validity of this correlation extends up to $y^+ = 26$; however, Dukler only used it up to $y^+ = 20$. Dukler used a value of 0.10 for n as suggested by Deissler. - Von Kármán's expression for the eddy diffusivity in highly developed turbulent flow is derived from his similarity theory, the suggested value for his universal constant κ being 0.38.*

Dukler included interfacial shears τ_i different from zero in his mathematical treatment. We already have equ. (29):

* Dukler's paper does not explicitly state that he used this value of κ , but the result of his calculations indicate that he apparently did so.

$$B^+ = \frac{B}{\nu} \sqrt{\frac{\tau_i g_c}{\rho} + Bg} \quad (29)$$

which for zero interfacial shear simplifies to:

$$B^+ = B^{3/2} \left(\frac{g}{\nu^2} \right)^{1/2} \quad (40)$$

To simplify the mathematical treatment, Dukler defined the dimensionless variable s , which is the ratio of the actual film thickness to the thickness the film would have if τ_i were zero, all other magnitudes (B^+ , ν , g) being the same:*

$$s \equiv \frac{B}{(B^+)^{2/3} \left(\frac{\nu^2}{g} \right)^{1/3}} \quad (41)$$

It can also be shown that:

$$s = \sqrt[3]{1 - \frac{\tau_i}{\tau_w}} \quad (42)$$

Substituting equ. (41) into equ. (29):

$$B^+ = s(B^+)^{2/3} (g\nu)^{-1/3} \sqrt{\frac{\tau_i g_c}{\rho} + s(B^+)^{2/3} (g\nu)^{2/3}} \quad (43)$$

Squaring both sides, dividing by $(B^+)^2$ and re-arranging, we obtain:

$$s^3 + s^2 \frac{\tau_i g_c}{(B^+)^{2/3} (g^2 \nu^2 \rho^3)^{1/3}} - 1 = 0 \quad (44)$$

Define

$$\beta \equiv \frac{\tau_i g_c}{(g^2 \nu^2 \rho^3)^{1/3}} \quad (45)$$

* In Dukler's paper the symbols σ , m , η are used in place of our s , B , B^+ , respectively.

with $\beta > 0$ for co-current, $\beta < 0$ for countercurrent gas flow; τ_i is computed from the gas-phase frictional pressure drop, equ. (31).

The final equation for s is then:

$$s^3 + s^2 \frac{\beta}{(B^+)^{2/3}} - 1 = 0 \quad (46)$$

Dukler solved this equation by means of a digital computer* for values of $\beta/(B^+)^{2/3}$ from 0 to 2,000.

The force balance:
$$\tau_{gc} = \tau_w g_c - y \rho g \quad (47)$$

can be reduced to the dimensionless form:

$$\frac{\tau}{\tau_w} = 1 - \frac{s^3}{B^+} y^+ \quad (48)$$

Combining with equ. (38) and (39), we obtain:

$$1 - \frac{s^3}{B^+} y^+ = \left[1 - n^2 u^+ y^+ (1 - e^{-n^2 u^+ y^+}) \right] \frac{du^+}{dy^+} \quad (0 \leq y^+ < 20) \quad (49)$$

$$1 - \frac{s^3}{B^+} y^+ = \frac{2 \left(\frac{du^+}{dy^+} \right)^4}{(d^2 u^+ / dy^{+2})^2} \quad (y^+ \geq 20) \quad (50)$$

These two equations were integrated on a computer for a wide range of $\frac{s^3}{B^+}$, and the results were plotted as a universal velocity profile on a graph of u^+ vs. y^+ , $\frac{s^3}{B^+}$ being a parameter.

The flowrate equation
$$(Re) = 4 \int_0^{B^+} u^+ dy^+ \quad (23)$$

was integrated on a computer using the above velocity profile. The

* This could have been done quite easily without a computer.

results are given as B^+ vs. (Re) , the interfacial shear number being a parameter. For $\beta > 30$, B^+ is a function of (Re) only.

$$\text{The film thickness equation } B = s(B^+)^{2/3} \left(\frac{\nu^2}{g} \right)^{1/3} \quad (51)$$

obtained from equ. (41) was similarly computed, and plotted as B vs. (Re) , with β as parameter. For $\beta = 0$, B merges with the Nusselt equation for $(Re) < 200$. At a (Re) of 1,600, Nusselt's film thickness is only about 10% below that of Dukler. -

Anderson and Mantzouranis⁽¹⁾ in 1960 presented a mathematical analysis based on the Nikuradze velocity profile. It is identical to the work of Dukler and Bergelin except that the authors considered a finite radius of curvature of the wall, i.e., a small-bore tube instead of a flat plate. They also considered the effect of gas velocity.

It can be seen from their resulting curves that the tube bore would have to be very small for the curvature to have any noticeable effect on the film thickness; certainly much smaller than the tube sizes used in our work.

Their experimental data were obtained with water flowing down a 0.427-in. I. D. glass tube and a moving air core, and scattered widely. The authors attempted to explain this scatter by entrainment, or by the formation of a "double profile", i.e., laminar flow at the interface as well as at the tube wall, with the two developing velocity profiles meeting at mid-film. - They found no influence of the ripples on the film thickness. They found that the surface tension affected the ripple regime but not the mean film thickness.

C) LITERATURE RESEARCH: HEAT TRANSFER (NON-BOILING)

The main interest in the study of the whole field of falling-film flow has been its application to falling-film condensers and coolers. Nusselt(37), (38) extended his fluid mechanics to the solution of the heat transfer problem. For his analysis he postulated pure saturated vapor, streamline flow, no interfacial shear, a flat condensing surface, and constant physical properties.

$$h = \frac{k}{B} \quad (52)$$

From Nusselt's film thickness expression, equ. (14),

$$h = \left(\frac{k^3 \rho^2 g}{\mu^2} \right)^{1/3} \left(\frac{3}{4} \text{Re} \right)^{-1/3} \quad (53)$$

Defining
$$\phi \equiv \left(\frac{k^3 \rho^2 g}{\mu^2} \right)^{1/3} \quad , \quad (54)$$

then
$$\frac{h}{\phi} = \left(\frac{3}{4} \text{Re} \right)^{-1/3} \quad (55)$$

The heat transfer coefficient decreases with the one-third power of the flowrate. - Nusselt also solved the Graetz problem for a laminar film:

$$\frac{hL}{\Gamma_{c_p}} = \frac{4.46 \psi^{0.565}}{2 - 2.235 \psi^{0.565}} \quad (\psi \leq 0.05) \quad (56)$$

$$\frac{hL}{\Gamma_{c_p}} = 0.0942 + 5.65 \psi \quad (\psi > 0.05) \quad (57)$$

where
$$\psi \equiv \left(\frac{3}{4} \text{Re} \right)^{-4/3} \left(\frac{g}{\nu^2} \right)^{1/3} (\text{Pr})^{-1} L \quad (58)$$

Equ. (38) and (39) can be approximated by the expression:

$$\frac{h_L}{c_p} = 2.62 \psi^{2/3} \quad (59)$$

Nusselt applied his analysis to the study of falling-film condensers. He found that for a constant steam-to-tube temperature difference Δt ,

$$h_m = \frac{4}{3} h_L = 1.47 (\text{Re}_L)^{-1/3} \quad (60)$$

where

$$h_m \equiv \frac{1}{L} \int_0^L h dL \quad (61)$$

and h_L is the heat transfer coefficient at the bottom end of the condensing surface, i.e., at length L . - It we define a Nusselt

number:

$$(\text{Nu}) \equiv \frac{hB}{k} \quad (62)$$

then according to Nusselt's theory:

$$(\text{Nu}) = 1 \quad (\text{Pure conduction}) \quad (63)$$

and

$$(\text{Nu})_m \equiv \frac{h_m B_L}{k} = \frac{4}{3} \quad (64)$$

Most industrial condensate films become so thick as they flow down the condensing surface that they reach turbulence. Values of h_m are, therefore, generally higher than according to Nusselt's correlation, and increase rather than decrease with flowrate.* Falling-film condensation research since Nusselt has been oriented chiefly towards quantitative

* Dropwise condensation will not be considered at this point.

expressions that take turbulence into account. - Kirkbride⁽³³⁾ and Badger^{(2), (3)} proposed an empirical correlation above a $(Re)_L$ of 1,800, expressing h_m/ϕ as function of $(Re)_L$. - Colburn⁽¹⁵⁾ suggested a semi-empirical relation based on the j-factor analogy, for $(Re)_L$ above 2,100; he expressed h_m/ϕ as a function of (Pr) as well as of $(Re)_L$. - Grigull⁽²⁸⁾ used the Prandtl analogy and the one-seventh-power law to derive an expression which was not explicit in h_m and could only be represented graphically, using $(Re)_L$ and (Pr) ; the trends were similar to those of Colburn's correlation. Grigull decided on a critical Reynolds number by taking that which would best correlate all experimental heat transfer coefficient determinations. In a later paper⁽²⁹⁾ in 1952 he presented an empirical correlation of h_m/ϕ as function of $(Re)_L$ only, for $(Re)_L > 1,600$. - Seban⁽⁴²⁾ in 1954 applied the Prandtl analogy and the Nikuradze velocity profile for $(Re)_L > 1,600$, and obtained h_m/ϕ as a complicated function of $(Re)_L$ and (Pr) . - Rohsenow, Webber and Ling⁽⁴⁰⁾ in 1956 extended this treatment to condensation with high vapor velocities, and concluded that the critical Reynolds number decreased with increasing values of τ_i to a lower limit of 70.

This list of research studies on condensation heat transfer is by no means complete, but serves to illustrate the trends in condensation research. Most of the correlations depend on some critical Reynolds number that varies from author to author; above this $(Re)_{crit}$ the authors postulate laws of momentum and heat transfer that do not necessarily apply to film flow. They also ignore departures from Nusselt's correlation in the subcritical range; even for zero vapor velocity and

no dropwise condensation, coefficients are usually reported between 12 and 35% higher than predicted by Nusselt's equ. (55) or (60). For design purposes, McAdams⁽³⁴⁾ recommends a value for the subcritical region 28% high than theoretical* and for turbulent flow the relation of Kirkbridge - Badger or that of Colburn.

There have been several falling-film sensible-heat transfer studies since Nusselt. Bays and McAdams⁽⁵⁾ used three steam-jacketed copper tubes to determine local heat transfer coefficients for two mineral oils in laminar flow down the inside wall. Temperature differences were obtained with wall thermocouples or by using dropwise condensation. Nusselt's equ. (59) was found to be valid when modified by a Sieder-Tate-type viscosity ratio; Nusselt's postulate of constant physical properties was too unrealistic with regard to oil viscosity in these runs. As in equ. (59), h was found to be proportional to $\mu^{1/9}$.

Turbulent flow was investigated by Sexauer⁽⁴³⁾. Water at room temperature flowed down the outside of vertical tubes that were heated from the inside by upflowing warm water. Flowrates were determined by weighing; film temperatures were measured with a thermometer, local wall temperatures with thermocouples. Temperature drops across the film were of the order of 1 - 2 °F. The results were correlated by the equation:

$$\frac{h_m L}{k} = a(\text{Re})^{0.5}(\text{Pr})^{0.15} \frac{L}{L_0}^{0.935} \quad (65)$$

* For the same $(\text{Re})_L$.

Here, L_0 is a reference length, a a numerical factor. - This equation correlated results for all diameters and lengths, but the factor a varied according to tube material; for steel tubes it had 72.5% of the value for brass tubes. Tube length is shown to be immaterial in turbulent flow.

McAdams, Drew and Bays⁽³⁵⁾ used the same equipment as Bays and McAdams to investigate water films in turbulent flow. For a mean water temperature of 190° F they correlated their data by the equation:

$$h_m = 120 \Gamma^{1/3} \quad (66)$$

with h_m in Btu/(hr)(sq ft)(°F), Γ in lb/(hr)(ft). - Drew⁽²¹⁾ tentatively suggested a more general correlation in dimensionless form:

$$\frac{h_m}{\phi} = 0.01 (\text{Re})^{1/3} (\text{Pr})^{1/3} \quad (67)$$

which at ca. 190°F would reduce to equ. (66). - This is the equation generally recommended by handbooks for the design of falling-film heaters at $(\text{Re}) > 1,800$.

Garwin and Kelly⁽²⁷⁾ in 1955 measured the heat transfer coefficient across turbulent water films flowing over an inclined brass plate. A steam chest was flanged to the underside of the plate. Wall temperatures were measured to within ca. 0.5°F with thermocouples. The mean film temperature was ca. 93°F. The results were correlated by the equation:

$$h_m = 87 \Gamma^{1/3} \sin^{0.2} \theta \quad (68)$$

with h_m in Btu/(hr)(sq ft)(°F), Γ in lb/(hr)(ft). For the vertical plate, of course, $\sin \theta$ reduces to one, and the resulting equation is similar to that of McAdams, Drew and Bays, equ. (66). - Equ. (67) for water at 93°F has a numerical coefficient of 65, instead of 87 as found by Garwin and Kelly.

Brauer⁽⁷⁾, 1957, ⁽⁸⁾, 1958, extended his results on falling-film momentum transfer to heat transfer by means of a theoretical study. In his mathematical model the entire resistance to heat transfer is concentrated into an equivalent thermal sublayer of thickness ϵ , in pure streamline motion. For smooth Nusselt-type film flow, $\epsilon = B$; in the presence of ripples and waves, ϵ is smaller than the trough film thickness. Let u' be the (unknown) velocity at $y = \epsilon$. Then:

$$\tau_w g_c = \mu \frac{u'}{\epsilon} \quad (69)$$

$$h = \frac{k}{\epsilon} = \frac{kg_c}{\mu} \frac{\tau_w}{u'} \quad (70)$$

$$(Nu) = \frac{hB}{k} = \frac{g_c}{\mu} \frac{\tau_w B}{u'} \quad (71)$$

Since both τ_w and B were expressed as functions of (Re) in his previous work on fluid mechanics, he was able to express h and (Nu) as functions of (Re) ; see Table IV. - Brauer postulated u' as solely dependent on physical properties, and defined a dimensionless viscosity number K_v :

$$K_v \equiv \frac{g \nu}{(u')^3} \quad (72)$$

K_V (or u') could be calculated from any one actual heat transfer measurement. - Brauer considered K_V rather than (Pr) as indicating the effect of viscosity on falling-film heat transfer.

TABLE IV

(Re)	$\tau_w g_c$	h/ϕ	(Nu)
c-crit	$2.73(g^2 \nu^2 \rho^3)(Re)^{1/5}$	$2.73K_V^{1/3}(Re)^{1/5}$	$1.64K_V^{1/3}(Re)^{8/15}$
crit	$2.73(g^2 \nu^2 \rho^3)(Re)_{crit}^{-1/5}(Re)^{2/5}$	$2.73K_V^{1/3}(Re)_{crit}^{-1/5}(Re)^{2/5}$	$1.64K_V^{1/3}(Re)_{crit}^{-2/5}(Re)^{14/15}$

Based on his heat transfer theory, Brauer developed equations for the critical tube length that would divide the tube into a laminar section and a turbulent section, and for overall heat transfer coefficients of condensate films extending into the turbulent section. He found his correlation satisfactory for the results of Badger⁽²⁾ with diphenyl, of Badger⁽³⁾ with diphenyl - diphenyl oxide, and of Baker, Kazmark and Stroebe⁽⁴⁾ with steam. He used whatever value of u' gave the best correlation; for steam at atmospheric pressure, $u' = 2.5$ ft/sec. - Brauer also compared his correlation with those of Kirkbride, Colburn for $(Pr) = 5$, Grigull, Seban, and Rohsenow, Webber and Ling. He showed that above a (Re) of 3,000 they all fell within a $\pm 15\%$

scatter band.*

Dukler⁽²³⁾ in 1960 extended his study of falling-film fluid flow to the heat transfer problem. As in fluid flow, he considered eddy transfer in superposition on molecular transfer at all points in the film. The basic heat transfer equation is, therefore:

$$q = -(k + \rho c_p E_H) \frac{dt}{dy} \quad (73)$$

Supposing physical properties and heat flux to be radially constant, and defining a dimensionless temperature as:

$$t^+ = \left(\frac{\rho c_p}{q} \right)_{wall} u^+ (t_w - t) \quad , \quad (74)$$

the basic heat transfer equation in dimensionless form is:

$$1 = \left[\frac{1}{(Pr)} + \frac{E_H}{\nu} \right] \frac{dt^+}{dy^+} \quad (75)$$

* Though of no direct bearing on our subject matter, it may be of interest to point out that Brauer⁽⁹⁾ in 1958 also extended his theory to mass transfer in falling liquid films. Replacing thermal conductivity with diffusivity, and the heat transfer coefficient with the liquid-film mass transfer coefficient, he obtained mass transfer Nusselt numbers as functions of (Re) and K_V analogous to his heat transfer work. He successfully correlated the results of Kamei and Oishi⁽³²⁾ on absorption of carbon dioxide in water, and previous work on absorption and desorption of carbon dioxide. For all these results he used u' equal to 0.22 ft/sec. He used the same value of u' to correlate mass transfer test results on soluble-wall columns. Brauer explained the fact that u' had a lower value for mass transfer than for heat transfer by ascribing the physical transfer mechanism to radial motions of particles from interface into the bulk due to wave action; this should have more effect on mass transfer than on heat and momentum transfer, since the latter two rely on molecular collision in addition to bulk movement. - Since the liquid Schmidt number was not used at all, Brauer's theory established proportionality between the liquid-film mass transfer coefficient and the liquid diffusivity.

From the definition of t^+ , equ. (74), the definition of B^+ , equ. (22), and the definition of β , equ. (41), it also follows that:

$$\frac{h}{\phi} = \frac{(\text{Pr})(B^+)^{1/3}}{st^+} \quad (76)$$

As in his fluid flow study, Dukler integrated the rate equation for $0 < y^+ < 20$ with the Deissler correlation, and for $y^+ \geq 20$ with the von Kármán correlation and the assumption that $E_H = E_M$:

$$1 = \left[\frac{1}{(\text{Pr})} + n^2 u^+ y^+ (1 - e^{-n^2 u^+ y^+}) \right] \frac{dt^+}{dy^+} \quad (0 < y^+ < 20) \quad (77)$$

$$\frac{1}{1 - \frac{s}{B^+} y^+} = \frac{dt^+}{du^+} \quad (y^+ \geq 20) \quad (78)$$

The integration was carried out on a digital computer, using the velocity profile obtained in the fluid flow study. For each value of t^+ so obtained, the value of h/ϕ was calculated by means of equ. (76). The results were plotted as curves of h/ϕ vs. (Re) , β and (Pr) being two independent parameters.

For condensers, similar curves were obtained for h_m/ϕ vs. $(\text{Re})_L$, β and (Pr) being parameters. They were arrived at by integrating the local heat transfer coefficients along the entire tube:

$$\frac{h_m}{\phi} = \frac{(\text{Re})_L}{\int_0^L \frac{d(\text{Re})}{h/\phi}} \quad (79)$$

Dukler tested his theoretical development against experimental results. For zero interfacial shear, the heat transfer coefficients merge with Nusselt's straight line at a (Re) of ca. 50. For steam condensing at $(Re)_L$ between 150 and 1,000, we have found the Dukler correlation to fall within $\pm 7\%$ of McAdams' recommended use of 1.28 times h_m from Nusselt's equ. (60)

An extreme test for Dukler's work is the correlation of the results obtained by Misra and Bonilla⁽³⁶⁾ in 1956 on the condensation heat transfer coefficients of mercury and sodium vapors. These authors' values of h_m were only 5 - 15% of the values predicted from the Nusselt theory; Reynolds numbers ranged up to 1,500.* Dukler found his theory to correlate these results in a satisfactory manner; all previous attempts of other authors had failed.

For film flow under turbulent conditions, we have found Dukler's correlation to fall within $\pm 6\%$ of that of Bays, equ. (66), and within $\pm 5\%$ of that of Garwin and Kelly, equ. (68), for the range ^{**} of Reynolds and Prandtl numbers employed by these authors. It also falls close to the correlations of Kirkbride - Badger and of Colburn at high flow rates.

In the case of significant interfacial shear stress, Dukler's correlation also proved satisfactory. Such tests were reported by Carpenter⁽¹¹⁾, who condensed water, methanol, ethanol, trichloroethylene

* Incidentally, ripples formed in the mercury at $(Re) \approx 66$.

**Despite the fact that these authors used the liquid bulk temperature, not the interface temperature as does Dukler.

and toluene inside vertical tubes at very high vapor velocities. His results had been correlated by Carpenter and Colburn⁽¹²⁾ and Colburn⁽¹⁶⁾ who used a semi-empirical expression derived in part from Nikuradze's velocity profile. Dukler satisfactorily correlated Carpenter's test results by calculating β via τ_i and using the appropriate β parameter in his curves; τ_i was calculated from the Martinelli-Lockhart correlation.

SECTION III

LITERATURE RESEARCH ON NUCLEATE BOILING FUNDAMENTALS

RATE OF HEAT TRANSFER IN NUCLEATE BOILING

McAdams, Addoms et al.⁽³⁰⁾ used improved measurement techniques to repeat work by early investigators on the boiling of saturated water on submerged platinum wires. Pressures up to 1,200 psig were used, causing wire superheats from 2 to 2,500°F. For superheats up to 10°F, the heat transfer rates were roughly those predicted from convective heat transfer correlations. From 17°F upwards, i.e., above the "knee" of the curve in Figure 4, the heat flux rose very steeply with increased superheat until a maximum ("burn-out point") was reached at a superheat of 420 F; film-boiling set in at higher superheats. Heat transfer coefficients are thus seen to be much higher in nucleate boiling than in non-boiling convective heat transfer.

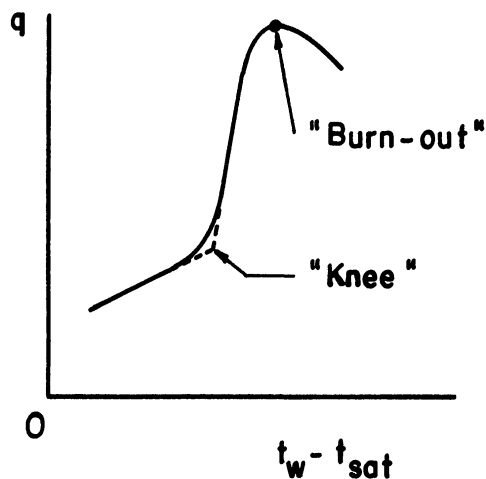


Figure 4

McAdams, Kennel et al.⁽³¹⁾ observed the upward flow of degassed distilled water through an annulus, the inner surface being a cylindrical heating element composed of a copper and a stainless steel section. Heat transfer measurements were made for wide ranges of subcooling, water flowrates and equivalent diameters. For $t_w < t_{sat}$ no boiling occurred, and the heat transfer rate were predictable from the Sieder-Tate correlation. For $t_w \geq t_{sat}$ the same applied up to a transition

wall temperature t_{tr} . At this transition point, corresponding to the knee in Figure 4, vapor first appeared and surface boiling commenced. Below the knee, the driving potential was $t_w - t_1$; above, it was $t_w - t_{sat}$, i.e., wall superheat Δt_{sat} , and t_1 was no longer a significant variable. For $t_w \geq t_{tr}$ all their points followed the correlation:

$$q = C (\Delta t_{sat})^{3.86} \quad (1)$$

The constant C was higher for tap water than for de-aerated water.*

Kreith and Summerfield performed similar tests for a wider range of variables, with water⁽²⁶⁾ and with aniline and n-butanol⁽²⁷⁾. Similar results as those of McAdams, Kennel et al. were obtained.

One of the practical interests of this field is the possibility of accurately predicting boiling heat transfer rates at high heat flux and high pressure in order to design smaller and more compact boilers. Rohsenow and Clark⁽⁴⁰⁾ performed tests up to pressures of 2,000 psia. They found results similar in form to those at lower pressures. The significant parameters in nucleate boiling were found to be, first, pressure (i.e. t_{sat}), and in second place velocity, which ceases to be significant at high heat fluxes.

For the nucleate boiling range, the heat transfer curve has generally been found to follow a correlation similar in form to equ. (1). The exponent of Δt_{sat} is mostly reported to be between 3 and 4⁽²⁵⁾,⁽²⁸⁾,⁽³²⁾,⁽³⁸⁾. The uncertainty lies in C , i.e., the location of

* Extrapolating these results to zero subcooling ($t_1 = t_{sat}$) would place the transition point at a wall superheat of 22° F.

the transition point.

Bernath and Begell⁽⁷⁾ have made a thorough study on the effect of velocity and subcooling. They plotted the results of hundreds of tests for de-ionized water flowing up a heated annulus, as wall superheat Δt_{sat} vs. degree of subcooling $\Delta t_{\text{sub}} \equiv t_{\text{sat}} - t_1$ (see Figure 5).

It was shown that the degree of subcooling had no effect on the rate of heat transfer unless a critical degree of subcooling Δt_{sub}^0 was exceeded; for $\Delta t_{\text{sub}} \geq \Delta t_{\text{sub}}^0$, the curve in Figure 5 was a straight line of slope m.

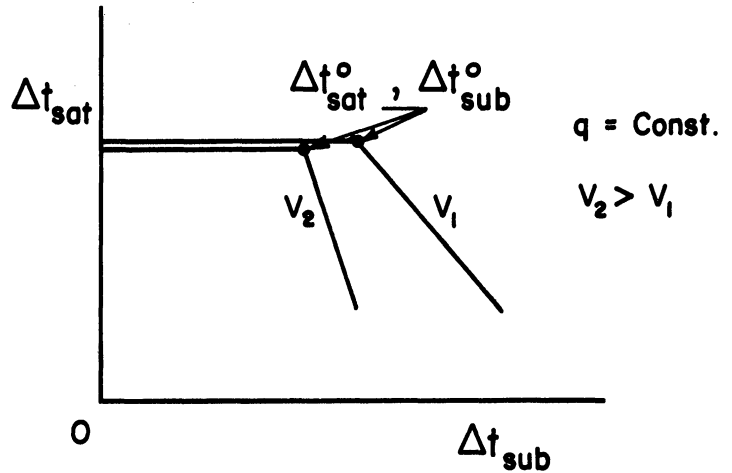


Figure 5

The following are the empirical correlations:

$$\Delta t_{\text{sat}}^0 = 54.0 - \frac{V}{1.81} + \frac{q - 3.24 \times 10^5}{4.1 \times 10^4 (D_e)^{0.43}} \quad (2)$$

$$\Delta t_{\text{sub}}^0 = 1.2(30.0 - V) \left(\frac{q}{3.24 \times 10^5} \right)^{1.8} \quad (3)$$

and for $\Delta t_{\text{sub}} > \Delta t_{\text{sub}}^0$, $m = \frac{7.5}{V} + 2.54 \times 10^{-7} q - 1.297$ * (4)

with temperatures in °F, velocity V in ft/sec, heat flux q in

* Note interaction of velocity and subcooling for $\Delta t_{\text{sub}} > \Delta t_{\text{sub}}^0$; also, minimum value of V.

Btu/(hr)(sq ft)(°F), equivalent diameter D_e in in. - These results were obtained on an aluminum surface at pressures between 25 and 125 psia. According to Averin⁽²⁾, Δt_{sat} for aluminum is $6.0 \pm 0.5^\circ C$ higher than that for copper, nickel, or stainless steel. If this correction is applied to the data of McAdams, Kennel et al., their data as well as the data of Bernath and Begell are reported to follow the above correlation within $4^\circ F$.

The role of additives on boiling heat transfer rates has not been correlated or completely explained. Lowery and Westwater⁽²⁹⁾ suggested that the determining variable might be a change in interfacial tension between the liquid and some solid nucleus, as well as in liquid-metal and liquid-air interfacial tension; the later two also have direct bearing on the wettability of the heating surface and the bubble contact angle. It is known that surface-tension depressants raise the boiling heat transfer rate of water⁽³³⁾.

The literature contains various correlations for the burn-out point. Rohsenow and Griffith⁽⁴¹⁾ presented a theoretical correlation based on calculating the heat flux at which the bubbles would come so close to each other laterally as to touch, thus coalescing and producing film boiling.

BUBBLE FORMATION

Let p be the pressure of a small spherical gas bubble of principal radii r_1 and r_2 . Let the bubble be completely surrounded by a liquid phase at pressure p_1 . If bubble and liquid are the same temperature, then⁽¹⁷⁾:

$$p - p_1 = \sigma \left(\frac{1}{r_1} + \frac{1}{r_2} \right) \quad \text{(Gibbs equation)} \quad (5)$$

If the gas is the pure vapor of the liquid, the liquid is, therefore, superheated; the superheat is easily calculated from equ. (5) by means of the Clapeyron equation.

It we knew σ to be constant down to molecular dimensions, p for a bubble consisting of one molecule of water would be 7,500 atm, according to equ. (1). In order to form a bubble "de novo" inside a mass of liquid would require that a number of molecules must simultaneously obtain sufficient kinetic energy to overcome the forces of attraction between them. It has been calculated that the probability of this occurring is virtually nil except in the region of the critical points.

To prove this experimentally, de-gassed and purified water has been heated to 520° F without boiling; such water has also been saturated with gases at 100 atm and de-pressurized to atmospheric pressure without effervescence.

Bubble formation cannot occur without the presence of available gas

* Developed previously by Laplace, based on force balance; Gibbs is credited with its development based on thermodynamic energy considerations.

particles, contaminants, mechanical shock, etc. Bubble formation is not promoted by edges or points unless these contain absorbed gas on the surface or trapped gas in capillary spaces⁽¹¹⁾.

Equ. (5), then, does not necessarily apply to commercial boiling systems, where the superheat needed to initiate boiling may be far less than calculated due to the nucleating influence of gas absorbed or occluded by foreign particles or by the heating surface itself. Besides, Gibbs' equation is based on a simplified model in which there is a unique surface between phases. In reality there seems to exist a transition layer several molecules thick between phases. For diameters smaller than, say, 20 molecules (ca. 80 \AA) the theory cannot be applied⁽²⁰⁾. Also, Gibbs' theory assumes static equilibrium and therefore a reversible process of formation; the apparently instantaneous nature of bubble formation would appear to invalidate this assumption.

Experimental evidence, however, indicates that the inaccuracies involved in Gibbs' simplified model are tolerable small. Jakob and Fritz⁽²⁴⁾ boiled water at atmospheric pressure on a copper surface having cubical cavities of 0.25 mm per side. The measured superheat, 1° C , corresponds to a Gibbs-equation bubble of 0.07 mm diameter, ca. $1/3$ of what could be expected from the cavities. - Bankoff^{(3), (4)} discussed cavities and grooves in metal heating surfaces. He calculated the maximum width of a cavity into which the meniscus of a given liquid can advance at given values of temperature, pressure, surface tension and contact angle; he performed a similar calculation for the maximum radius of a semi-circular groove. He reviewed the data of Rinaldo⁽³⁷⁾,

Addoms⁽¹⁾, and Vos and van Stralen⁽⁴²⁾, who had measured the minimum superheat in saturated pool boiling of water at pressures from 14.7 to 1,985 psia. For each experimental determination he calculated the critical cavity or groove dimension; these fell amazingly close to the Gibbs-equation bubble diameters. - Griffith and Wallis⁽¹⁹⁾ used gramophone needles to punch cavities of known radius in the surface of their metal heating surface; the measured superheat corresponded to Gibbs-equation bubble radii that fell very close to those of the needles.

Corty and Foust⁽¹⁰⁾ made a detailed experimental study of the size and shape distributions of the microroughnesses in their heating surface, and correlated them qualitatively with the nucleation site density and the wall superheat for several liquids. - Clark, Strenge and Westwater⁽⁸⁾ took photomicrographs and electron micrographs of nucleation sites on a single zinc crystal, on polycrystalline zinc, and on aluminum alloy 2024, using ether and n-pentane and applying extreme precautions against contamination. They found that grain boundaries had little or no effect on boiling nucleation and that nucleation sites were not regions of special atomic density in the metal (effect of anisotropy). Of the 20 sites studied, 13 were pits of 0.3 to 3 mils width, 4 were scratches of 0.1 to 0.8 mils width. The measured superheats in all cases corresponded to Gibbs-equation bubble sizes larger than the widths of the nucleation sites. - Averin⁽²⁾ found no effect of surface roughness on boiling heat transfer at all, near the burn-out point.

McAdams, Kennel et al.⁽³¹⁾, and later Pike, Miller and Beatty⁽³⁴⁾, investigated the influence of the presence of gas on nucleation.

De-aerated tap water initiated boiling at a much higher superheat (70° F) than tap water (20° F) or water saturated with carbon dioxide, in pool boiling on a wire. Wire gage or wire position relative to the liquid surface had no influence on superheat. - Bankoff, Hajjar and McGlothin⁽⁵⁾ measured superheats in the pool boiling of 7 organic liquids that had been allowed to stand exposed to the air, in order to prove that nucleation occurs on the wire and not in the liquid phase. The wire was annealed in air. They noted that with time the superheat increased, probably due to the desorption of air from the wire due to boiling. Also, the bulk of the nuclei were observed on the wire, not on the dust particles within the liquid phase.

BUBBLE GROWTH

The expansion rate of bubbles is of interest because of the agitation effect on the liquid and the resulting acceleration of the rate of heat transfer. Plesset⁽³⁵⁾ combined the Gibbs equation with the Rayleigh equation and derived a differential equation in which figure the first and second derivatives of the bubble radius with time. (The Rayleigh equation is a more general fluid flow equation and applies to any bubble pressure, irrespective of its relationship to the radius via the surface tension.) The mathematical model on which it is based assumes a spherically symmetrical pressure field, a liquid of infinite extent, inviscid flow, and a spherical bubble. Foster and Zuber⁽¹⁵⁾ combined Plesset's equation with the Clapeyron equation and solved for the expansion rate in terms of the superheat, after considerable simplifying assumptions. A similar mathematical analysis by Plesset and Zwick⁽³⁶⁾ yielded a much simpler expression for the bubble radius as function of time. Its validity was experimentally proved by Faneuff, McLean and Scherrer⁽¹⁴⁾, who sent periodic current pulses of very short duration (1 μ sec) through a nichrome wire submerged in 180° F water; a stroboscopic light source actuated by the same timer allowed bubble growth to be photographed with a high-speed camera.

Griffith⁽¹⁸⁾ reasoned that the principal stirring action occurred during the visible life of the bubble, and that during this time the growth rate was essentially dependent on the heat transfer in the liquid to the bubble wall. Assuming laminar flow and constant physical properties,

he solved the heat diffusion equation for the velocity, and obtained an expression that successfully correlated the experimental results of Dergarabedian⁽¹²⁾ for the expansion rate of bubbles in boiling water (ca. 0.22 ft/sec).

BUBBLE BEHAVIOR

Fritz⁽¹⁶⁾ has shown that the maximum diameter of a steam bubble is:

$$D = C_b \beta' \sqrt{\frac{2g_c \sigma}{g(\rho_l - \rho_g)}} \quad (6)$$

where β' is the contact angle, C_b an empirical constant. Jakob⁽²³⁾ showed furthermore that the bubble diameter was inversely proportional to the number of bubbles per hour, for the same heat flux; that the number of bubbles per square foot of heating surface at any moment was directly proportional to the heat flux; and that the velocity of bubble detachment was equal to the product of bubble diameter and number of bubbles per hour.

Gunther and Kreith⁽²²⁾ and Gunther⁽²¹⁾ made detailed photographic measurements of bubble behavior while heating a flow of subcooled water with a submerged electrically heated metal strip. For low velocity and subcooling, bubbles were observed to have a period of steep initial growth, followed by a rather long period of slow growth and a period of slow decay. As velocity and subcooling increased, the growth and collapse curves tended to steepen and to become mirror images of each other; both bubble size and bubble life span decreased, and changes in heat flux only caused a change in the bubble population. - While attached to the wall, the bubbles were roughly hemispherical in shape; with less subcooling they began to detach themselves, since the quenching boundary had moved further away from the wall.

SUGGESTED HEAT TRANSFER MECHANISMS IN NUCLEATE BOILING

The following are some mechanisms that have been suggested:

- 1) Bubble activity excites microconvection in the normally laminar sublayer. According to this theory, though, heat flux should depend on subcooling, which it does not. Also, the translational motion of bubbles is of the order of 10 ft/sec; it does not seem logical that it should cause higher heat transfer rates than convection, which may well reach linear velocities of 20 - 30 ft/sec. Another reason against this theory is the fact that bubbles only occupy 25% of the heating surface⁽¹³⁾.
- 2) Bubbles act as surface roughness. However, in that case the heat flux should again depend on subcooling, and also on the "relative roughness" (ratio of bubble size to tube size); neither of the two apply.⁽¹³⁾
- 3) Latent heat transport: the bubble absorbs latent heat, which it transfers to the liquid upon collapsing. - Rohsenow and Clark⁽³⁹⁾ analyzed this possibility by making a rigorous thermodynamic calculation of the amount of heat thus transported by a bubble of given size, specific volume, and specific heat of vaporization. The heat per bubble was multiplied by the bubble density and bubble frequency from the high-speed motion pictures of McAdams, Kennel et al. It was found that, of the increase in heat transfer over convection due to boiling, at most 2% could be due to the bubbles acting as "carriers". - A similar conclusion can be drawn from the photographic analysis of Gunther and Kreith⁽²²⁾.

4) Bubble pumping action: the bubble leaves an empty space upon collapsing or detaching itself, which is filled up by cold liquid. This mechanical pumping action is far more effective than convective heat transfer, which is based on diffusion by eddies. - Yamagata, Hirano et al.⁽⁴³⁾ reported direct proportionality between the heat transfer Nusselt number and the cube root of the number of vapor columns formed in water boiling over a horizontal heating surface. - Rohsenow⁽³⁸⁾ calculated the bubble Reynolds number, which should characterize this agitation, and correlated the bubble Nusselt number as function of (Re) and (Pr); the final Rohsenow correlation is:

$$\frac{c_l \Delta t_{sat}}{\Delta H_{vap}} = C_{sf} \left(\frac{q}{\mu \Delta H_{vap}} \sqrt{\frac{g_c \sigma}{g(\rho_l - \rho_g)}} \right) (Pr)_l^{1.7} \quad (7)$$

Here, q is the heat flux in excess of the convective heat flux, C_{sf} an empirical constant. Rohsenow found his correlation to be satisfactory for the experimental pool boiling results of previous investigators. - Clark and Rohsenow⁽⁹⁾, investigating boiling heat transfer to water at high pressures, also found the Rohsenow correlation to hold. - Other correlations based on heat transfer from heating surface to liquid with stimulation due to bubble agitation have been suggested by Bankoff and Mikesell⁽⁶⁾, Engelberg-Foster and Greif⁽¹³⁾, and others.

5) Film model, suggested by Bernath and Begell⁽⁷⁾ and others; the film is defined as having the thickness which is the distance from the heating surface to the point where the average temperature of the mixed phases is the saturation temperature of the liquid: i.e., the region where

there is superheat. Bernath and Begell postulate that wall superheat is proportional to film thickness. Film thickness is a function of heat flux, subcooling, and free-stream turbulence. Qualitatively, the effect of heat flux is described as tending to increase film thickness (and hence superheat) because of greater bubble population; the effect of subcooling and/or convection, as tending to decrease film thickness because of the bubble-quenching zone moving closer to the wall; the effect of velocity is described as causing increased wall shear stress, hence a thinner film. The interaction of velocity and subcooling, as per equ. (4), is explained by the negligible quenching effect of subcooling on the thickness of a thick film (low velocity) as compared to the considerable effect of the same degree of subcooling on a thin film (high velocity). Photographic evidence for this concept was taken from the work of authors such as Gunther and Kreith⁽²²⁾, and Gunther⁽²¹⁾.

SECTION IV

LITERATURE RESEARCH ON GAS-LIQUID FLOW

The practical interest in this field is mainly to be able to predict pressure drop with reasonable accuracy; preferably in the case of passage of mass from one phase to the other, as in evaporation or condensation. Due to the extreme complexity of the process, however, there is no unified general theoretical treatment. Experiment is still far ahead of theory, but as yet there is no general empirical correlation either.

Boelter and Kepner⁽⁵⁾, Martinelli, Boelter et al.⁽²¹⁾, Martinelli, Putnam and Lockhart⁽²³⁾, Lockhart and Martinelli⁽¹⁹⁾, and Martinelli and Nelson⁽²²⁾ proposed a simplified model. Designed for isothermal air-liquid flow through horizontal pipes, its basic assumptions are that pressure drop is only frictional, that gas pressure drop is equal to liquid pressure drop (i.e., no radial pressure gradients), and that the two phases are in thermodynamic equilibrium and fill the pipe completely. For the purposes of the Martinelli model, a phase is arbitrarily considered in laminar or turbulent motion, irrespective of its actual flow behavior, according to whether its superficial* Reynolds number is below 1,000 or above 2,000 respectively. Using these superficial Reynolds numbers, friction factors are calculated for each phase: $\frac{16}{(Re)}$ if "laminar", $\frac{0.046}{(Re)^{0.2}}$ if "turbulent". From the friction factors, superficial* pressure drops are calculated separately for gas and liquid, and are denominated $\left(\frac{\Delta p}{\Delta L}\right)_g$ and $\left(\frac{\Delta p}{\Delta L}\right)_l$, respectively. It can then be shown that the actual two-phase pressure drop $\left(\frac{\Delta p}{\Delta L}\right)_{TP}$ is a unique

* Superficial in the sense that for the purpose of this calculation the phase in question is fictitiously assumed to fill the whole cross-sectional flow area in single-phase flow.

function of either one of the two superficial pressure drops and of the (unknown) actual hydraulic radii and cross-sectional surface forms of the two phases. By defining:

$$\bar{\Phi}_1 \equiv \sqrt{\frac{(\Delta p / \Delta L)_{TP}}{(\Delta p / \Delta L)_1}} \quad (1)$$

$$\bar{\Phi}_g \equiv \sqrt{\frac{(\Delta p / \Delta L)_{TP}}{(\Delta p / \Delta L)_g}} \quad (2)$$

$$X \equiv \sqrt{\frac{(\Delta p / \Delta L)_1}{(\Delta p / \Delta L)_g}} \quad (3)$$

the above can be stated more conveniently by saying that $\bar{\Phi}_1$ and $\bar{\Phi}_g$ are unique functions of X . - Calling the liquid and the gas volumetric holdups R_1 and R_g , respectively, it can also be shown that R_1 and R_g should be unique functions of X . - Since the actual hydraulic radii and the cross-sectional surface forms of the two phases are unknown, the functions must be experimentally determined. This was done by the investigators for the horizontal flow of air-water mixtures.

Due to the many simplifying assumptions contained in the Martinelli model, it correlates two-phase pressure-drop data within a scatter of ca. $\pm 50\%$. Despite its drawbacks, it is much used because of its ease of manipulation. It has even been applied, with empirical modifications, to cases that directly contradict its initial assumptions, as in upward or downward flow with and without vaporization, where frictional pressure drop is far from being the total pressure drop, and in stratified or plug flow, where radial pressure gradients cannot be neglected. Analytical

modifications of the Martinelli model were proposed by Levy⁽¹⁶⁾ and Gazley⁽¹³⁾; neither correlation improves the predictions of pressure drop and liquid holdup. Far more numerous are the empirical modifications of the Martinelli model: Johnson and Abou-Sabe⁽¹⁵⁾ for horizontal non-isothermal air-water flow; Lieberson⁽¹⁷⁾ for isothermal vertical upflow; Van Wingen⁽³¹⁾, Chenoweth and Martin⁽⁹⁾ and Baker⁽¹⁾ for gas-oil flow in large-diameter pipe lines; Stein, Hoopes et al.⁽²⁸⁾ for downflow through concentric internally-heated annuli; Martinelli and Nelson⁽²²⁾ for horizontal forced-circulation evaporator tubes; Dengler⁽¹¹⁾ and Untermeyer⁽³⁰⁾ for vertical upflow evaporator tubes.

A different approach from the Martinelli model is the homogeneous flow model. Its basic assumptions are equal linear velocity for both phases ("fog" flow) and interphase thermodynamic equilibrium.* This model permits the use of friction factors. The pressure drop equation can thus be integrated along the tube. - The friction factors in all correlations are empirically determined. Several authors applying the homogeneous flow model correlated their friction factors against modified Reynolds numbers, without offering any theoretical justification: Shugaeff and Sorokin⁽²⁷⁾, Marcy⁽²⁰⁾, and Dittus and Hildebrand⁽¹²⁾ used the liquid-phase viscosity in their Reynolds number, and McAdams, Wood and Heroman⁽²⁴⁾ employed a weighted viscosity; Shugaeff and Sorokin for air-water flow, Marcy for the flow of flashing refrigerants, and the

* The latter assumption is not axiomatic: Styrikovich and Miropolski⁽²⁹⁾ reported superheated steam in the upper part of a heated horizontal pipe carrying steam-water mixtures.

others for the flow of oil with vaporization. Bottomley⁽⁶⁾ and Benjamin and Miller^{(2), (3)} successfully applied the homogeneous flow model to water-steam flashing.

Jakob, Leppert and Reynolds⁽¹⁴⁾ measured pressure drop for the forced-convection boiling of water in a horizontal heating tube, and recalculated their results according to the homogeneous flow model and the (separated-flow) Martinelli-Nelson model; their actual results fell between the two widely-spreading curves without showing preference for either model. In general, the homogeneous flow model is best applicable to high-speed flow, as in flashing. Davidson, Hardie, et al.⁽¹⁰⁾, investigating forced-circulation boiler tubes, found that pressure drops calculated with friction factors were several times greater than the actual values except at high Reynolds numbers.

Linning⁽¹⁸⁾ proposed a model for vaporization two-phase flow in which he postulated annular flow. This model has not had much application, due perhaps to the unwieldiness of the final equation.

Other methods that have been used to analyze gas-liquid flow are dimensional analysis, suggested by Schmidt⁽²⁶⁾, and the approach of Calvert⁽⁷⁾, who obtained velocity profiles by applying the principles of Prandtl and von Kármán to two-phase annular vertical air-water upflow. Calvert calculated the gas-phase pressure drop from the interfacial shear; the latter was assumed to be a function of interfacial roughness, and was obtained by taking some fraction of the stagnation pressure times the area of drag caused by the roughness. Since the degree of roughness

at the interface is unknown, the final equation contained unknown constants which were calculated from empirical data obtained by Calvert and by Radford⁽²⁵⁾.

There are hardly any data in the literature on two-phase pressure drop for liquid phase in downward falling-film flow through pipes of more than capillary size. Carpenter⁽⁸⁾ measured pressure drops in a vertical-tube condenser for condensing vapors at high vapor velocities. The substances used were water, methanol, ethanol, trichloroethylene and toluene. Since for falling-film flow the film thicknesses were negligibly small as compared to tube size, superficial Reynolds numbers were used for gas-phase Reynolds numbers. Also, total pressure drop was equated to gas-phase pressure drop, and the gas friction factor plotted against the gas Reynolds number for varying liquid flowrates. For zero liquid flowrate, the friction factor plot was identically equal to that for pure gas flow. The shape of the friction factor curve for increasing liquid rates was closely akin in form to single-phase flow friction factor curves for increasing tube-wall roughness. - The parameter in

these curves was taken as $\frac{\Gamma}{\rho l}$ rather than as $(Re)_l$, since the viscosity did not vary sufficiently to warrant the use of a Reynolds number. For liquids other than water, the parameter was furthermore divided by the ratio of surface tension to water surface tension (see Figure 6). It can be

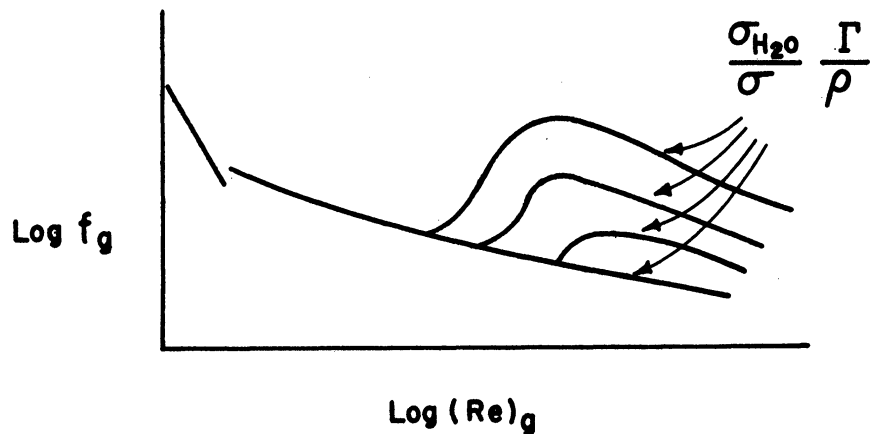


Figure 6

seen that the pressure drop was equal to the dry-wall pressure drop except at high gas and liquid flowrates.

Bergelin, Kegel et al.⁽⁴⁾ performed tests for co-current down-flow of air-water mixtures through 1-in. tubes. Their results followed Carpenter's correlation fairly closely, but deviated $\pm 30\%$ from the Lockhart-Martinelli correlation.

SECTION V

LITERATURE RESEARCH ON PERTINENT EVAPORATOR STUDIES

There is a large amount of published evaporator literature in existence. The following is an abstract of several studies that may contribute to a better understanding of falling-film evaporation.

A. Climbing-Film LTV's

Dengler⁽³⁾ in 1952 made a fundamental study of heat transfer and pressure drop, evaporating water in a single-tube LTV. With regard to pressure drop, he found that the Lockhart-Martinelli model could be used if sufficiently modified; to do this he employed radioactive tracers. For heat transfer he used thermocouples to measure wall temperature, and found that for temperature drops of up to ca. 10 °F, heat transfer obeyed an essentially convective mechanism and could be predicted by using a Dittus-Boelter type of correlation. For higher temperature drops the heat transfer coefficients became higher than the corresponding convective coefficients would have been, and varied with powers of the temperature drop greater than unity, as in nucleate boiling.

Guerrieri and Talty⁽⁴⁾ in 1956 performed similar tests with 5 organic liquids over a wide range of operating variables. They essentially corroborated the findings of Dengler in all respects.

Sonic choking at the tube ends was discussed by Schweppe and Foust⁽¹⁸⁾ and by Harvey and Foust⁽⁶⁾ in 1953. They found that critical flow in their experimental evaporator was occasionally reached at flow-rates lower than predicted. Their discussion was incomplete in that it tacitly assumed a homogeneous flow model, and because void fraction, i.e., linear velocity, was not measured.

B. Wiped-Surface Evaporators

Several studies have been published on evaporators in which the heating surface is mechanically wiped in order to produce a very thin film of liquor. This has special application in cases of heat-sensitive liquids where low hold-up and low temperature difference are desirable.

Climbing-film evaporators of this type have been described by Hadley and Thomas⁽⁵⁾, and falling-film wiped-surface evaporators by Hausschild⁽⁷⁾, Schneider⁽¹⁷⁾, Billet⁽¹⁾, Poócza⁽¹⁵⁾, Kirschbaum and Dieter⁽¹²⁾, Kern and Karakas⁽⁹⁾, and Lustenader, Richter and Neugebauer⁽¹³⁾. In most cases the experimental results apply only to the particular machine being studied, and consist of empirical correlations of hold-up and heat transfer in terms of wiper-blade velocity and feed rate. The theoretical studies assume streamline flow only. There is also a considerable number of patents in this field.

C. Falling-Film LTV's

The literature on falling-film LTV's is practically non-existent. Chambers and Peterson⁽²⁾ described a falling-film sulfuric acid concentrator, but did not present sufficient data to study the heat transfer characteristics. Kerry⁽¹⁰⁾ qualitatively described a falling-film machine used as a liquid-oxygen vaporizer in an air separation plant. Keville⁽¹¹⁾ described the performance of a falling-film LTV used for concentrating milk; his published numerical data are not sufficient for the formulation of a sound heat transfer correlation.

Karetnikov⁽⁸⁾ in 1954 made a laboratory investigation of heat transfer through a falling film of de-aerated water at ca. 140° F, under boiling and non-boiling conditions. The apparatus was a vertical 16mm OD x 600 mm copper tube, inside a glass shell. The tube was electrically heated from inside and had thermocouples caulked into the walls. The water flowed down the outer tube surface from a special feed distributor. The glass shell was provided with a manometer. Reynolds numbers ranged from 570 to 2,600, and the heat load from 1,800 to 12,500 Btu/(hr)(sq ft). - Boiling heat transfer experiments were carried out under a vacuum of ca. 24 in. Hg. Non-boiling tests were performed under identical conditions but at atmospheric pressure. - The following observations were made:

- 1) In non-boiling heat transfer the film was transparent and offered a visual appearance similar to that found by previous investigators.
- 2) When boiling, the film was never transparent, being full of bubbles all the time.
- 3) When the heat flux reached maximum values ranging from 3,500 Btu/(hr)(sq ft) at (Re) 570 to 12,500 Btu/(hr)(sq ft) at (Re) 2,600, the film was actually repelled from the wall and falling-film evaporation became impossible.
- 4) Boiling heat transfer coefficients varied little with heat load; if anything, they decreased with increasing heat load.
- 5) Boiling heat transfer coefficients increased with increasing flow rate.
- 6) Boiling heat transfer coefficients were lower than the non-boiling coefficients for the same flowrate and heat load. - At extremely

low flowrates, the boiling coefficients reached and even exceeded the non-boiling coefficients. However, this may be due to the fact that the author used the arithmetic mean rather than the log-mean temperature difference to compute the non-boiling coefficient. This error, which causes coefficients to appear too low, becomes all the more severe as the flowrate decreases, and may thus account for this reversal of trend at extremely low flowrates.

- 7) The non-boiling heat transfer coefficients deviated considerably from any known falling-film heat transfer correlation. The author did not indicate his method of measuring temperature differences, and this deviation can therefore not be explained. This does not mean that his conclusions under heading 6) are necessarily untrue, since the relative relationship between boiling and non-boiling coefficients may be sound despite the fact that their absolute magnitudes may be questionable. - The author did not mention the heat transfer work of any previous investigators.

Richkov and Pospelov⁽¹⁶⁾ in 1959 studied the falling-film evaporation of preheated water and caustic soda solutions flowing down the outside wall of a 30 mm OD x 1,200 mm vertical nickel-plated copper tube, at atmospheric pressure. The tube was electrically heated from inside and was provided with wall thermocouples. - The range explored was (Re) 3,100 to 4,100, q from 4,800 to 52,000 Btu/(hr)(sq ft) - Feed and exit liquor temperatures were measured with mercury thermometers (to an accuracy of 0.1° C) and their average used as the boiling temperature of the liquid; although not expressly stated, this value was then apparently

subtracted from the wall temperature in order to compute the heat transfer coefficient. - The conclusions made were as follows:

- 1) The visual appearance of the boiling film was described at great length though not supplemented by sketches or photographs. For heat fluxes not in excess of 9,000 Btu/(hr)(sq ft), steam bubbles formed continuously, rapidly growing to the same size as the film thickness itself; they flowed down the tube in this manner until surfacing and bursting. The liquor film had the aspect of a descending deposit of large bubbles.
- 2) At high heat fluxes, of the order of 50,000 Btu/(hr)(sq ft), the film seemed to disintegrate with the formation of large falling droplets. - This is similar to the observation of Karetnikov.
- 3) An empirical correlation for water was derived:

$$h = 2.12 q^{0.32} (\text{Re})^{0.435}$$

All magnitudes are in British engineering units, Btu - hr - ft - °F.

- 4) Similar correlations were derived for caustic solutions of different strengths. These correlations differ in the value of all three numerical factors; besides, for all caustic solutions the exponents of q were negative.

The ease with which an excessive heat load destroys the typical falling-film flow regime was also commented on by Mueller⁽¹⁴⁾ in 1961. He cited the case of a falling-film vaporizer which under a temperature drop of 16°F still maintained a falling-film flow regime, but which under higher heat loads had a temperature drop of 45 - 55°F as in pool boiling. He explained this by assuming that in a falling-film evaporator the critical temperature drop was so low because of the absence of a force that would bring the fluid back to the tube walls once it had left them.

SECTION VI

DESIGN AND RESULTS OF EXPERIMENTS

INTRODUCTION

Each run was characterized by a different set of magnitudes for the 6 independent variables. The object of each run was the measurement of the overall heat transfer coefficient.

The 6 independent variables were: tube diameter, feed rate, steam rate, vapor-head temperature, feed temperature, and feed salinity.

The experimental work was initiated with a 2-level experiment of 5 variables, for a constant tube diameter. The experiment, the LWCI runs, consisted of 32 randomized runs, and its results indicated the significance of each variable. Further experiments were designed on the basis of this information in order to explore the entire region, defined by the upper and lower levels of each one of the 6 variables, with as few runs as possible. A total of 105 runs was performed.

Since the overall heat transfer coefficient is a function of all 6 variables, it was found impossible to make a clear representation of the results in graphical form. They are therefore presented as numerical tables.

SECTION VI

DESIGN AND RESULTS OF EXPERIMENTS

INTRODUCTION

Each run was characterized by a different set of magnitudes for the 6 independent variables. The object of each run was the measurement of the overall heat transfer coefficient.

The 6 independent variables were: tube diameter, feed rate, steam rate, vapor-head temperature, feed temperature, and feed salinity.

The experimental work was initiated with a 2-level experiment of 5 variables, for a constant tube diameter. The experiment, the IWCI runs, consisted of 32 randomized runs, and its results indicated the significance of each variable. - Further experiments were designed on the basis of this information in order to explore the entire region, defined by the upper and lower levels of each one of the 6 variables, with as few runs as possible. A total of 105 runs was performed.

Since the overall heat transfer coefficient is a function of all 6 variables, it was found impossible to make a clear representation of the results in graphical form. They are therefore presented as numerical tables.

SECTION VI

DESIGN AND RESULTS OF EXPERIMENTS

A. RUNS LWCI-1 TO LWCI-32

Design of Experiment

Runs LWCI-1 to -32 constitute the initial study. Their object was to determine which of all possible variables had a significant effect on the heat transfer coefficient, and to determine the sign and magnitude of this effect, in 2-in. tubes.

Table V gives the variables that were studied, together with their range of magnitude.

Variable	Lower Level	Higher Level
Vapor-head saturation temperature, °F	150	230
Feed concentration factor	1	2
Feed "superheat" * , °F	0	20
Feed rate, lb/hr	1,500	6,000
Steam rate, lb/hr	250	450

TABLE V

The low and high levels of the operating variables were set by practical considerations. 150° F was the lowest vapor-head saturation temperature that could be reached with the existing condenser, cooling water and vacuum equipment. 230° F was the highest because of possible scale formation at higher temperatures; the danger of scale also

* i.e., feed temperature minus vapor-head saturation temperature

determined the choice of 2 for the highest feed concentration factor. The range of feed superheat, 0 to 20°, covers the practical range of interest for falling-film LTV operation. The flowrates for feed and steam were limited by the equipment, but cover the practical range of interest; liquor Reynolds numbers vary from 1,400 to 10,300 and feed-to-evaporation ratios from 3.3 to 24.

In order to run a completely balanced experiment⁽⁴⁾, each level of each variable was tested at all the levels of all the other variables. Since each variable was run at 2 levels (low and high), and the number of variables was 5, the number of experimental runs was $(2)^5 = 32$.

The runs were assigned the letters LWCI, followed by consecutive numbers from 1 to 32, this being the order in which they were performed. They were arranged in a randomized fashion, shown in Table VI, in order to cancel out any time trends.

Feed rate		1,500				6,000			
Steam rate		250		450		250		450	
Conc. factor		1	2	1	2	1	2	1	2
VH sat. temp.	Feed superh.								
150	0	18	4	2	30	6	32	21	1
	20	15	20	22	7	13	11	27	31
230	0	5	23	24	14	26	16	8	29
	20	17	10	9	19	3	28	25	12

TABLE VI

Accuracy of Results

Errors may have originated from the following causes:

- 1) Malfunctioning of the test equipment.
- 2) Malfunctioning of the measuring instruments.
- 3) Random error.
- 4) Error in data on physical properties used in order to calculate heat transfer coefficients.
- 5) Personal error in reading the instruments.
- 6) Personal error in recording, transcribing, and calculating.

Test equipment malfunctioning was mainly due to poor performance of the automatic control instrumentation. This was due to the fact that the range of operation was too wide for the existing instrumentation. A steady steam rate and good feed temperature regulation were often very hard to obtain. Results obtained under doubtful conditions were afterwards discarded.

The instrument errors having the greatest effect on heat transfer coefficients are errors in steam-chest pressure and in vapor-head pressure. Since overall temperature differences were of the order of a few degrees only, even small errors in absolute pressure would cause large errors in heat transfer coefficient. - At 150° F, mercury manometers were used to read both pressures. At 230°, however, the steam-side pressure was read on a Bourdon gage. A series of precision pressure gages were tried; none were satisfactory, since their calibration (against a mercury manometer) would often change after several days of operation. The vapor-head

pressure at 230° was measured with a mercury manometer, vapor being prevented from entering the instrument piping by means of a small but positive hand-controlled purge of compressed air through the manometer pipe into the vapor-head. (A similar scheme for the steam-side pressure would have introduced air into the steam chest, thus inhibiting condensation.) A larger instrument error at 230° than at 150° F was therefore expected.

The boiling-point rise data* were taken from Report No. 438, W. L. Badger and Associates, Inc., written for the U. S. Department of the Interior, Office of Saline Water⁽⁵⁾. They are based on the correlation of the work of several investigators on sea water concentrates and on pure sodium chloride solutions, and involve a small degree of interpolation and extrapolation. They are presented as curves of (BPR) vs. concentration, with temperature as parameter. Any error due to the use of these data would be expected to be larger at 230° than at 150° F, first, because boiling-point rise at 230° is larger than at 150° F, and secondly, because at 230 the heat transfer coefficients are higher, and (BPR) thus constitutes a larger percentage of the apparent temperature difference than at 150° F. - The (BPR) was calculated for the average chlorosity in the tube, and for the film temperature (roughly, the average between steam temperature and vapor-head temperature).

Personal error in instrument reading, and in recording, transcribing and calculating, was held down as much as possible. Instrument readings

* Graph No. 1 of Appendix E..

were generally performed by the engineers, not the operators; the steam tables of Keenan and Keyes⁽²⁾ were used in the calculations; readings with poor mass or energy balances were discarded; and the written work was checked several times. Several runs were re-run at a later date, and the results were found to be practically the same.

Experimental Results

A summary of the experimental results is presented in Appendix A. These data represent the last 2 sets of readings for each run. In cases where there was evidence of equipment or instrument malfunctioning during one of the readings, only the more reliable set or sets of readings are presented in Appendix A.

The average overall heat transfer coefficient for each run is presented in Table VII, expressed in Btu/(hr)(sq ft)(°F).

Feed rate		1,500				6,000			
Steam rate		250		450		250		450	
Conc. factor		1	2	1	2	1	2	1	2
VH sat. temp.	Feed superh.								
150	0	445	464	472	435	565	498	520	500
	20	418	438	441	422	468	480	481	470
230	0	645	678	606	573	868	774	794	745
	20	590	606	600	587	737	687	701	647

TABLE VII

From Table VII it can be seen that the temperature and the flow-rate are significant variables. This was expected, since it is similar to most cases of heat transfer to a moving fluid. - Feed salinity, as expected, is a variable of little or no significance. At these low concentrations, concentration has little influence on density, viscosity or Prandtl number, and it is quite probable that the discrepancy between runs that differ only in concentration factor is due to small errors in estimating the boiling point rise.

Perhaps the most surprising result is the insensitivity of the overall heat transfer coefficient to the steam rate, i.e., the heat load. This is the kind of result one would expect from a sensible-heat transfer run, not a boiling run; in nucleate boiling, an increase in heat load of 80% normally causes an increase in heat transfer coefficient of 220 - 480%. * This is certainly not the case here.

The effect of feed superheat is also surprising; it depresses the heat transfer coefficient by roughly 6%.

With regard to the accuracy of the results, some of the results at 230° F seem to be off; run 14 seems to be too low, whereas 26 and 8 are definitely too high. The error must be ascribed to the causes previously mentioned. on page 85.

*See page 58.

B, RUNS LWCJ-1 TO LWCJ-16

AND

C, RUNS LWCK-10 TO LWCK-29

The results of the LWCI runs permitted an intelligent planning of further research. In the LWCI runs, the variables had been tested only at their lowest and at their highest possible values; the runs had shown that temperature and feed rate might bring additional information if run at intermediate values, but obviously not so the steam rate and the feed concentration.

The LWCJ series was designed essentially to complement the LWCI series by running tests at intermediate vapor-head saturation temperatures (175 and 200° F); runs were also made at the intermediate feed rate of 3,000 lb/hr at all temperatures. These runs, 16 in all, were all run at a concentration factor of 1 and a steam rate of 450 lb/hr; 8 of them at a feed superheat of 0, the others at a superheat of 20°F.

At a later date, the pilot plant was modified by adding a steam-jet air ejector to the Nash vacuum pump, and by substituting the steam shell of an idle FC evaporator for the old overhead condenser. This allowed operation at higher vacuum, and the range of vapor-head saturation temperature was extended down to 100° F. These are runs LWCK-10 to LWCK-29, run at 100 and 125° F. - This concluded the work on 2-in. tubes.

Table VIII indicates the runs for the entire test program on 2-in. tubes (series LWCI, LWCJ, LWCK), constituting a total of 68 runs. The letters LWC have been omitted for brevity.

Feed rate		1,500				3,000		6,000					
Steam rate		250		450		250		450		250		450	
Conc. factor		1	2	1	2	1	1	1	2	1	2		
VH sat. temp.	Feed sup.												
100	0	K-18		K-19		K-15	K-12	K-16		K-10			
	20	K-21	K-29	K-20		K-14	K-13	K-17	K-28	K-11			
125	0			K-22			K-24			K-26			
	20			K-23			K-25			K-27			
150	0	I-18	I-4	I-2	I-30		J-1	I-6	I-32	I-21	I-1		
	20	I-15	I-20	I-22	I-7		J-2	I-13	I-11	I-27	I-31		
175	0			J-11			J-3			J-7			
	20			J-12			J-4			J-8			
200	0			J-5			J-15			J-9			
	20			J-6			J-16			J-10			
230	0	I-5	I-23	I-24	I-14		J-13	I-26	I-16	I-8	I-29		
	20	I-17	I-10	I-9	I-19		J-14	I-3	I-28	I-25	I-12		

TABLE VIII

The experimental data of the LWCJ and LWCK runs are summarized in Appendices B and C, respectively.

The overall heat transfer coefficients for the entire test program on 2-in. tubes are presented in Table IX, expressed in $\text{Btu}/(\text{hr})(\text{sq ft})(^\circ\text{F})$. The conclusions that were reached after the LWCI runs regarding the effect of the different variables on the heat transfer coefficient are

shown to be valid for the entire region. It is because of this that 68 runs were sufficient to explore this region, which consisted of 144 possible combinations of the different levels of variables involved.

Feed rate		1,500				3,000		6,000			
Steam rate		250		450		250	450	250		450	
Conc. factor		1	2	1	2	1	1	1	2	1	2
VH sat. temp.	Feed sup.										
100	0	314		305		327	315	329		327	
	20	331	325	304		293	290	291	299	254	
125	0			373				404		428	
	20			380				391		388	
150	0	445	464	472	435	460		565	498	520	500
	20	418	438	441	422	446		468	480	481	470
175	0			491				527		574	
	20			469				495		528	
200	0			530				576		556	
	20			553				557		591	
230	0	645	678	606	573	641		868	774	794	745
	20	590	606	600	587	618		737	687	701	647

TABLE IX

D. RUNS LWDA-2 TO LWDA-38

These 37 runs comprise the test program using 1-in. tubes. They were performed after the runs with 2-in. tubes had been completed, and had a similar choice of variables. Vapor-head saturation temperatures were 100, 125, 150, 175, 200, and 230°F, as with the 2-in. tubes; feed superheats were also 0 and 20° F. The feed rates were 1,500 and 3,000 lb/hr. (Flows higher than 4,000 lb/hr proved impossible for these narrow tubes: one of the 7 tubes would revert to full-pipe flow and starve the other 6 tubes of feed.) The steam rates were 150 and 250 lb/hr. The latter gave roughly the same heat flux of ca. 6,000 Btu/(hr)(sq ft) as 450 lb/hr of steam gave with the 2-in. tubes. The 150 lb/hr steam rate was really too low for adequate process control; it was used in 12 of the 37 runs, chiefly to test the assertion that steam rate had little significance on heat transfer coefficient. Only 1 run was made with a feed concentration factor higher than 1, to test the assertion that concentration had little or no significance.

Feed rate		1,500			3,000	
Steam rate		150	250		150	250
Conc. factor		1	1	2	1	1
VH sat. temp.	Feed superh.					
100	0	34	2		37	4
	20	35	3	38	36	5
125	0		8			6
	20		9			7
150	0	33	10		30	12
	20	32	11		31	13
175	0		14			16
	20		15			17
200	0		19			18
	20		20			21
230	0	23	22		25	24
	20	28	27		29	26

TABLE X

Table X shows the run numbers of our work with 1-in. tubes. Appendix D) gives a summary of the experimental results of each run. Table XI gives the measured overall heat transfer coefficients, in Btu/(hr)(sq ft)(°F).

Feed rate		1,500			3,000	
Steam rate		150	250		150	250
Conc. factor		1	1	2	1	1
VH sat. temp.	Feed superh.					
100	0	191	172		177	162
	20	162	153	161	130	133
125	0	267			231	
	20	245			190	
150	0	391	381		350	319
	20	368	364		284	280
175	0	494			436	
	20	484			405	
200	0	626			529	
	20	605			577	
230	0	652	773*		599	643
	20	656	687		631	674

TABLE XI

The following conclusions may be drawn from the tests on 1-in. tubes:

- 1) The significance of the variables in 1-in. tubes is very similar to that in 2-in. tubes except that of feed rate.
- 2) At high temperatures (200 - 230° F) the heat transfer coefficients are practically the same as in 2-in. tubes; they become increasingly lower than those in 2-in. tubes as temperature is lowered. This effect

* This figure is evidently too high.

of vapor-head saturation temperature appears to be the only difference between operation with 2-in. and 1-in. tubes.

SECTION VII

THEORETICAL MODEL OF FALLING-FILM EVAPORATIVE HEAT TRANSFER MECHANISM

FUNDAMENTAL MODEL

Figure 7 serves to illustrate the definition of the heat transfer coefficient through the liquid film, h_f . If t_w is the temperature at the inner tube wall, t_v the temperature of the film at or close to the vapor interface, then:

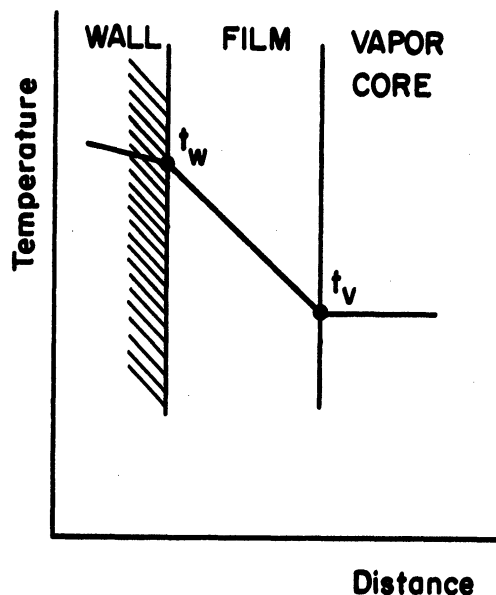


Figure 7

$$\Delta t_f \equiv t_w - t_v \quad (1)$$

$$h_f \equiv \frac{q}{\Delta t_f} \quad (2)$$

Our experimental work shows conclusively that the heat transfer coefficient remains practically unchanged even when the heat load is increased by 80%, and that this is valid for all temperatures, flow-rates, feed superheats, concentration factors and tube diameters employed. This indicates that the heat transfer mechanism should be convective. In view of the low temperature drops involved, this explanation is plausible, especially in view of the analogous results of Dengler and of Guerrieri and Talty with climbing-film LTV's.

The available correlations for convective heat transfer through

falling liquid films are those of Drew, Brauer, and Dukler.* Drew's correlation is not supported by any experimental evidence except for water at 190° F. - Brauer's correlation contains an empirical factor, namely, the velocity at the "equivalent" film thickness; we have no way of predicting this factor, which seems to depend on the nature of the liquid and its temperature.

Dukler's analysis is the direct computer solution of the basic differential equations for momentum and heat transfer. Except for the use of the Deissler and the von Kármán universal velocity profiles, no simplifying assumptions or empirical factors of any kind are contained in this analysis. It successfully correlates experimental falling-film sensible-heat transfer and condensation data over an extremely wide range of variables; this shows that the two universal velocity profiles, though derived from tests with full-pipe flow, are valid for falling-film flow. We used this correlation as our theoretical model.

The Dukler correlation for our range of variables is presented ** in graphs 2 and 3. Graph 2 is a plot of the dimensionless film thickness group $B \left(\frac{\rho g}{\mu^2} \right)^{1/3}$ versus Reynolds number, for negligible interfacial shear. Graph 3 is a plot of the dimensionless heat transfer coefficient $\frac{h_f}{\phi}$ as function of the Reynolds and Prandtl numbers, also for negligible shear. Graph 2 is taken directly from Dukler's paper. Graph 3 resulted from a cross-plot of Dukler's curves of $\frac{h_f}{\phi}$ vs. (Re) for values of (Pr) of 1.0, 2.0, and 5.0.

* See pages 50, 51 and 53 respectively.

** See Appendix E.

Graph 4 is a plot of ϕ , computed for sea water concentrates as function of temperature and chlorosity.

The heat transfer coefficients thus calculated are essentially local coefficients. The mean value of the coefficient with respect to the entire tube length should, in all rigor, be calculated by integrating the local coefficients along the tube. This may be avoided, however, by considering that in our tests the vaporization rate was low compared to the feed rate; the average between feed rate and blow-down rate should be satisfactory for computing the mean Reynolds number, especially since the flowrate varies linearly due to the constant heat flux along the tube. The small change in salinity during vaporization has little effect on the physical constants of the liquor, and can be satisfactorily taken into account by using the mean salinity.

Graphs 5 and 6 are plots of viscosity and Prandtl number, respectively, of sea water concentrates. They were calculated from data on physical properties contained in Report 438 of W. L. Badger Associates, Inc., for the Office of Saline Water⁽⁵⁾.

BOILING POINT ELEVATION

According to our theoretical model, Figure 7, a precise knowledge of t_v as well as of the wall temperature is required in order to calculate Δt_f . However, t_v would be extremely difficult to measure, and must therefore be calculated from the local vapor pressure, p_v . This pressure is equal to the measured vapor-head pressure plus any (usually very low) pressure drop Δp caused by friction, acceleration

and elevation, and can be computed.

$$\text{Let the general function } t \equiv f(p) \quad (3)$$

be the equation of the temperature vs. vapor pressure of the volatile solvent; for aqueous solutions it is tabulated in the steam tables. If the vapor phase in falling-film evaporator tubes consisted of saturated steam, it would then follow that $t_v = f(p_v)$. For boiling liquids, however, the equilibrium vapor is not saturated but superheated: $t_v > f(p_v)$. This superheat is due to two causes: the presence of bubbles, and the presence of solute.

Let a spherical bubble of radius r be in equilibrium with the surrounding liquid phase. Let p' be the pressure of the gas inside the bubble. Let p_v be the pressure of the liquid, which is the same as the pressure of the extended equilibrium gas phase (no curvature). A balance on the tangential tensile forces acting on the bubble surface yields the well-known relation:

$$\sigma \cdot 2\pi r = (p' - p_v) \cdot \pi r^2 \quad (4)$$

$$\text{or: } p' - p_v = \frac{2\sigma}{r} \quad (5)$$

The presence of solute lowers the vapor pressure of the solution below that of the pure solvent. This causes the equilibrium vapor to be superheated by a temperature difference (BPR), the boiling-point rise. If t_v and p'' are the temperature and pressure, respectively, of the vapor in equilibrium with the liquid, then:

$$(\text{BPR}) \equiv t_v - f(p'') \quad (6)$$

Consider now the case of both bubble and solute action occurring simultaneously, as in boiling sea water. The vapor in equilibrium with the boiling liquid is in bubble form; hence p' of the discussion on bubble action becomes identical with p'' mentioned under solute action. Combining equ. (5) and (6), we arrive at the conclusion that in this case the boiling-point elevations due to bubbles and to solute are additive:

$$t_v = f(p_v + \frac{2\sigma}{r}) + (\text{BPR}) \quad (7)$$

Using our symbols, $f(p_v)$ is the "apparent" vapor temperature, and $f(p_v) + (\text{BPR})$ the "corrected" vapor temperature, in the parlance of industrial evaporator practice. The neglect* of the $\frac{2\sigma}{r}$ term in industry is due to the fact that in most cases it is negligibly small except for very small bubbles, and because there is little information regarding the size and behavior of bubbles in commercial evaporators.

In falling-film evaporation, both Karetnikov and Richkov et al.** report observations on bubble size, namely, that the bubbles become stable when they reach the same proportions as the film thickness itself. This stands to reason. First, a stable bubble can certainly not be larger than the film. Second, suppose there exists an array of bubbles of different sizes, ranging from very small up to a maximum with diameter equal to the film thickness B . These bubbles cannot all exist at equilibrium with each other, for the same reason that small crystals cannot exist in equilibrium with large crystals when suspended

* See Appendix F for the effect of neglecting $\frac{2\sigma}{r}$ in falling-film evaporation.

** See pages 79 and 80 respectively.

in a saturated solution: according to the second law of thermodynamics, the smaller bubbles (or crystals) shrink spontaneously until they disappear.

The Dukler analysis offers the needed information on the thickness of falling films, and the surface tension of sea water concentrates can be found in the work of Sverdrup et al.⁽³⁾. The bubble boiling-point elevation $\frac{4\sigma}{B}$ may be calculated as follows:

$$\frac{4\sigma}{B} = \frac{\chi}{B \left(\frac{\rho^2 g}{\mu^2} \right)^{1/3}} \text{ in. Hg} \quad (8)$$

where χ is defined as:

$$\chi = 3.876 \times 10^{-6} \sigma \left(\frac{\rho^2 g}{\mu^2} \right)^{1/3} \text{ in. Hg}, \quad (9)$$

σ being expressed in dynes/cm, $\left(\frac{\rho^2 g}{\mu^2} \right)^{1/3}$ in ft⁻¹.

The convenience of this formulation is that χ is a function of temperature and chlorosity only, whereas $B \left(\frac{\rho^2 g}{\mu^2} \right)^{1/3}$ is a function of the Reynolds number only. Graph 7 shows χ ; $B \left(\frac{\rho^2 g}{\mu^2} \right)^{1/3}$ can be read from Graph 2, the Dukler film thickness correlation.

The film thicknesses for our experimental work range from 11 to 28 mils, when calculated with the Dukler correlation. Values of $\frac{4\sigma}{B}$ range from 0.11 to 0.25 in. Hg. Neglect of the bubble boiling-point elevation* is unimportant at 230° F, but at low temperatures it can cause considerable error due to the slope of the vapor-pressure curve of water at low temperatures. This may explain the reason why Karetnikov**

* See Appendix F

**See page 79

found his boiling coefficients to be lower than his non-boiling coefficients, especially since he worked at very low Reynolds numbers (and hence low film thicknesses).

Boiling-point elevations from bubble action and from solute action change little along the length of the tube*; the values for the average values of film temperature and chlorosity were always used in our calculations.

LONGITUDINAL PRESSURE-DROP MODEL

It is necessary to know the pressure-drop in order to be able to calculate p_v :

$$p_v = p_{vH} + \Delta p \quad (10)$$

This pressure-drop is the friction, acceleration and elevation pressure-drop due to the downward two-phase flow through the tube, with eventual sonic choking.

No sonic choking was encountered during the experimental work. It was calculated that the highest vapor exit velocity, ca. 950 ft/sec, was less than 70% of the speed of sound at that temperature. Vapor exit velocities were calculated from a separated-flow model, which of itself yields higher values than the homogeneous-flow model such as used by Harvey and Foust and by Schweppe and Foust.**

Acceleration-pressure drops were calculated according to the

* See Appendix F for a discussion of this point.

** See page 77.

separated-flow model, which should be applied in falling-film flow. To do this, the film thickness was calculated from the Dukler correlation, and the liquid cross-sectional area subtracted from the total tube cross-sectional area to give the gas flow cross-section.

Elevation heads were also calculated.

A certain degree of conjecture had to be used in order to calculate frictional pressure-drop. A thorough search of the literature on two-phase flow had failed to yield a satisfactory universal correlation for two-phase pressure-drop in falling-film flow.

Bergelin, Kegel et al. reported that for gas flowrates below a critical value, the pressure-drop in falling-film two-phase flow was equal to the pressure-drop of the gas phase alone. Our highest calculated exit gas velocity in 2-in. tubes was 386 ft/sec, with a gas Reynolds number of 20,000. For the low liquor rates employed, this gas rate is lower than the critical gas rate for 1.025 in. tubes as employed by the authors. Pressure-drop for 2-in. tubes was therefore calculated for dry-tube flow as follows:

$$-\frac{dp}{dL} = f \frac{2G^2v}{g_c D} \quad (11)$$

$$\therefore -\Delta p = \int_0^{L_T} f \frac{2G^2v}{g_c D} dL \quad (12)$$

Let G_T be the terminal value of the gas flow density G . Let L_T be the terminal length of the tube (24 ft in our case).

Basic assumption: uniform heat flux along the tube.

$$\therefore G = \frac{G_T}{L_T} L \quad (13)$$

$$\therefore -\Delta p = \int_0^L f \frac{2G_T^2 v L^2}{g_c D L_T^2} dL \quad (14)$$

$$-\Delta p = \frac{2G_T^2}{g_c D L_T^2} \int_0^L f v L^2 dL \quad (15)$$

This integral can be solved by dividing the tube into a laminar length where the Reynolds number varies from zero to 2,100 and $f = \frac{16}{(Re)}$, and a turbulent length with $f = 0.046 (Re)^{-0.2}$. It can be shown that the pressure-drop arising from the laminar section is negligibly small and that the laminar section is negligibly short. Hence:

$$-\frac{dp}{dL} = \frac{(0.046)(2)G_T^{1.8} \mu^{0.2} v L^{1.8}}{g_c D^{1.2} L_T^{1.8}} \quad (16)$$

$$\therefore -\Delta p = \frac{(0.046)(2)G_T^{1.8} \mu^{0.2} v}{2.8 g_c D^{1.2} L_T^{1.8}} L^{2.8} \quad (\mu, v \text{ const.}) \quad (17)$$

The pressure-drop increases with the 2.8th power of the tube length. In fact, for the typical case of 2-in. tubes, with vapor-head temperature 100° F, steam rate 450 lb/hr, we have 90% of the pressure-drop concentrated in the bottom 3.7% of the tube length. It is practically an "exit pressure-drop". In order, therefore, to avoid an integration of pressure-drop with length, we simplified the pressure-drop model by calculating the whole pressure-drop as an exit pressure-drop. The error

involved in this assumption is small because of the low magnitude of the pressure-drops involved, so low, in fact, that they could not be experimentally determined during the tests with 2-in. tubes.

Table XII presents the calculated values of the total pressure-drop, in in. Hg, this being the sum of friction, acceleration and elevation pressure-drops. Friction accounts for one-half to two-thirds of the total, and was calculated for dry-tube flow as described. Graph 8 reproduces Table XII for purposes of interpolation, for temperatures below 200° F.

Tube size, in.	1				2			
	150		250		250		450	
Steam rate, lb/hr	1,500	3,000	1,500	3,000	1,500	6,000	1,500	6,000
Feed rate, lb/hr	1,500	3,000	1,500	3,000	1,500	6,000	1,500	6,000
Vapor temp., °F								
100	0.708	0.725	1.827	1.879	0.067	0.069	0.205	0.211
125	0.359	0.368	0.928	0.958	0.033	0.034	0.103	0.106
150	0.195	0.200	0.506	0.518	0.016	0.017	0.054	0.055
175	0.108	0.111	0.288	0.295	0.005	0.006	0.027	0.028
200	0.059	0.061	0.168	0.173	-0.003	-0.003	0.010	0.011
230	0.024	0.024	0.085	0.088	-0.015	-0.014	-0.006	-0.006

TABLE XII

It can be seen from Table XII that for 2-in. tubes the vapor pressure-drops are extremely small; so small, in fact, that at the higher temperatures the pressure gains due to the weight of the 24-ft column of

vapor is higher than the combined friction and acceleration pressure-drops, thus producing a total vapor pressure-drop that is negative, i.e., a pressure gain.

As mentioned earlier, the upper tube ends were provided with entrance orifices in order to equalize the feed distribution among the 7 tubes. The unavoidable disadvantage of this scheme was our resulting inability to measure feed pressure directly; feed pressure minus vapor-head pressure would then have given us the vapor pressure-drop. As it was, the measured quantity was the sum of the vapor pressure-drop plus the orifice pressure-drop, the latter amounting to a major portion of this sum. This disadvantage was circumvented by the following procedure: after a sufficient number of hourly heat transfer readings for a given run, the steam was shut off but nothing else was changed. Under these conditions the pressure-drop was due only to the orifice pressure-drop, since the tube did not contain any vapor. The orifice pressure-drop was measured, and subtracted from the measurements taken during the run itself; this should yield the vapor pressure-drop.

The values thus obtained scattered considerably. This was not unexpected, because:

- 1) the orifice pressure-drops amounted to several inches Hg, while the vapor pressure-drops were very small;
- 2) the orifice pressure-drops themselves fluctuated strongly due to momentary pressure changes in the feed line;
- 3) any amount of flashing through the orifice, due to even a very low feed superheat, raised the orifice pressure-drop considerably.

The theoretical minimum for the two-phase pressure-drop is the dry-tube pressure-drop as per Table XII . The vapor pressure-drops observed in the 2-in. tubes were of the same order of magnitude; hence the values of Table XII were used in our calculations as the two-phase pressure-drops.

For 1-in. tubes the problem was more complex because:

- 1) orifices were smaller*, hence orifice pressure-drops were higher;
- 2) the measured two-phase pressure-drops were higher than the dry-tube pressure-drops for runs at lower temperatures and at the high steam rate.

The two-phase pressure-drops were approximated as follows: the dry-tube values of Table XII were corrected by adding the empirical corrections of Table XIII; this roughly correlates the experimentally obtained two-phase pressure-drops. Data are in in. Hg.

Feed rate	1,500		3,000	
Steam rate	150	250	150	250
Vapor temp.				
100 - 175° F	0.00	0.60	0.00	1.20
200	0.00	0.00	0.00	0.60
230	0.00	0.00	0.00	0.00

TABLE XIII

* Preliminary work with the 1-in. tubes had shown a tendency for full-pipe flow to occur in any one tube, which then completely starved the other six of feed. This could only be avoided by installing smaller orifices. - For the same reason feed rates in excess of 4,000 lb/hr could not be used.

CALCULATION OF TUBE-SIDE HEAT TRANSFER FILM COEFFICIENT FROM THEORETICAL MODEL

This is best illustrated by taking a typical example from the Appendix; say, the first of the two sets of data of run CI-1:

μ , the film viscosity, is found on Graph No. 5: 1.17 lb/(hr)(ft).

(Re), the film Reynolds number, is calculated as $4w/b\mu$: 5,900.

(Pr), the film Prandtl number, is found on Graph No. 6: 2.88.

h_f/ϕ , the dimensionless Nusselt heat transfer group, is found on Graph No. 3: 0.319 (Dukler's correlation).

ϕ , the Nusselt heat transfer coefficient group, is taken from Graph No. 4: 4,060 Btu/(hr)(sq ft)(°F) .

χ , the bubble superheat magnitude, is taken from Graph No. 7: 2.83 in. Hg.

$B\left(\frac{\rho_g^2}{\mu^2}\right)^{1/3}$, the dimensionless Nusselt film thickness group, is taken from Graph No. 2: 23.4 (Dukler's correlation).

Δp , the tube exit pressure-drop, is taken from Graph No. 8; for 1-in. tubes we correct for liquid effect by adding values from Table XIII. For the set of data of this example, the result is:

$$\underline{0.06 \text{ in. Hg}} .$$

p_v , the actual pressure in the tube vapor core, is the VH sat. press. plus Δp : $7.61 + 0.06 = \underline{7.67 \text{ in. Hg}}$.

$\frac{4\sigma}{B}$, the bubble superheat pressure, is calculated as $\chi/B\left(\frac{\rho_g^2}{\mu^2}\right)^{1/3}$:
 $2.83/23.4 = \underline{0.12 \text{ in. Hg}}$.

$f(p_v + \frac{4\sigma}{B})$, the tube vapor core temperature corrected for bubble superheat, is found in the steam tables: $f(7.67 + 0.12) =$
 $f(7.79 \text{ in. Hg abs.}) = \underline{151.16 \text{ °F}}$.

t_v , the tube vapor core temperature (corrected for BPR as well as bubble superheat): $f(p_v + \frac{4\sigma}{B}) + \text{BPR} = 151.16 + 2.03 = \underline{153.19^\circ \text{ F}}$.

h_f , the heat transfer coefficient for actual conduction-convection (Dukler) through the falling film itself, is calculated by multiplying $\frac{h_f}{\phi}$ by ϕ : $(0.319)(4,060) = \underline{1,295 \text{ Btu}/(\text{hr})(\text{sq ft})(^\circ\text{F})}$.

Δt_f , the temperature drop through the falling film (see Figure 7 , page 9), is calculated by dividing the heat load Q by the inner tube surface (78.3 sq ft) and by h_f : $458,000/(78.3)(1,295) = \underline{4.52^\circ \text{ F}}$.

This solves the heat transfer problem, since it gives the wall temperature: $t_v + \Delta t_f = 153.19 + 4.52 = 157.71^\circ \text{ F}$. - Heat transfer occurs only across the film itself, over a temperature drop of $\Delta t_f = 4.52^\circ \text{ F}$. However, in experimental work and for evaporator design the important temperature difference is between the wall temperature and the BPR-corrected vapor-head saturation temperature, Δt_{corr} . It must be emphasized that in a falling-film evaporator Δt_{corr} is not a temperature drop across a film, but simply the difference between two temperatures. Still, the BPR-corrected vapor-head saturation temperature has the advantage of being experimentally measurable*, and heat transfer coefficients based on it are the usual way of reporting heat transfer information. Δt_{corr} is therefore calculated here from our theoretical model;

$$\Delta t_{\text{corr}} = 157.71 - (150.22 + 2.03) = \underline{5.46^\circ \text{ F}}$$

* The vapor-head saturation temperature is experimentally measurable, and BPR is added to it.

Calculation of heat transfer coefficients as illustrated on the previous two pages may be summarized as follows:

VH pressure	$p_{VH} = 7.61 \text{ in.}; f(7.61) = 150.22^\circ$
<u>+ Tube exit pressure drop</u>	<u>$+ \Delta p = 0.06 \text{ in.}$</u>
Vapor core pressure	$p_V = 7.67 \text{ in.}; f(7.67) = 150.53^\circ$
+ Bubble superheat	<u>$+ 4\sigma/B = 0.12 \text{ in.}$</u>
	$7.79 \text{ in.}; f(7.79) = 151.16^\circ$
<u>+ Boiling-point rise (solutes)</u>	<u>$+ \text{BPR} = 2.03^\circ$</u>
Vapor core temperature	$t_V = 153.19^\circ$
<u>+ Temp. drop across film (Dukler)</u>	<u>$+ \Delta t_f = 4.52^\circ$</u>
Wall temperature	$t_W = 157.71^\circ$

Hence $\Delta t_{app} = 157.71 - 150.22 = 7.49^\circ\text{F}$

and $\Delta t_{corr} = \Delta t_{app} - \text{BPR} = 7.49 - 2.03 = 5.46^\circ\text{F}$

Figure 8 shows temperatures and pressures at different points according to the proposed model.

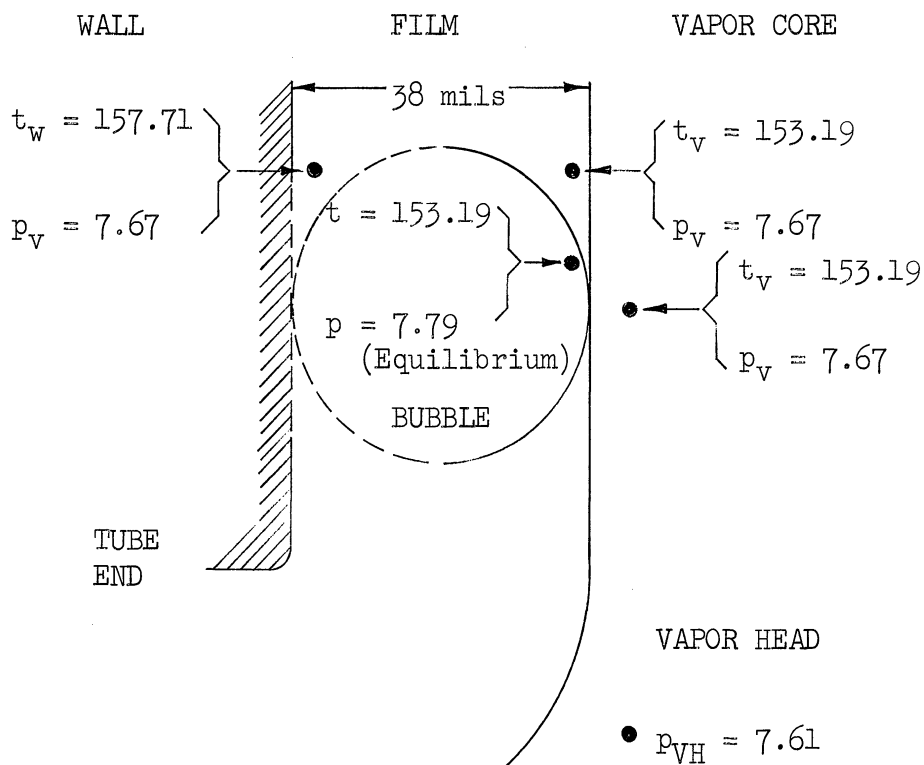


Figure 8.

Adoption of the proposed model implies that several basic assumptions must be postulated:

- 1) The liquid contains bubbles. This is based on the observations of Richkov and Pospelov, and of Karetnikov; the films at Wrightsville Beach could not be observed due to the nature of the equipment.
- 2) There is not enough relative motion between bubbles and liquid to create turbulence. Heat transfer therefore follows the laws of convection for liquid films. - The assumption of little relative motion is also based on the observations of Richkov and Pospelov and of Karetnikov, who report that the bubbles float downwards at the same velocity as the liquid.
- 3) There are not enough bubbles to destroy the essentially liquid texture of the film; for heat transfer calculations, the physical properties of the film are those of the liquid phase.
- 4) There are, however, sufficient bubbles so that the liquid temperature at the vapor core interface is determined by the bubble superheat.
- 5) The bubble diameters are of the same order of magnitude as the film thickness.
- 6) The bubble surface is spherical in shape, at least near the vapor core interface.

The model does not contain any suggestions regarding the form, temperature and pressure of that part of the bubble that is close to the wall. Neither does it contain any assumption regarding what fraction of the vapor enters the core by evaporation of the plane interface, and what fraction enters the core due to the emergence and bursting of bubbles.

Transfer of vapor does not necessarily have to occur solely by bubble bursting, because according to the model the liquid at the plane interface is superheated, and will spontaneously form superheated vapor of the same temperature and pressure. This constitutes a driving force that forces the liquid to lose enthalpy to the vapor core.

The thermodynamics of this statement are readily illustrated by the temperature-entropy diagram, Figure 9. The T-S curve is that of the (plane-surface) vapor-liquid equilibrium of a salt solution having a BPR of 2.03°F.

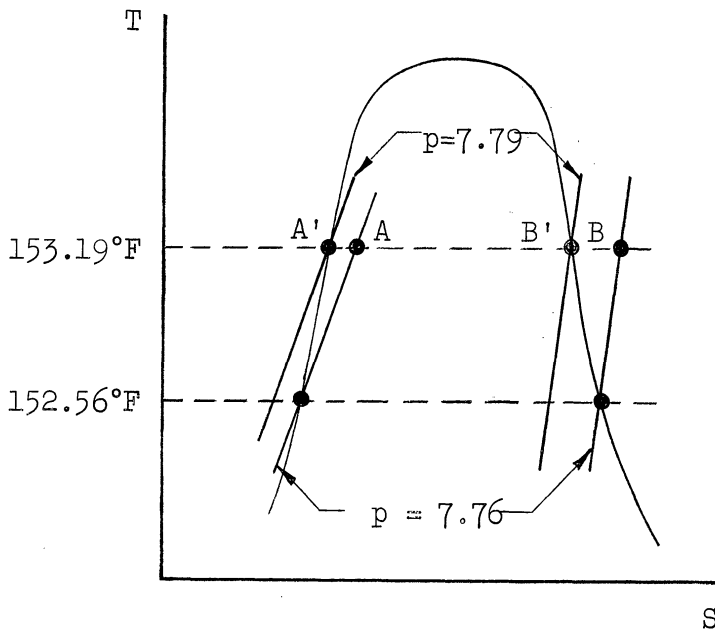


Figure 9.

Point A represents the condition of the (superheated) liquid near the plane interface with the gas core; point B represents the condition of the (superheated) vapor in the core. We have the following relationships in terms of F , the free energy:

$$F_{B'} - F_{A'} = 0 \quad (\text{equilibrium})$$

$$F_B - F_{B'} = \int_{7.79}^{7.67} v_g dp \quad (\text{reversible isothermal single-phase expansion})$$

$$F_A - F_{A'} = \int_{7.79}^{7.67} v_l dp \quad (\text{reversible isothermal single-phase expansion})$$

$$\therefore \Delta F = F_B - F_A = \int_{7.79}^{7.67} (v_g - v_l) dp < 0 \quad (\text{spontaneous process})$$

Hence superheated liquid (A) is spontaneously transformed into superheated vapor (B).

The proposed model is necessarily limited by assumptions 1) to 6), all of which are postulated without there being any experimental proof of their validity. It must be emphasized, therefore, that this is by no means the only possible model for falling-film evaporative heat transfer. However, the present model appears to be thermodynamically sound, and is shown in the next Section to yield a satisfactory prediction of heat transfer coefficients under widely varying operating condition.

SECTION VIII

PREDICTION OF OVERALL HEAT TRANSFER COEFFICIENTS
FOR RUNS WITH ZERO FEED SUPERHEAT
FROM THEORETICAL MODEL

INTRODUCTION

Overall heat transfer coefficients were predicted for all combinations of operating conditions that were actually tested in our experimental work for runs at zero feed superheat.

In order to calculate the overall coefficients, the tube-side temperature drops were predicted from our theoretical model; the steam-side temperature drops were predicted from the experimental results of Baker, Kazmark and Stroebe and from the recommendation of McAdams.

It was found that overall heat transfer coefficients thus estimated agreed within 10% with those measured in our experimental work.

CALCULATION OF STEAM-SIDE TEMPERATURE DROP

In heat transfer studies it is usual to measure the wall temperature directly, chiefly by means of thermocouples. These give readings with a scatter of $\pm 0.5\%$, say, for good operation. For our runs, however, this degree of scatter would have meant a scatter in liquor-side film coefficient of up to $\pm 65\%$, not counting scatter from any other source. This is due to the unusually low temperature differences encountered in falling-film LTV evaporation. - In addition, the installation and operation of thermocouples would have presented problems of a practical nature for which the pilot plant was not equipped.

Another possibility was the experimental determination of the steam-side film coefficient by means of a Wilson plot. Steam condensate Reynolds numbers ranged from ca. 200 to ca. 1,500. At these very low steam rates it proved impossible to determine the steam-side coefficient in this manner, since temperature drops at the hot end of the tube became immeasurably small. This was predicted by calculation and proved in an experimental attempt to make a Wilson-type determination.

The only alternative was to estimate the temperature drop through the condensate and the tube wall. Little dropwise condensation of steam could have taken place because the tubes had been in continuous operation for weeks or months before these tests took place; because no oily layer was ever observed in the steam-condensate drip tank; because the tube metals used do not tend to promote dropwise condensation as does, say, stainless steel; because the outside of the tubes before,

during and after the tests never showed any trace of oil; because no time trends in overall heat transfer coefficient were ever observed; because of the excessive continuous venting of the steam chest; and because the steam condensate passed through 2 vertical storage tanks before returning to the boiler, whose main consumer of steam was our pilot plant.

For such cases, McAdams* recommends the use of a film coefficient 28% higher than that obtained from the Nusselt correlation with the same Reynolds number. - Dukler** has recently presented a correlation that we have found to fall within $\pm 7\%$ of that of McAdams. - The curves in Graph 9 were constructed according to the McAdams recommendation and were used to determine the steam-side temperature drop for each set of readings. This recommendation is particularly applicable to the LTV, as shown by Baker, Kazmark and Strobe⁽¹⁾ in 1939. Their tests were conducted on a single-tube LTV consisting of a 2-in. tube 20 ft long. Tube wall temperatures were determined with thermocouples embedded at intervals of 1 ft. In the particular region of interest, namely, $(Re) < 900$, the steam-side heat transfer coefficients averaged 1.28 times the Nusselt correlation; see Appendix F for a discussion of the scatter in Δt_{stm} .

CALCULATION OF TUBE-WALL TEMPERATURE DROP

The temperature drops through the tube walls were determined as follows:

* See page 49.

** See page 53.

a) 2-in. tubes: 7 2-in. 12 BWG x 24'-0" tubes:

<u>No. of tubes</u>	<u>Material</u>	<u>k, Btu/(hr)(ft)(°F)</u>
2	Aluminum brass	58
2	Copper	200
1	Ampco grade 8	43
1	Admiralty	64
1	90-10 Cupronickel	26

Average conductivity (arithmetic mean): 92.7 Btu/(hr)(ft)(°F)

Log-mean diameter: 1.895 in.

Temperature drop, °F: $1.177 \times 10^{-6} Q$, where Q is the total LTV heat load, in Btu/hr (i.e., not the load per tube).

b) 1-in. tubes: 7 1-in. 16 BWG x 24'-0" tubes:

<u>No. of tubes</u>	<u>Material</u>	<u>k, Btu/(hr)(ft)(°F)</u>
3	Aluminum brass	58
2	Copper	200
1	Admiralty	64
1	90-10 Cupronickel	26

Average conductivity: 94.9 Btu/(hr)(ft)(°F)

Log-mean diameter: 0.932 in.

Temperature drop, °F: $1.39 \times 10^{-6} Q$

The tube-wall temperature drops turned out to be so small, even when compared to the steam-side and liquor-side temperature drops, that the effect of using mixed tube bundles on the distribution of the heat load among the 7 tubes was insignificant.*

* The purpose of installing mixed tube bundles was to make simultaneous corrosion studies on different tube metals.

CALCULATION OF OVERALL HEAT TRANSFER COEFFICIENT

The overall heat transfer coefficient is calculated by dividing the heat flux Q/A by the overall temperature difference ($\Delta t_{stm} + \Delta t_w + \Delta t_{corr}$). This is best illustrated by a typical calculation; again, take the first set of data of run CI-1, Appendix A, as example.

h_{stm} , the steam-side heat transfer coefficient, is read from Graph No. 9:

$$\underline{1,089 \text{ Btu}/(\text{hr})(\text{sq ft})(\text{ }^\circ\text{F})}$$

Δt_{stm} , the mean temperature drop through the condensate layer, is calculated by dividing the heat load Q , 458,000 Btu/hr, by h_{stm} and the outer tube surface, 87.9 sq ft: 4.78 $^\circ\text{F}$

Δt_w , the temperature drop through the metal tube wall, is calculated as $1.177 \times 10^{-6} Q$: 0.54 $^\circ\text{F}$

U_{VH} , the overall coefficient, is calculated by dividing Q , 458,000 Btu/hr, by the inner tube surface, 78.3 sq ft, and by the overall temperature difference, $4.78 + 0.54 + 5.46 = 10.78 \text{ }^\circ\text{F}$:

$$\underline{542 \text{ Btu}/(\text{hr})(\text{sq ft})(\text{ }^\circ\text{F})}$$

COMPARISON OF THEORETICAL MODEL WITH EXPERIMENTAL RESULTS

Table XIV shows the comparison of the values for the experimentally obtained heat transfer coefficients and the values predicted from our theoretical model for U_{VH} in the 2-in. tubes. It is interesting to observe that there is agreement with a maximum deviation of 10%, except for the two runs whose results are in parentheses. These two runs are the very same ones whose experimental values were considered to be definitely too high, from an analysis of the experimental data alone

(see page 88). Our theoretical model corroborates this; the error in the two runs is probably due to experimental error, therefore, and cannot be ascribed to a defect in the theoretical model.

Feed rate	1,500				3,000		6,000			
Steam rate	250		450		250	450	250		450	
Conc. factor	1	2	1	2	1	1	1	2	1	2
VH sat. temp.	<u>Experimental Values of U_{VH}</u>									
100	314		305		327	315	329		327	
125			373			404			428	
150	445	464	472	435		460	565	498	520	500
175			491			527			574	
200			530			576			656	
230	645	702	621	573		641	(868)	774	(794)	745
	<u>Theoretical Values of U_{VH}</u>									
100	291		297		326	317	363		362	
125			392			431			469	
150	471	471	470	465		513	571	529	551	548
175			530			566			607	
200			578			615			656	
230	650	650	623	629		659	759	749	694	698
	<u>% Deviation</u>									
100	-8		-3		-0	+1	+9		+10	
125			+5			+6			+9	
150	+6	+2	-0	+7		+10	+1	+6	+6	+9
175			+7			+7			+5	
200			+8			+6			0	
230	+1	-8	+0	+9		+3	(-14)	-3	(-14)	-7

TABLE XIV

Table XV compares the experimental values of U_{VH} in the 1-in. tubes with those derived from the theoretical model. For some runs, deviation between experiment and theory is higher than with the 2-in. tubes. This is because pressure-drop dominates the whole picture. Take, for example, the first set of readings of run LWDA-12. Here, Δt_{corr} is $13.80^{\circ} F.$, of which $8.70^{\circ} F$ are accounted for by pressure-drop alone (the rest is made up of $\Delta t_f = 4.61^{\circ} F$, and a bubble superheat of $0.49^{\circ} F$). For tubes as narrow as these, then, a good two-phase pressure-drop prediction is far more important than a good heat transfer prediction, and the % deviation of Table XV is a test of the pressure-drop accuracy rather than of our falling-film heat transfer model.

The test enclosed in parentheses is the same one whose experimental value is evidently too high (see page 94). - Also, the runs with 150 lb/hr steam have little significance, since adequate control at this low steam rate was impossible in our experiments.

Except for the runs mentioned in the previous paragraph, whose experimental values are unreliable, our theoretical model predicts U_{VH} for the 1-in. tubes with a maximum deviation of 9%.

Figure 8 shows the agreement between theory and experiment in graphical form, for both 2-in. and 1-in. tubes. It refers to all runs with saturated feed.

Feed rate	1,500		3,000	
Steam rate	150	250	150	250
Conc. factor	1	1	1	1
VH sat. temp.	<u>Exptl. U_{VH}</u>			
100	191	172	177	162
125		267		231
150	391	381	350	319
175		494		436
200		626		529
230	652	(773)	599	643
	<u>Theor. U_{VH}</u>			
100	200	174	202	158
125		265		237
150	466	374	486	335
175		473		446
200		608		580
230	707	671	769	712
	<u>% Deviation</u>			
100	+5	1	+12	-2
125		-1		+3
150	+16	-2	+28	+5
175		-4		+2
200		-3		+9
230	+8	(-13)	+22	+10

TABLE XV

CORRELATION OF U_{VH}

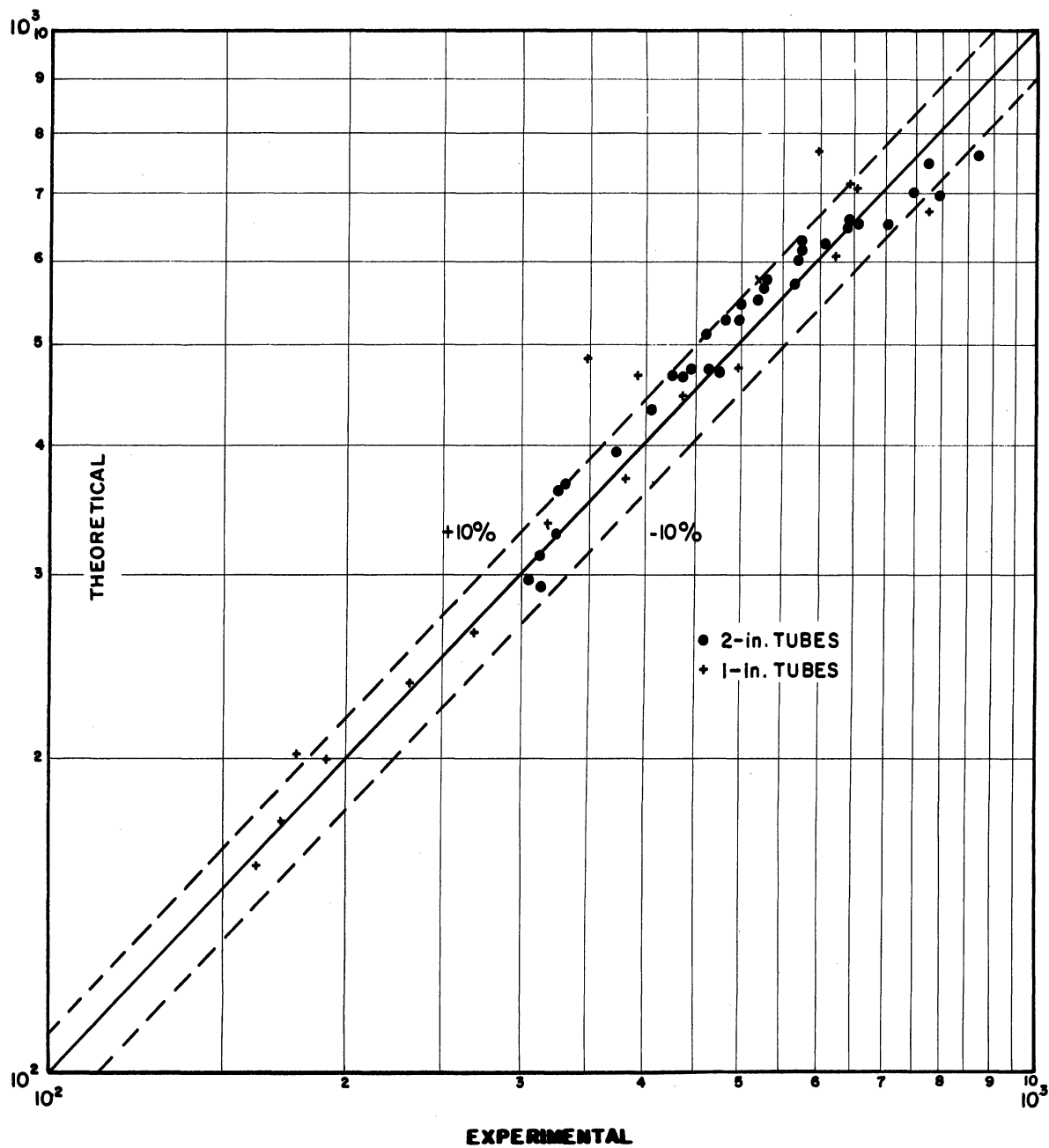


Figure 10

A more stringent test of the model is the prediction of the liquid-side heat transfer coefficient. The predicted value of h_{VH} can be compared with experimental values; although the latter were not measured directly, they can be computed by taking

$$\frac{1}{h_{VH} \text{ exptl.}} = \frac{1}{U_{VH} \text{ exptl.}} - \left(\frac{A_{stm}/A_f}{h_{stm}} \right) - \left(\frac{A_w/A_f}{h_{wall}} \right)$$

Table XVI and XVII show the comparison for 2-in. and 1-in. tubes, respectively; agreement is generally within 20%. Figure 11 illustrates the correlation of predicted with measured values of the experimental h_{VH} .

Feed rate	1,500				3,000		6,000			
Steam rate	250		450		250	450	250		450	
Conc. factor	1	2	1	2	1	1	1	2	1	2
VII sat. temp.	Experimental Values of h_{VH}									
100	438		447		462	470	482		492	
125			583			665			738	
150	683	690	824	719		777	1025	925	998	918
175			854			967			1148	
200			928			1095			1431	
230	1147	1221	1161	1004		1289	(2100)	1591	(2125)	1813
	Theoretical Values of h_{VH}									
100	398		430		460	475	543		577	
125			632			743			867	
150	747	707	818	802		942	1047	1040	1124	1092
175			978			1110			1283	
200			1088			1245			1431	
230	1160	1151	1220	1170		1361	1524	1487	1529	1557
	% Deviation									
100	-10		-4		-0	+1	+11		+15	
125			+8	+10		+11			+15	
150	+9	+2	-1			+18	+2	+11	+11	+16
175			+13			+13			+11	
200			+15			+12			0	
230	+1	+6	+5	+14		+5	(-38)	-7	(-39)	-16

TABLE XVI

Feed rate	1,500		3,000	
Steam rate	150	250	150	250
Conc. factor	1	1	1	1
VH sat. temp.	<u>Exptl. h_{VH}</u>			
100	229	205	209	191
125		354		291
150	560	572	488	442
175		839		685
200		1246		904
230	1135	(1821)	979	1258
	<u>Theor. h_{VH}</u>			
100	242	208	245	185
125		350		301
150	727	558	799	471
175		776		709
200		1178		1060
230	1311	1343	1529	1549
	<u>% Deviation</u>			
100	+5	-1	+15	-3
125		-1		+3
150	+23	-3	+39	+6
175		-8		+3
200		-6		+15
230	+13	(-36)	+36	+19

TABLE XVII

CORRELATION OF h_{VH}

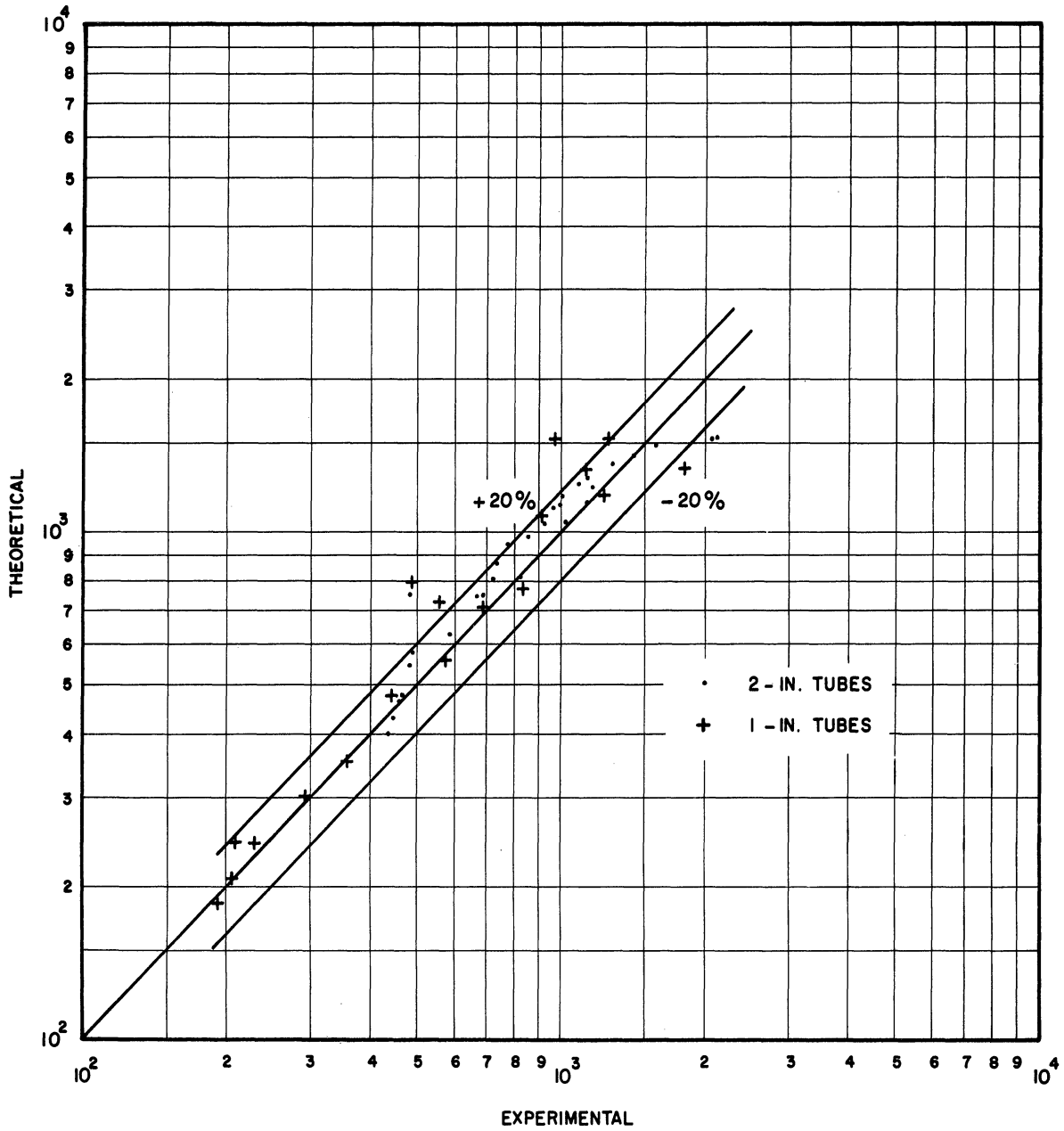


Figure 11

SECTION IX

THEORETICAL ANALYSIS OF RESULTS FOR TESTS WITH 20°F FEED SUPERHEAT

The test results show that the overall heat transfer coefficients for runs with 20°F feed superheat are always somewhat lower than the corresponding runs with zero feed superheat.

The only possible explanation for this unforeseen result is, that flashing at the tube entrance produces such linear velocities that falling-film flow is only established a few feet further down. - The ease with which falling-film flow is destroyed due to high local vaporization rates is quoted by Karetnikov (page 79), Richkov and Pospelov (page 80), and Mueller (page 81); it is attributed to the absence of any force (except surface tension) that would bring the fluid back to the tube wall once it leaves it.

The theoretical model for the runs with 20°F feed superheat is then as follows. The feed flashes, and falling-film flow is only established a few feet further down. At this point the feed has lost all its superheat, and proceeds downwards with evaporative heat transfer just as the corresponding runs with zero feed superheat. - Heat transfer occurs only where there is falling-film flow.

Breaking down the overall heat transfer resistance into its steam-side, wall, and falling-film components is out of place here, because we do not know the square footage of actual heat transfer surface. This latter quantity is the only unknown magnitude, and it determines the difference between the results of any run and the results of the corresponding run with zero feed superheat.

If the tube length taken up by the flashing could be calculated, it could be subtracted from the total tube length to yield the actual heat transfer length. Unfortunately, too little is known concerning the exact mechanism of flashing. The problem is exceedingly complex; it involves inertial, viscous, and surface forces; a separate long-range research would be necessary to study it.

In order to get an approximate idea of the flash lengths involved, we have divided the overall heat transfer coefficients by the theoretical values of U_{VH} for the zero-superheat runs. The quotients, expressed as %, will then give the percentage of the total tube length where actual heat transfer takes place, i.e., where falling-film flow exists. These values are given in Table XVI for 2-in. tubes, and in Table XVII for 1-in. tubes.

Feed rate	1,500				3,000		6,000			
Steam rate	250		450		250	450	250		450	
Conc. factor	1	2	1	2	1	1	1	2	1	2
VH sat. temp.										
100	70	101	102		90	92	82	84	72	
125			97				91		83	
150	89	93	94	91			87	82	91	87 86
175			89				88		87	
200			96				91		90	
230	91	93	96	93			94	97	92	101 93

TABLE XVIII

Feed rate	1,500		3,000		
Steam rate	150	250		150	250
Conc. factor	1	1	2	1	1
VH sat. temp.					
100	81	88	92	64	87
125		92			80
150	79	97		58	84
175		102			91
200		100			99
230	93	102		82	95

TABLE XIX

Control of the feed temperature, and hence superheat, was not always as accurate as might have been desired. Despite this, and despite the wide variations of tube diameter and all other variables between runs, the figures in Tables XVI and XVII are remarkably alike. With very few exceptions they amount to ca. 90%. This means that flashing takes place in the top 2-3 ft., the rest of the tube being heat-transfer area. One can therefore predict U_{VH} for the runs with 20° F superheat by calculating U_{VH} for saturated feed and considering the tube shorter by 2-3 ft. from its real length.

APPENDIX A

EXPERIMENTAL DATA AND CALCULATIONS, COLUMNS 1-14

THEORETICAL PREDICTIONS, COLUMNS 15-33

RUNS LWCI-1 TO LWCI-32

2-in. Tubes, CI Series, Zero Feed Superheat

Run No. (1)	VH sat. temp. °F (2)	VH press. in. Hg (3)	Feed rate lb/hr (4)	Vapor rate lb/hr (5)	Ave. flow lb/hr (6)	BD Cl gpl (7)	Feed Cl gpl (8)	Ave. Cl gpl (9)	Steam rate lb/hr (10)	Qx10 ⁻³ Btu/hr (11)	Stm. sat. temp. °F (12)	BPR °F (13)	EXPTL UvH Btu/ft ² -hr-°F (14)	μ lb/hr-ft (15)	(Re) (16)	(Pr) (17)
CI- 1	<u>150</u>		<u>6,000</u>				<u>40</u>		<u>450</u>							
	150.22	7.61	5,857	457	5,628	44.77	40.97	42.87	447	458.0	163.83	2.03	505	1.17	5,900	2.88
	150.22	7.60	6,251	444	6,029	37.29	34.60	35.95	445	451.1	163.55	1.69	495	1.14	6,485	2.83
CI- 2	<u>150</u>		<u>1,500</u>				<u>20</u>		<u>450</u>							
	150.16	7.60	1,510	453	1,283	29.31	20.79	25.05	439	448.1	163.55	1.17	468	1.10	1,430	2.78
	150.27	7.62	1,505	462	1,274	29.68	20.93	25.31	446	456.3	163.75	1.19	475	1.10	1,417	2.78
CI- 4	<u>150</u>		<u>1,500</u>				<u>40</u>		<u>250</u>							
	150.01	7.57	1,519	249	1,395	46.87	39.55	43.21	246	247.4	158.98	2.04	474	1.18	1,448	2.91
	150.16	7.60	1,496	243	1,374	46.87	39.55	43.21	237	238.6	158.94	2.04	453	1.18	1,428	2.91
CI- 5	<u>230</u>		<u>1,500</u>				<u>20</u>		<u>250</u>							
	230.13		1,477	258	1,348	25.33	20.88	23.11	264	241.2	236.48	1.42	625	0.68	2,425	1.58
	230.08	42.41	1,483	251	1,357	25.15	20.90	23.03	257	234.8	236.01	1.42	665	0.68	2,442	1.58
CI- 6	<u>150</u>		<u>6,000</u>				<u>20</u>		<u>250</u>							
	150.11	7.59	5,865	256	5,737	21.26	20.41	20.84	252	254.2	156.72	0.98	577	1.10	6,380	2.80
	149.73	7.52	6,279	331	6,114	22.10	21.07	21.59	285	289.3	157.41	1.01	553	1.11	6,750	2.80
CI- 8	<u>230</u>		<u>6,000</u>				<u>20</u>		<u>450</u>							
	229.98	42.29	6,085	442	5,864	22.54	21.07	21.81	447	417.3	237.89	1.34	811	0.67	9,220	1.58
	230.06	42.36	5,968	436	5,750	22.18	20.96	21.57	442	411.8	238.18	1.34	776	0.67	9,030	1.58
CI-14	<u>230</u>		<u>1,500</u>				<u>40</u>		<u>450</u>							
	229.91	42.24	1,662	362	1,481	50.83	40.14	45.49	353	325.0	240.22	2.92	562	0.74	2,455	1.67
	229.89	42.22	1,649	356	1,471	48.93	40.78	44.86	362	333.6	240.05	2.86	583	0.74	2,439	1.67
CI-16	<u>230</u>		<u>6,000</u>				<u>40</u>		<u>250</u>							
	229.92	42.25	6,212	236	6,094	40.02	38.76	39.39	245	222.9	236.04	2.47	780	0.73	10,220	1.68
	230.03	42.36	6,244	229	6,129	41.05	39.71	40.38	245	222.8	236.27	2.53	768	0.73	10,290	1.68
CI-18	<u>150</u>		<u>1,500</u>				<u>20</u>		<u>250</u>							
	149.90	7.55	1,542	268	1,408	24.52	20.50	22.51	260	258.6	158.36	1.06	447	1.10	1,568	2.79
	150.00	7.57	1,520	270	1,385	25.07	20.42	22.75	259	260.0	158.58	1.07	442	1.10	1,541	2.79
CI-21	<u>150</u>		<u>6,000</u>				<u>20</u>		<u>450</u>							
	150.32	7.63	6,395	500	6,145	21.20	20.00	20.60	490	499.1	163.43	0.97	525	1.09	6,900	2.77
	150.27	7.62	5,879	468	5,645	22.18	20.40	21.29	444	450.8	162.49	1.00	514	1.09	6,345	2.77
CI-23	<u>230</u>		<u>1,500</u>				<u>40</u>		<u>250</u>							
	230.08	42.37	1,527	238	1,408	34.52	29.58	32.05	251	227.9	236.25	2.00	697	0.69	2,500	1.62
	230.14	42.42	1,523	236	1,405	34.12	29.62	31.87	252	228.7	236.25	1.98	707	0.69	2,495	1.62
CI-24	<u>230</u>		<u>1,500</u>				<u>20</u>		<u>450</u>							
	229.94	42.26	1,540	439	1,320	28.03	21.17	24.60	445	412.8	239.95	1.53	622	0.66	2,450	1.57
	229.77	42.13	1,545	440	1,325	27.95	20.96	24.46	443	411.0	239.75	1.52	620	0.66	2,460	1.57
CI-26	<u>230</u>		<u>6,000</u>				<u>20</u>		<u>250</u>							
	230.15	42.43	5,880	243	5,766	21.55	20.53	21.04	237	215.6	234.62	1.30	878	0.67	10,540	1.58
	230.11	42.40	5,950	245	5,827	21.55	20.57	21.06	244	222.2	234.72	1.30	858	0.67	10,650	1.58
CI-29	<u>230</u>		<u>6,000</u>				<u>40</u>		<u>450</u>							
	230.23	42.49	6,107	438	5,888	31.52	29.44	30.48	457	424.7	239.46	1.90	740	0.70	10,300	1.62
	230.24	42.50	6,015	443	5,793	31.55	29.36	30.46	456	423.7	239.35	1.90	750	0.70	10,120	1.62
CI-30	<u>150</u>		<u>1,500</u>				<u>40</u>		<u>450</u>							
	150.27	7.62	1,515	472	1,279	55.20	38.38	46.79	454	459.3	166.08	2.26	432	1.17	1,339	2.87
	150.27	7.62	1,519	471	1,284	55.20	38.38	46.79	458	464.1	166.04	2.26	438	1.17	1,344	2.87
CI-32	<u>150</u>		<u>6,000</u>				<u>40</u>		<u>250</u>							
	150.06	7.58	6,244	258	6,115	34.57	33.36	33.97	256	256.5	158.22	1.60	500	1.15	6,510	2.88
	149.95	7.56	6,180	256	6,052	34.58	33.20	33.89	256	256.3	158.18	1.60	495	1.15	6,450	2.88

2-1a. Tubes, CI Series, Zero Feed Superheat (Cont'd.)

(18)	(19)	(20)	(21)	(22)	(23)	(24)	(25)	(26)	(27)	(28)	(29)	(30)	(31)	(32)	(33)
h_f/ϕ	ϕ	χ	$B \left(\frac{p^2 g}{\mu^2} \right)^{1/3}$	Δp	P_v	$4\sigma/B$	$f(P_v + \frac{H\sigma}{B})$	t_v	h_f	Δt_a	Δt_{corr}	t_{stim2}	Δt_{stim}	Δt_v	U_{FM}
	Btu/ft ² -hr-°F	in. Hg		in. Hg	in. Hg	in. Hg		°F	Btu/ft ² -hr-°F	°F	°F	Btu/ft ² -hr-°F	°F	°F	Btu/ft ² -hr-°F
0.319 0.323	4,060 4,130	2.83 2.84	23.4 24.6	0.06 0.05	7.67 7.65	0.12 0.12	151.16 151.06	153.19 152.75	1,295 1,332	4.52 4.33	5.46 5.17	1,089 1,090	4.78 4.71	0.54 0.53	542 554
0.252 0.252	4,220 4,210	2.88 2.88	11.7 11.7	0.06 0.06	7.66 7.68	0.25 0.25	151.78 151.89	152.95 153.08	1,062 1,060	5.38 5.50	7.00 7.12	1,090 1,097	4.67 4.75	0.53 0.54	469 470
0.257 0.257	3,980 3,980	2.82 2.82	11.8 11.7	0.02 0.02	7.59 7.62	0.24 0.24	151.37 151.52	153.41 153.56	1,022 1,022	3.09 2.98	4.45 4.34	1,312 1,377	2.14 1.96	0.29 0.28	478 464
0.207 0.207	6,260 6,260	3.53 3.53	14.9 14.9	-0.02 -0.02	42.39 42.35	0.24 0.24	230.40 230.35	231.82 231.77	1,297 1,297	2.38 2.32	2.65 2.59	1,518 1,530	1.81 1.75	0.28 0.28	650 650
0.321 0.325	4,180 4,180	2.85 2.85	24.4 25.2	0.02 0.03	7.61 7.55	0.12 0.11	150.85 150.48	151.83 151.49	1,340 1,359	2.42 2.72	3.16 3.47	1,293 1,243	2.24 2.64	0.30 0.34	570 572
0.254 0.253	6,250 6,270	3.52 3.53	30.0 29.7	-0.01 -0.01	42.28 42.35	0.12 0.12	230.11 230.20	231.45 231.54	1,588 1,587	3.36 3.32	3.49 3.46	1,276 1,280	3.72 3.66	0.49 0.48	696 692
0.213 0.213	5,980 5,980	3.45 3.45	15.0 14.9	-0.01 -0.01	42.23 42.21	0.23 0.23	230.19 230.18	233.11 233.04	1,272 1,272	3.26 3.35	3.54 3.64	1,388 1,373	2.67 2.76	0.38 0.39	630 627
0.269 0.269	5,980 5,980	3.44 3.44	31.9 32.0	-0.01 -0.01	42.24 42.35	0.11 0.11	230.05 230.19	232.52 232.72	1,609 1,609	1.77 1.77	1.90 1.93	1,557 1,558	1.63 1.63	0.26 0.26	751 746
0.255 0.255	4,200 4,200	2.86 2.86	12.2 12.1	0.02 0.02	7.57 7.59	0.23 0.24	151.21 151.37	152.27 152.44	1,070 1,070	3.09 3.10	4.40 4.47	1,287 1,287	2.29 2.30	0.30 0.31	472 469
0.325 0.318	4,240 4,230	2.87 2.87	25.6 24.3	0.07 0.06	7.70 7.68	0.11 0.12	151.26 151.21	152.23 152.21	1,379 1,344	4.62 4.29	5.56 5.23	1,056 1,088	5.38 4.72	0.59 0.53	552 550
0.210 0.210	6,130 6,130	3.47 3.47	15.0 15.0	-0.01 -0.01	42.36 42.41	0.23 0.23	230.35 230.41	232.35 232.39	1,288 1,288	2.26 2.27	2.53 2.54	1,541 1,541	1.68 1.69	0.27 0.27	650 650
0.207 0.207	6,310 6,310	3.54 3.54	15.0 15.0	-0.01 -0.01	42.25 42.12	0.24 0.24	230.23 230.06	231.76 231.58	1,308 1,308	4.03 4.01	4.32 4.30	1,280 1,283	3.67 3.65	0.49 0.48	622 623
0.261 0.262	6,260 6,260	3.52 3.52	33.2 33.5	-0.01 -0.01	42.42 42.39	0.11 0.11	230.28 230.24	231.58 231.54	1,635 1,641	1.68 1.73	1.81 1.86	1,570 1,557	1.56 1.63	0.25 0.26	760 757
0.264 0.263	6,120 6,120	3.47 3.47	32.0 31.7	-0.01 -0.01	42.48 42.49	0.11 0.11	230.35 230.36	232.25 232.26	1,617 1,610	3.35 3.36	3.47 3.48	1,274 1,274	3.79 3.78	0.50 0.50	699 697
0.253 0.253	4,080 4,080	2.83 2.83	11.4 11.4	0.06 0.06	7.68 7.68	0.25 0.25	151.89 151.89	154.15 154.15	1,032 1,032	5.67 5.74	7.29 7.36	1,092 1,092	4.78 4.83	0.54 0.55	464 465
0.326 0.325	4,080 4,080	2.80 2.80	24.7 24.5	0.02 0.02	7.60 7.58	0.11 0.11	150.74 150.64	152.34 152.24	1,330 1,326	2.46 2.47	3.14 3.16	1,062 1,062	2.75 2.75	0.30 0.30	530 528

2-in. Tubes, CI Series, 200° F Feed Superheat

Run No.	VH sat. temp. °F	VH press. in. Hg	Feed rate lb/hr	Vapor rate lb/hr	ND Cl gpl	Feed Cl gpl	Ave. Cl gpl	Feed super-heat °F	Stm. rate lb/hr	Q x 10 ⁻³ Btu/hr	Stm. sat. temp. °F	Δt _o A _{app} °F	BPR °F	Δt _o A _{corr} °F	U _{VH} Btu/ft ² -hr-°F
CI- 3	<u>230</u>		<u>6,000</u>			<u>20</u>		<u>20</u>	<u>250</u>						
	230.15	42.43	5,983	369	22.27	20.91	21.59	20.2	242	219.6	235.27	5.12	1.34	3.78	741
	229.97	42.28	6,040	374	22.08	20.55	21.32	20.0	245	222.1	235.16	5.19	1.32	3.87	733
CI- 7	<u>150</u>		<u>1,500</u>			<u>40</u>		<u>20</u>	<u>450</u>						
	149.74	7.52	1,531	476	43.05	29.68	36.37	21.9	440	441.5	164.83	15.09	1.73	13.36	422
CI- 9	<u>230</u>		<u>1,500</u>			<u>20</u>		<u>20</u>	<u>450</u>						
	229.89	42.22	1,437	477	30.23	20.57	25.40	18.6	450	420.3	240.49	10.60	1.59	9.01	596
	229.86	42.20	1,552	465	30.10	20.84	25.47	21.3	443	411.0	240.15	10.29	1.59	8.70	604
CI-10	<u>230</u>		<u>1,500</u>			<u>40</u>		<u>20</u>	<u>250</u>						
	230.40	42.63	1,460	240	39.83	33.80	36.82	16.0	250	227.2	237.45	7.05	2.31	4.74	612
	230.59	42.78	1,453	256	39.10	33.08	36.09	19.3	252	225.8	237.65	7.06	2.26	4.22	600
CI-11	<u>150</u>		<u>6,000-</u>			<u>40</u>		<u>20</u>	<u>250</u>						
	150.22	7.61	6,029	364	33.54	31.39	32.47	18.0	254	254.9	158.54	8.32	1.53	6.79	480
CI-12	<u>230</u>		<u>6,000</u>			<u>40</u>		<u>20</u>	<u>450</u>						
	229.80	42.15	5,763	589	35.42	31.83	33.63	22.6	455	423.3	240.30	10.50	2.12	8.38	645
	229.91	42.24	5,725	565	35.17	31.88	33.53	18.2	463	430.7	240.51	10.60	2.11	8.49	649
CI-13	<u>150</u>		<u>6,000</u>			<u>20</u>		<u>20</u>	<u>450</u>						
	150.32	7.63	5,880	535	22.37	20.38	21.38	23.4	386	390.5	161.99	11.67	1.01	10.66	468
	150.27	7.62	5,908	536	22.31	20.36	21.34	24.2	386	390.2	161.91	11.64	1.01	10.63	468
CI-15	<u>150</u>		<u>1,500</u>			<u>20</u>		<u>20</u>	<u>250</u>						
	149.68	7.51	1,587	295	24.35	20.30	22.33	21.5	267	264.5	158.94	9.26	1.05	8.21	412
	149.90	7.55	1,601	321	24.35	20.30	22.33	26.6	280	279.3	159.38	9.48	1.05	8.43	423
CI-17	<u>230</u>		<u>1,500</u>			<u>20</u>		<u>20</u>	<u>250</u>						
	229.73	42.10	1,421	262	24.71	20.41	22.56	19.4	244	221.5	235.95	6.22	1.40	4.82	586
	229.73	42.10	1,424	259	24.74	20.38	22.56	19.3	241	218.9	235.84	6.11	1.40	4.71	594
CI-19	<u>230</u>		<u>1,500</u>			<u>40</u>		<u>20</u>	<u>450</u>						
	229.96	42.28	1,518	485	40.50	27.56	34.03	19.2	457	423.5	241.29	11.33	2.15	9.18	589
	229.90	42.23	1,528	493	39.31	26.50	32.92	19.2	459	426.1	241.30	11.40	2.09	9.31	585
CI-20	<u>150</u>		<u>1,500</u>			<u>40</u>		<u>20</u>	<u>250</u>						
	150.01	7.57	1,586	289	38.55	32.01	35.28	17.6	254	253.9	158.94	8.93	1.67	7.26	446
	150.32	7.63	1,553	286	36.73	31.55	34.14	-17.9	254	253.7	159.47	9.15	1.61	7.54	430
CI-22	<u>150</u>		<u>1,500</u>			<u>20</u>		<u>20</u>	<u>450</u>						
	150.22	7.61	1,556	514	32.81	22.31	27.56	15.7	478	481.9	165.46	15.24	1.32	13.92	442
	150.11	7.59	1,570	510	32.81	22.32	27.57	16.8	475	478.1	165.30	15.19	1.32	13.87	440
CI-25	<u>230</u>		<u>6,000</u>			<u>20</u>		<u>20</u>	<u>450</u>						
	230.30	42.55	6,049	551	22.58	20.87	21.73	19.6	438	407.5	239.06	8.76	1.35	7.41	702
	230.24	42.50	5,973	545	22.97	20.83	21.90	19.8	437	406.6	239.04	8.80	1.36	7.44	699
CI-27	<u>150</u>		<u>6,000</u>			<u>20</u>		<u>20</u>	<u>250</u>						
	149.73	7.52	6,265	418	22.10	20.36	21.23	20.9	282	283.8	158.31	8.58	1.00	7.58	478
	149.41	7.46	6,257	395	22.10	20.36	21.23	21.5	257	257.9	157.22	7.81	1.00	6.81	483
CI-28	<u>230</u>		<u>6,000</u>			<u>40</u>		<u>20</u>	<u>250</u>						
	230.48	42.69	6,022	352	34.07	32.47	33.27	19.9	244	222.4	236.74	6.26	2.08	4.18	680
	230.49	42.70	5,995	346	34.00	31.96	32.98	19.0	243	220.3	236.60	6.11	2.06	4.05	695
CI-31	<u>150</u>		<u>6,000</u>			<u>40</u>		<u>20</u>	<u>450</u>						
	150.16	7.60	6,250	550	38.45	35.18	36.82	20.6	444	449.4	164.08	13.92	1.76	12.16	471
	150.00	7.57	6,251	551	38.45	35.18	36.82	20.9	442	447.4	163.95	13.95	1.76	12.19	469

APPENDIX B

EXPERIMENTAL DATA AND CALCULATIONS, COLUMNS 1-14

THEORETICAL PREDICTIONS, COLUMNS 15-33

RUNS LWCJ-1 TO LWCJ-16

2-in. Tubers, C2 Series, Zero Feed Supplement

(1)	(2)	(3)	(4)	(5)	(6)	(7)	(8)	(9)	(10)	(11)	(12)	(13)	(14)	(15)	(16)	(17)	(18)	(19)	(20)	(21)	(22)	(23)	(24)	(25)	(26)	(27)	(28)	(29)	(30)	(31)	(32)	(33)
Run No.	VII Sls. Temp. °F	VII Sls. In. Hg	Feed Rate 20/HR	Wagon Rate 20/HR	Avg. Flow 20/HR	SD Cl. 1	Feed Cl. Ave. 20/HR	Cl. Steam Rate 20/HR	Q20/3 20/HR	Q20/3 20/HR	Wt. Me. 20/HR	Wt. Me. 20/HR	Wt. Me. 20/HR	Wt. Me. 20/HR	Wt. Me. 20/HR	Wt. Me. 20/HR	Wt. Me. 20/HR	Wt. Me. 20/HR	Wt. Me. 20/HR	Wt. Me. 20/HR	Wt. Me. 20/HR	Wt. Me. 20/HR	Wt. Me. 20/HR	Wt. Me. 20/HR	Wt. Me. 20/HR	Wt. Me. 20/HR	Wt. Me. 20/HR	Wt. Me. 20/HR	Wt. Me. 20/HR	Wt. Me. 20/HR	Wt. Me. 20/HR	Wt. Me. 20/HR
C2-1	150		1,000	436	2,788	23,146	20,09	404	407.4	162.65	1.03	463	1,08	1,168	2,775	2,775	4,240	2,88	16.8	0.05	7.66	0.17	153.37	152.40	1,188	4.38	5.53	1,123	4.13	0.48	513	
	150.32	7.63	1,014	434	2,797	23,146	20,09	405	411.2	162.69	1.03	463	1,08	1,170	2,775	2,775	4,240	2,88	16.8	0.05	7.68	0.17	153.47	152.40	1,188	4.42	5.57	1,123	4.13	0.48	513	
C2-3	175		1,000	460	2,788	23,146	20,09	404	412.5	162.69	1.03	463	1,08	1,170	2,775	2,775	4,240	2,88	16.8	0.05	7.68	0.17	153.47	152.40	1,188	4.42	5.57	1,123	4.13	0.48	513	
	174.07	13.46	1,000	460	2,788	23,146	20,09	404	412.5	162.69	1.03	463	1,08	1,170	2,775	2,775	4,240	2,88	16.8	0.05	7.68	0.17	153.47	152.40	1,188	4.42	5.57	1,123	4.13	0.48	513	
C2-5	200		1,500	432	1,306	26,429	19,448	428	409.7	211.40	1.29	530	0.79	2,624	1.89	0.221	5,300	3.33	13.6	0.01	23.59	0.24	260.74	262.03	1,226	4.30	4.28	1,238	3.76	0.48	578	
	200.23	23.58	1,522	432	1,306	26,429	19,448	428	409.7	211.40	1.29	530	0.79	2,624	1.89	0.221	5,300	3.33	13.6	0.01	23.59	0.24	260.74	262.03	1,226	4.30	4.28	1,238	3.76	0.48	578	
C2-7	173		5,000	475	5,656	22,03	20,27	457	431.2	185.20	1.09	574	0.82	7,240	2.28	0.298	4,840	3.11	26.8	0.03	13.60	0.12	172.16	176.25	1,342	4.00	4.49	1,347	4.48	0.53	607	
	174.67	13.57	5,000	475	5,656	22,03	20,27	457	431.2	185.20	1.09	574	0.82	7,240	2.28	0.298	4,840	3.11	26.8	0.03	13.60	0.12	172.16	176.25	1,342	4.00	4.49	1,347	4.48	0.53	607	
C2-9	200		5,000	457	5,786	21,86	20,23	446	427.1	209.18	1.18	656	0.89	8,890	1.91	0.281	5,460	3.31	29.4	0.01	23.33	0.11	199.94	201.12	1,594	3.36	3.28	1,226	4.00	0.50	666	
	199.69	23.32	5,000	457	5,786	21,86	20,23	446	427.1	209.18	1.18	656	0.89	8,890	1.91	0.281	5,460	3.31	29.4	0.01	23.33	0.11	199.94	201.12	1,594	3.36	3.28	1,226	4.00	0.50	666	
C2-11	173		1,500	437	1,281	27,32	19,31	432	445.7	187.24	1.21	491	0.91	1,726	2.27	0.236	4,860	3.13	12.8	0.03	13.71	0.24	172.89	177.10	1,348	4.36	5.28	1,355	4.40	0.53	530	
	174.03	13.68	1,509	437	1,281	27,32	19,31	432	445.7	187.24	1.21	491	0.91	1,726	2.27	0.236	4,860	3.13	12.8	0.03	13.71	0.24	172.89	177.10	1,348	4.36	5.28	1,355	4.40	0.53	530	
C2-13	220		3,000	435	2,759	22,69	19,54	438	443.8	229.25	1.32	647	0.67	5,600	1.27	0.228	6,300	3.24	21.1	0.01	42.36	0.17	228.28	231.66	1,437	3.28	3.28	1,226	3.56	0.48	629	
	220.69	44.33	3,000	435	2,759	22,69	19,54	438	443.8	229.25	1.32	647	0.67	5,600	1.27	0.228	6,300	3.24	21.1	0.01	42.36	0.17	228.28	231.66	1,437	3.28	3.28	1,226	3.56	0.48	629	
C2-15	200		3,000	442	2,797	23,27	19,55	446	426.5	210.95	1.22	576	0.79	4,340	1.89	0.246	5,000	3.32	19.8	0.01	23.61	0.17	200.63	201.85	1,293	4.02	4.38	1,222	3.98	0.50	633	
	200.27	23.60	3,018	442	2,797	23,27	19,55	446	426.5	210.95	1.22	576	0.79	4,340	1.89	0.246	5,000	3.32	19.8	0.01	23.61	0.17	200.63	201.85	1,293	4.02	4.38	1,222	3.98	0.50	633	

2-in. Tubes, CJ Series, 20^o F Superheat

Run No.	VH sat. temp. °F	VH press. in. Hg	Feed rate lb/hr	Vapor rate lb/hr	BD Cl	Feed Cl	Ave. Cl	Feed super-heat °F	Stm. rate lb/hr	q x 10 ⁻³ Btu/hr	Stm. sat. temp. °F	t _{OA} app °F	BFR of	t _{OA} corr of	U _{VH} Ft ² -hr-°F
CJ- 2	<u>150</u>		<u>3,000</u>		<u>20</u>	<u>20</u>		<u>20</u>	<u>450</u>						
	150.16	7.60	2,992	476	23.66	20.08	21.87	20.9	405	410.3	162.94	12.78	1.04	11.74	446
CJ- 4	<u>175</u>		<u>3,000</u>		<u>20</u>	<u>20</u>		<u>20</u>	<u>450</u>						
	174.83	13.62	2,986	510	24.45	20.06	22.26	20.4	451	445.9	187.48	12.65	1.15	11.50	495
CJ- 6	<u>200</u>		<u>1,500</u>		<u>20</u>	<u>20</u>		<u>20</u>	<u>450</u>						
	200.17	23.55	1,511	470	28.22	19.47	23.85	18.8	430	411.8	211.46	11.29	1.36	9.93	553
CJ- 8	<u>175</u>		<u>6,000</u>		<u>20</u>	<u>20</u>		<u>20</u>	<u>450</u>						
	174.60	13.55	5,952	594	22.50	20.38	21.44	20.2	448	441.3	186.39	11.79	1.10	10.69	528
CJ-10	<u>200</u>		<u>6,000</u>		<u>20</u>	<u>20</u>		<u>20</u>	<u>450</u>						
	199.61	23.28	6,104	547	22.42	20.47	21.45	14.6	433	414.8	209.80	10.19	1.22	8.97	591
CJ-12	<u>175</u>		<u>1,500</u>		<u>20</u>	<u>20</u>		<u>20</u>	<u>450</u>						
	174.70	13.58	1,523	474	27.52	19.25	23.39	16.8	438	430.9	187.66	12.96	1.21	11.75	469
CJ-14	<u>230</u>		<u>3,000</u>		<u>20</u>	<u>20</u>		<u>220</u>	<u>450</u>						
	230.05	42.35	2,939	494	23.14	19.62	21.38	19.6	434	402.8	239.70	9.65	1.33	8.32	618
CJ-16	<u>200</u>		<u>3,000</u>		<u>20</u>	<u>20</u>		<u>20</u>	<u>450</u>						
	200.25	23.59	2,969	491	23.55	19.65	21.60	15.9	442	424.0	211.21	10.96	1.23	9.73	557

APPENDIX C

EXPERIMENTAL DATA AND CALCULATIONS, COLUMNS 1-14

THEORETICAL PREDICTIONS, COLUMNS 15-33

RUNS LWCK-10 TO LWCK-29

2-in. Tubes, CR Series, Zero Feed, Submergent

(1)	(2)	(3)	(4)	(5)	(6)	(7)	(8)	(9)	(10)	(11)	(12)	(13)	(14)	(15)	(16)	(17)	(18)	(19)	(20)	(21)	(22)	(23)	(24)	(25)	(26)	(27)	(28)	(29)	(30)	(31)	(32)	(33)
Run No.	VR wt. of temp. of in. lg.	VR pres. in. lg.	Feed rate lb/hr	Vapor rate lb/hr	Ave. flow lb/hr	100.01 lb/hr	Feed Cl Ave. Cl in.	in.	VR wt. of temp. of in. lg.	VR pres. in. lg.	VR wt. of temp. of in. lg.	VR wt. of temp. of in. lg.	VR wt. of temp. of in. lg.	VR wt. of temp. of in. lg.	VR wt. of temp. of in. lg.	VR wt. of temp. of in. lg.	VR wt. of temp. of in. lg.	VR wt. of temp. of in. lg.	VR wt. of temp. of in. lg.	VR wt. of temp. of in. lg.	VR wt. of temp. of in. lg.	VR wt. of temp. of in. lg.	VR wt. of temp. of in. lg.	VR wt. of temp. of in. lg.	VR wt. of temp. of in. lg.	VR wt. of temp. of in. lg.	VR wt. of temp. of in. lg.	VR wt. of temp. of in. lg.	VR wt. of temp. of in. lg.	VR wt. of temp. of in. lg.	VR wt. of temp. of in. lg.	VR wt. of temp. of in. lg.
CR-10	100.14	2.00	6,000	433	5,758	20.35	19.08	19.69	150	445.6	119.30	0.78	398	3,155	2.38	20.0	0.19	2.19	2.12	106.00	106.78	1.188	4.86	9.82	862	2.31	0.52	562				
	100.04	1.97	5,966	428	5,754	20.35	19.08	19.69	150	442.7	118.77	0.78	396	3,145	2.37	20.0	0.19	2.16	2.12	106.00	106.33	1.185	4.84	9.80	859	2.29	0.52	562				
CR-12	100.30	1.95	2,992	513	2,738	23.08	19.36	21.22	150	474.2	120.66	0.85	310	3,125	2.38	14.0	0.26	2.24	2.24	107.05	107.87	0.94	6.09	12.04	935	5.77	0.56	316				
	100.61	1.96	3,027	510	2,772	23.08	19.59	21.42	150	474.8	120.66	0.85	319	3,125	2.38	14.0	0.26	2.24	2.24	107.05	108.30	0.94	6.09	12.04	935	5.77	0.56	316				
CR-15	100.81	1.98	3,007	255	2,809	21.63	19.80	20.72	250	258.0	112.01	0.82	320	3,060	2.33	14.0	0.27	2.08	2.08	108.05	109.47	0.86	3.33	7.17	1,107	2.64	0.30	304				
	101.31	2.01	3,013	254	2,886	21.73	19.64	20.51	250	258.0	112.01	0.82	333	3,060	2.33	14.0	0.27	2.08	2.08	108.05	109.84	0.86	3.34	7.17	1,107	2.65	0.30	304				
CR-16	100.13	1.90	5,965	250	5,800	19.03	19.15	19.53	250	261.8	110.10	0.76	324	3,030	2.32	16.6	0.27	1.97	1.97	106.62	103.36	1.121	2.98	6.17	1,098	2.73	0.31	293				
	100.63	1.91	5,959	251	5,813	20.00	19.18	19.59	250	261.5	110.12	0.76	323	3,030	2.32	16.6	0.27	1.97	1.97	106.62	103.94	1.121	2.98	6.17	1,098	2.73	0.31	293				
CR-18	100.13	1.88	1,499	256	1,457	24.67	19.88	21.24	250	262.1	111.88	0.87	328	3,060	2.33	16.4	0.27	2.05	2.05	106.41	106.30	0.884	3.86	8.46	1,098	2.76	0.31	295				
	100.63	1.88	1,499	256	1,457	24.67	19.88	21.24	250	262.1	111.88	0.87	328	3,060	2.33	16.4	0.27	2.05	2.05	106.41	106.30	0.884	3.86	8.46	1,098	2.76	0.31	295				
CR-19	100.13	1.86	1,499	479	1,253	24.67	19.88	21.24	250	469.3	121.29	0.86	306	3,060	2.33	16.4	0.27	2.05	2.05	106.41	106.30	0.884	3.86	8.46	1,098	2.76	0.31	295				
	100.63	1.86	1,499	479	1,253	24.67	19.88	21.24	250	469.3	121.29	0.86	306	3,060	2.33	16.4	0.27	2.05	2.05	106.41	106.30	0.884	3.86	8.46	1,098	2.76	0.31	295				
CR-22	124.68	3.92	1,499	475	1,253	24.67	19.88	21.24	250	469.3	121.29	0.86	306	3,060	2.33	16.4	0.27	2.05	2.05	106.41	106.30	0.884	3.86	8.46	1,098	2.76	0.31	295				
	124.68	3.92	1,499	475	1,253	24.67	19.88	21.24	250	469.3	121.29	0.86	306	3,060	2.33	16.4	0.27	2.05	2.05	106.41	106.30	0.884	3.86	8.46	1,098	2.76	0.31	295				
CR-24	124.68	3.89	3,093	468	2,855	23.78	20.11	21.95	250	469.1	121.68	0.95	376	3,650	2.64	10.7	0.12	4.04	4.04	128.01	129.08	0.979	6.11	9.44	1,024	5.46	0.55	326				
	124.68	3.89	3,093	468	2,855	23.78	20.11	21.95	250	469.1	121.68	0.95	376	3,650	2.64	10.7	0.12	4.04	4.04	128.01	129.08	0.979	6.11	9.44	1,024	5.46	0.55	326				
CR-26	124.77	3.93	5,968	468	5,700	21.57	19.74	20.66	250	471.2	129.66	0.90	425	3,640	2.66	22.1	0.11	4.04	4.04	128.01	127.77	1.011	4.82	6.97	1,027	5.34	0.56	469				
	124.68	3.92	5,958	468	5,700	21.75	20.09	20.96	250	471.1	129.79	0.91	425	3,640	2.66	22.1	0.11	4.03	4.03	128.01	127.69	1.011	4.82	6.97	1,027	5.34	0.56	469				

2-in Tubes, CK Series, 20° F Feed Superheat - Experimental Data and Calculations

Run No.	VH sat. temp. of	VH press. in. Hg	Feed rate lb/hr	Vapor rate lb/hr	BD Cl	Feed Cl	Ave. Cl	Feed super-heat of	Stm. rate lb/hr	Q x 10 ⁻³ Btu/hr	Stm. sat. temp. of	Δ t _{OA,app} of	EPR of	Δ t _{OA,corr} of	U _{VH} Btu/hr-ft ² -of
CK-11	<u>100</u>		<u>6,000</u>		<u>20</u>	<u>20</u>		<u>20</u>	<u>450</u>						
	99.61 100.80	1.91 1.98	5,997 5,996	593 593	21.08 21.21	19.07 19.12	20.08 20.17	20.5 18.5	433 454	457.9 478.7	123.97 125.06	24.36 24.26	0.84 0.84	23.52 23.42	248 260
CK-13	<u>100</u>		<u>3,000</u>		<u>20</u>	<u>20</u>		<u>20</u>	<u>450</u>						
	99.96 99.43	1.93 1.90	2,997 2,961	489 482	23.57 23.70	19.62 19.88	21.60 21.79	22.5 22.1	409 414	435.6 441.0	120.35 119.52	20.39 20.09	0.88 0.89	19.51 19.20	285 294
CK-14	<u>100</u>		<u>3,000</u>		<u>20</u>	<u>20</u>		<u>20</u>	<u>250</u>						
	100.13 99.96	1.94 1.93	3,004 3,020	330 340	21.47 21.29	19.10 19.02	20.29 20.16	22.2 22.0	253 252	269.2 268.3	112.63 112.51	12.50 12.55	0.82 0.81	11.68 11.74	294 292
CK-17	<u>100</u>		<u>6,000</u>		<u>20</u>	<u>20</u>		<u>20</u>	<u>250</u>						
	99.96 99.78	1.93 1.92	6,015 6,091	355 368	20.64 20.40	19.43 19.23	20.04 19.82	19.3 20.7	246 244	260.2 257.7	112.13 111.88	12.17 12.10	0.80 0.79	11.37 11.31	292 290
CK-20	<u>100</u>		<u>1,500</u>		<u>20</u>	<u>20</u>		<u>20</u>	<u>450</u>						
	100.13 100.13	1.94 1.94	1,537 1,538	502 501	28.90 28.94	19.17 19.31	24.04 24.13	20.5 19.2	453 446	479.3 471.7	121.27 120.97	21.14 20.84	0.99 0.99	20.15 19.85	304 304
CK-21	<u>100</u>		<u>1,500</u>		<u>20</u>	<u>20</u>		<u>20</u>	<u>250</u>						
	99.43 99.43	1.90 1.90	1,488 1,415	299 290	24.59 24.44	19.44 19.44	22.02 21.94	17.5 20.7	268 261	285.2 276.3	111.37 110.85	11.94 11.42	0.88 0.87	11.06 10.55	329 335
CK-23	<u>125</u>		<u>1,500</u>		<u>20</u>	<u>20</u>		<u>20</u>	<u>450</u>						
	125.61 125.52	4.02 4.01	1,498 1,482	492 498	29.86 30.92	20.03 20.61	24.95 25.77	18.6 18.2	455 447	473.4 464.6	142.56 142.37	16.95 16.85	1.10 1.15	15.85 15.70	381 378
CK-25	<u>125</u>		<u>3,000</u>		<u>20</u>	<u>20</u>		<u>20</u>	<u>450</u>						
	124.87 124.87	3.94 3.94	3,007 3,024	537 537	23.97 24.67	20.09 20.43	22.03 22.55	20.7 20.7	446 450	464.6 469.5	141.10 141.17	16.23 16.30	0.98 1.00	15.25 15.30	389 392
CK-27	<u>125</u>		<u>6,000</u>		<u>40</u>	<u>40</u>		<u>20</u>	<u>450</u>						
	124.49 124.59	3.90 3.91	5,941 6,043	585 584	21.60 20.77	19.48 18.71	20.54 19.74	21.1 21.0	449 448	468.4 467.4	140.91 140.78	16.42 16.19	0.92 0.88	15.50 15.31	386 390
CK-28	<u>100</u>		<u>6,000</u>		<u>40</u>	<u>40</u>		<u>20</u>	<u>250</u>						
	99.96 99.78	1.93 1.92	6,190 6,165	360 365	35.53 35.30	33.43 33.63	34.48 34.47	19.3 20.0	248 246	262.7 260.4	112.38 112.51	12.42 12.73	1.38 1.38	11.04 11.35	304 293
CK-29	<u>100</u>		<u>1,500</u>		<u>40</u>	<u>40</u>		<u>20</u>	<u>250</u>						
	100.64 101.14	1.97 2.00	1,532 1,523	279 271	38.50 38.47	31.34 32.05	34.92 35.26	18.9 18.2	245 241	260.2 255.6	112.26 112.65	11.62 11.51	1.40 1.42	10.22 10.09	325 324

APPENDIX D

EXPERIMENTAL DATA AND CALCULATIONS, COLUMNS 1-14

THEORETICAL PREDICTIONS, COLUMNS 15-33

RUNS LWDA-2 TO LWDA-38

1-in. Tubes, Series DA, Zero Feed Superheat

(1) Run No.	(2) VH sat. temp. °F	(3) VH press. in. Hg	(4) Feed rate lb/hr	(5) Vapor rate lb/hr	(6) Ave. flow lb/hr	(7) BD Cl gpl	(8) Feed Cl gpl	(9) Ave. Cl gpl	(10) Steam rate lb/hr	(11) Qx10 ⁻³ Btu/hr	(12) Stm. sat. temp. °F	(13) BPR °F	(14) U _{VH} Btu/ft ² -hr-°F	(15) μ lb/hr-ft	(16) (Re)	(17) (Pr)
DA-2	<u>100</u>		<u>1,500</u>				<u>20</u>		<u>250</u>							
	99.96	1.93	1,511	245	1,388	22.75	21.13	21.94	239	246.6	138.58	0.94	171	1.35	2,580	3.51
	99.96	1.93	1,491	243	1,369	23.02	21.73	22.37	246	254.5	139.46	0.96	173	1.34	2,561	3.50
DA-4	<u>100</u>		<u>3,000</u>				<u>20</u>		<u>250</u>							
	99.61	1.91	3,042	248	2,918	21.03	19.32	20.18	246	251.9	141.17	0.87	162	1.31	5,590	3.40
	99.43	1.90	3,071	248	2,947	20.83	19.23	20.03	247	252.7	140.91	0.87	162	1.31	5,650	3.41
DA-6	<u>125</u>		<u>3,000</u>				<u>20</u>		<u>250</u>							
	124.96	3.95	3,038	252	2,912	21.28	19.45	20.37	255	256.5	154.97	0.93	230	1.18	6,190	2.97
	124.96	3.95	3,039	251	2,914	21.22	19.48	20.35	257	258.9	155.06	0.93	232	1.18	6,200	2.97
DA-8	<u>125</u>		<u>1,500</u>				<u>20</u>		<u>250</u>							
	125.24	3.98	1,441	257	1,356	23.68	19.59	21.64	269	273.5	152.50	0.97	272	1.21	2,813	3.09
	124.87	3.94	1,528	258	1,398	23.91	19.91	21.91	260	263.9	152.19	0.99	262	1.21	2,900	3.09
DA-10	<u>150</u>		<u>1,500</u>				<u>20</u>		<u>250</u>							
	149.90	7.55	1,573	252	1,447	21.92	18.41	20.17	261	257.4	168.23	0.97	387	1.05	3,459	2.65
	149.95	7.56	1,535	252	1,409	22.26	18.66	20.46	252	248.6	168.33	0.99	374	1.05	3,362	2.65
DA-12	<u>150</u>		<u>3,000</u>				<u>20</u>		<u>250</u>							
	149.57	7.49	3,000	262	2,869	22.46	20.63	21.55	252	248.2	171.02	1.05	318	1.03	7,000	2.58
	149.79	7.53	3,022	258	2,893	21.19	19.45	20.32	250	246.7	170.88	0.99	320	1.02	7,110	2.58
DA-14	<u>175</u>		<u>1,500</u>				<u>20</u>		<u>250</u>							
	175.67	13.88	1,508	232	1,392	24.52	20.47	22.50	249	241.2	189.27	1.17	506	0.91	3,840	2.24
	175.29	13.76	1,550	235	1,434	24.83	20.74	22.79	243	234.6	189.17	1.19	483	0.91	3,960	2.24
DA-16	<u>175</u>		<u>3,000</u>				<u>20</u>		<u>250</u>							
	175.83	13.93	3,002	230	2,887	22.50	20.81	21.66	258	249.2	192.20	1.13	427	0.89	8,140	2.19
	177.49	14.46	2,991	239	2,871	22.39	20.81	21.60	261	252.0	193.44	1.14	444	0.88	8,190	2.17
DA-18	<u>200</u>		<u>3,000</u>				<u>20</u>		<u>250</u>							
	200.92	23.92	2,965	227	2,846	22.60	20.99	21.80	237	222.2	212.99	1.25	535	0.78	9,160	1.87
	200.17	23.55	2,942	216	2,824	23.14	21.71	22.43	236	219.2	212.38	1.28	523	0.78	9,090	1.87
DA-19	<u>200</u>		<u>1,500</u>				<u>20</u>		<u>250</u>							
	199.67	23.31	1,467	228	1,341	25.24	21.37	23.31	251	236.4	210.85	1.32	626	0.80	4,210	1.91
	200.15	23.54	1,505	254	1,379	25.76	21.58	23.67	251	236.1	211.36	1.34	625	0.80	4,325	1.90
DA-22	<u>230</u>		<u>1,500</u>				<u>20</u>		<u>250</u>							
	229.86	42.20	1,495	236	1,377	22.71	20.36	21.54	238	215.9	238.39	1.33	783	0.67	5,150	1.58
	229.79	42.15	1,490	242	1,369	22.59	19.90	21.25	231	209.3	238.28	1.32	762	0.67	5,120	1.58
DA-23	<u>230</u>		<u>1,500</u>				<u>20</u>		<u>150</u>							
	229.77	42.13	1,453	134	1,386	22.39	20.34	21.37	151	133.2	236.32	1.32	665	0.67	5,195	1.57
	230.03	42.33	1,431	125	1,368	23.25	21.31	22.28	144	126.6	236.58	1.38	639	0.67	5,120	1.57
DA-24	<u>230</u>		<u>3,000</u>				<u>20</u>		<u>250</u>							
	229.84	42.18	3,000	238	2,881	22.75	21.13	22.07	255	232.1	240.54	1.37	650	0.66	10,980	1.56
	229.82	42.17	3,049	230	2,934	23.02	21.37	22.20	248	224.6	240.43	1.38	636	0.66	11,150	1.56
DA-25	<u>230</u>		<u>3,000</u>				<u>20</u>		<u>150</u>							
	229.89	42.22	3,039	128	2,974	22.48	21.53	22.01	146	127.5	236.87	1.36	592	0.67	11,120	1.57
	229.93	42.25	2,995	128	2,931	22.80	21.71	22.26	145	126.5	236.76	1.38	606	0.67	10,990	1.57
DA-30	<u>150</u>		<u>3,000</u>				<u>20</u>		<u>150</u>							
	149.30	7.44	2,967	181	2,876	21.56	20.45	21.01	187	185.3	164.27	1.00	346	1.06	6,800	2.68
	149.09	7.40	2,973	184	2,881	21.71	20.45	21.08	192	190.2	164.15	1.00	354	1.06	6,820	2.68
DA-33	<u>150</u>		<u>1,500</u>				<u>20</u>		<u>150</u>							
	149.73	7.52	1,464	140	1,394	23.00	20.81	21.91	155	150.8	160.98	1.04	385	1.08	3,240	2.74
	149.73	7.52	1,429	142	1,358	23.14	20.92	22.03	162	157.5	161.15	1.04	396	1.08	3,155	2.74
DA-34	<u>100</u>		<u>1,500</u>				<u>20</u>		<u>150</u>							
	100.97	1.99	1,463	157	1,384	20.80	18.70	19.75	156	159.6	123.35	0.81	193	1.48	2,348	3.94
	99.96	1.93	1,500	153	1,423	20.77	18.69	19.73	158	162.6	123.16	0.81	189	1.48	2,418	3.94
DA-37	<u>100</u>		<u>3,000</u>				<u>20</u>		<u>150</u>							
	99.26	1.89	3,016	167	2,932	20.04	19.11	19.58	169	174.3	125.97	0.80	176	1.45	5,070	3.83
	98.91	1.87	3,042	166	2,959	20.04	19.11	19.58	173	178.6	126.06	0.80	177	1.45	5,120	3.83

1-in. Tubes, Series DA, Zero Feed Superheat (Cont'd.)

(18)	(19)	(20)	(21)	(22)	(23)	(24)	(25)	(26)	(27)	(28)	(29)	(30)	(31)	(32)	(33)
h_f/ϕ	\dot{p} Btu/ft ² -hr-°F	χ in. Hg	$B \left(\frac{p_g^2}{\mu^2} \right)^{1/3}$	ΔP in. Hg	P_v in. Hg	$4\sigma/B$ in. Hg	$f \left(\frac{P_v + \frac{4\sigma}{B}}{P} \right)$	t_v °F	h_f Btu/ft ² -hr-°F	Δt_F °F	Δt_{corr} °F	h_{gsm_2} Btu/ft ² -hr-°F	Δt_{gsm} °F	Δt_w °F	U_{vH} Btu/ft ² -hr-°F
0.301 0.301	3,590 3,610	2.60 2.61	15.3 15.2	1.90 1.90	3.83 3.83	0.17 0.17	125.43 125.43	126.37 126.39	1,080 1,087	5.96 6.12	31.43 31.59	982 975	5.71 5.94	0.34 0.35	172 175
0.342 0.343	3,670 3,670	2.63 2.63	22.7 22.8	2.50 2.50	4.41 4.40	0.12 0.12	130.04 129.96	130.91 130.83	1,255 1,260	5.24 5.24	35.67 35.77	983 981	5.83 5.85	0.34 0.34	157 158
0.327 0.327	4,020 4,020	2.79 2.79	24.0 24.0	2.16 2.16	6.11 6.11	0.12 0.12	142.25 142.25	143.18 143.18	1,315 1,315	5.10 5.14	22.39 22.43	1,017 1,013	5.63 5.66	0.36 0.36	236 238
0.289 0.290	3,920 3,920	2.75 2.75	16.0 16.1	1.59 1.59	5.57 5.53	0.17 0.17	139.06 138.78	140.03 139.77	1,131 1,137	6.30 6.05	20.12 19.96	991 1,001	6.27 5.98	0.38 0.37	267 262
0.279 0.278	4,340 4,360	2.92 2.93	17.6 17.3	1.11 1.11	8.66 8.67	0.17 0.17	156.29 156.34	157.26 157.33	1,210 1,212	5.55 5.35	11.94 11.74	1,047 1,060	5.59 5.34	0.36 0.35	376 372
0.315 0.315	4,460 4,450	2.96 2.96	25.9 26.0	1.77 1.75	9.26 9.28	0.11 0.11	158.76 158.85	159.81 159.84	1,405 1,402	4.61 4.60	13.80 13.66	1,068 1,070	5.29 5.25	0.35 0.34	334 335
0.262 0.264	4,890 4,890	3.14 3.14	18.5 18.8	0.85 0.85	14.73 14.61	0.17 0.17	178.83 178.47	180.00 179.66	1,280 1,290	4.92 4.75	8.08 7.93	1,120 1,129	4.89 4.73	0.34 0.35	473 472
0.296 0.297	4,980 5,000	3.16 3.17	28.3 28.4	1.45 1.47	15.38 15.93	0.11 0.11	180.58 182.33	181.71 183.47	1,474 1,485	4.41 4.43	9.16 9.27	1,112 1,112	5.09 5.15	0.35 0.35	445 446
0.280 0.279	5,520 5,510	3.34 3.33	30.0 29.9	0.74 0.73	24.66 24.28	0.11 0.11	202.62 201.87	203.87 203.15	1,546 1,539	3.76 3.72	5.46 5.42	1,198 1,197	4.22 4.16	0.31 0.30	581 578
0.247 0.247	5,450 5,470	3.31 3.32	19.2 19.3	0.14 0.17	23.45 23.71	0.17 0.17	200.31 200.84	201.63 202.18	1,349 1,351	4.58 4.56	5.22 5.25	1,171 1,172	4.59 4.58	0.33 0.33	609 607
0.231 0.231	6,260 6,260	3.53 3.53	21.7 21.6	0.08 0.08	42.28 42.23	0.16 0.16	230.16 230.10	231.49 231.42	1,448 1,448	3.89 3.77	4.19 4.08	1,250 1,263	3.92 3.76	0.30 0.29	670 672
0.229 0.229	6,280 6,280	3.53 3.53	21.7 21.6	0.02 0.02	42.15 42.35	0.16 0.16	230.00 230.25	231.32 231.63	1,439 1,439	2.42 2.30	2.65 2.52	1,451 1,461	2.08 1.97	0.19 0.18	707 707
0.261 0.262	6,310 6,310	3.54 3.54	33.1 33.2	0.08 0.07	42.26 42.24	0.11 0.11	230.08 230.05	231.45 231.43	1,649 1,654	3.68 3.55	3.92 3.78	1,223 1,237	4.31 4.13	0.32 0.31	709 715
0.263 0.262	6,290 6,290	3.54 3.54	33.2 33.1	0.02 0.02	42.24 42.27	0.11 0.11	230.05 230.09	231.41 231.47	1,652 1,648	2.02 2.00	2.18 2.16	1,469 1,470	1.97 1.96	0.18 0.18	770 768
0.286 0.287	4,310 4,310	2.91 2.91	25.4 25.4	0.29 0.31	7.73 7.71	0.11 0.11	151.42 151.32	152.42 152.32	1,233 1,238	3.92 4.01	6.04 6.24	1,158 1,148	3.64 3.77	0.26 0.26	487 484
0.255 0.254	4,250 4,250	2.89 2.89	17.0 17.0	0.17 0.18	7.69 7.70	0.17 0.17	151.52 151.58	152.56 152.62	1,083 1,080	3.63 3.80	5.42 5.65	1,220 1,205	2.81 2.97	0.21 0.22	467 465
0.312 0.313	3,320 3,310	2.46 2.46	14.7 14.8	0.77 0.76	2.76 2.69	0.17 0.17	114.23 113.38	115.04 114.19	1,036 1,036	4.02 4.09	17.28 17.51	1,070 1,064	3.39 3.46	0.22 0.23	199 200
0.356 0.357	3,370 3,370	2.49 2.49	21.5 21.6	0.92 0.91	2.81 2.78	0.12 0.12	114.23 113.87	115.03 114.67	1,200 1,203	3.80 3.87	18.77 18.83	1,048 1,041	3.78 3.90	0.24 0.25	200 203

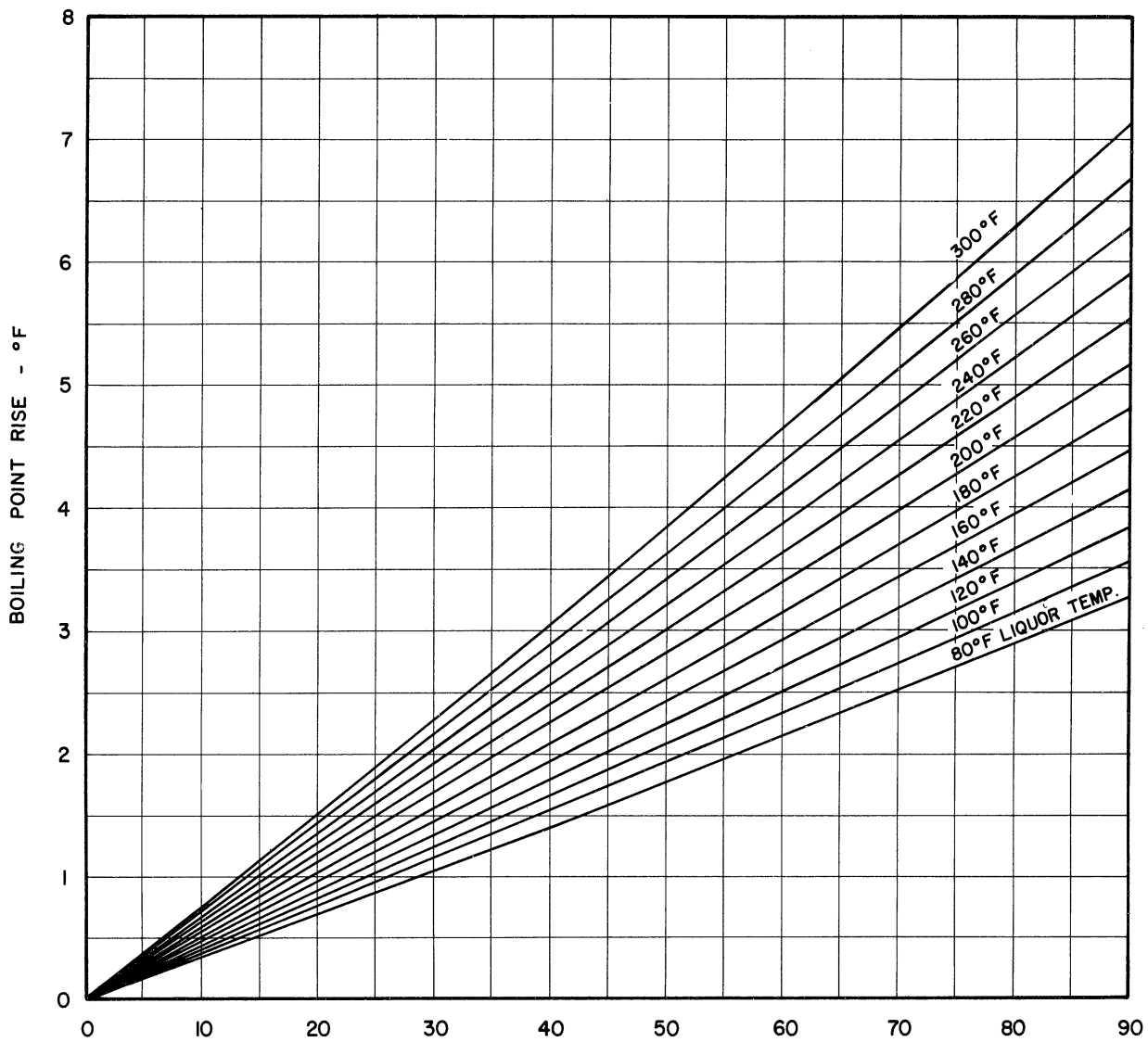
1-in. Tubes, DA Series, 20th F Feed superheat

Run No.	VH sat. temp. °F	VH press. in. Hg	Feed rate lb/hr	Vapor rate lb/hr	BD Cl gpl	Feed Cl gpl	Ave. Cl gpl	Feed super-heat °F	Stm. rate lb/hr	Q x 10 ⁻³ Btu/hr	Stm. sat. temp. °F	Δt _{OA} app °F	BPR °F	Δt _{OA} corr °F	U _{av} Btu/ft ² -hr-°F
DA- 3	100		1,500			20		20	250						
	99.61 99.78	1.91 1.92	1,520 1,554	268 268	22.73 22.98	19.02 19.09	20.88 21.04	19.9 19.3	244 237	249.5 242.7	143.00 142.44	43.39 42.66	0.93 0.93	42.46 41.73	153 152
DA- 5	100		3,000			20		20	250						
	98.91 99.43	1.87 1.90	3,012 3,000	335 316	21.72 21.53	19.38 19.46	20.55 20.50	22.4 20.7	256 250	259.2 253.5	150.43 149.57	50.52 50.14	0.95 0.95	49.57 49.19	131 135
DA- 7	125		3,000			20		20	250						
	124.96 124.96	3.95 3.95	3,099 3,064	306 309	21.62 21.69	19.48 19.54	20.55 20.62	17.4 18.2	256 260	255.0 259.1	161.15 161.40	36.19 36.44	0.98 0.98	35.21 35.46	189 191
DA- 9	125		1,500			20		20	250						
	124.96 125.06	3.95 3.96	1,549 1,481	280 280	24.08 23.77	19.72 19.73	21.90 21.75	19.3 20.2	256 268	258.3 270.6	154.24 154.33	29.28 29.27	1.02 1.01	28.26 28.26	239 250
DA-11	150		1,500			20		20	250						
	149.90 149.95	7.55 7.56	1,547 1,493	285 284	23.07 23.73	19.27 19.27	21.17 21.50	18.5 19.3	256 258	252.4 254.3	169.14 169.14	19.24 19.19	1.04 1.05	18.20 18.14	362 366
DA-13	150		3,000			20		20	250						
	149.79 149.79	7.53 7.53	3,002 3,003	323 324	21.49 21.42	19.11 19.07	20.30 20.25	20.8 21.6	267 258	262.9 255.0	175.13 174.73	25.34 24.94	1.00 1.00	24.34 23.94	282 278
DA-15	175		1,500			20		20	250						
	175.67 175.16	13.88 13.72	1,546 1,539	282 281	24.81 22.98	20.42 18.57	22.62 20.73	19.3 18.0	255 258	245.9 248.4	190.06 189.74	14.39 14.58	1.21 1.11	13.18 13.47	487 482
DA-17	175		3,000			20		20	250						
	176.27 175.09	14.07 13.70	3,118 3,065	306 292	23.14 23.16	20.95 20.95	22.05 22.06	18.0 19.2	243 244	232.9 234.5	192.18 191.71	15.91 16.62	1.19 1.19	14.72 15.43	413 397
DA-20	200		1,500			20		20	250						
	199.92	23.43	1,504	282	26.80	21.99	24.40	19.4	251	235.0	211.45	11.53	1.40	10.13	605
DA-21	200		3,000			20		20	250						
	202.34 202.28	24.63 24.60	2,904 2,910	286 274	22.78 22.89	20.67 20.74	21.73 21.82	16.7 15.9	250 248	233.7 231.7	214.10 214.05	11.76 11.77	1.26 1.27	10.50 10.50	579 575
DA-26	230		3,000			20		20	250						
	230.38 230.48	42.61 42.69	2,962 2,903	301	22.75 23.12	20.40 20.76	21.58 21.94	18.9 23.0	258 260	234.5 236.0	240.80 241.03	10.42 10.55	1.37 1.38	9.05 9.17	677 672
DA-27	230		1,500			20		20	250						
	230.09 230.35	42.38 42.59	1,518 1,502	258 262	25.69 25.76	19.70 20.99	22.70 23.38	17.9 17.2	252 253	229.0 231.1	240.27 240.58	10.18 10.23	1.44 1.48	8.74 8.75	685 689
DA-28	230		1,500			20		20	150						
	230.51 230.49	42.72 42.70	1,531 1,520	200 189	25.13 25.10	21.53 20.86	23.33 22.98	12.0 14.7	172 171	153.5 152.4	238.05 238.05	7.54 7.56	1.47 1.45	6.07 6.11	660 651
DA-29	230		3,000			20		20	150						
	230.14 230.20	42.42 42.47	2,994 2,989	239 244	22.23 23.32	20.58 21.71	21.41 22.52	21.4 20.8	177 175	157.4 155.7	238.03 238.04	7.89 7.84	1.35 1.42	6.54 6.42	629 633
DA-31	150		3,000			20		20	150						
	149.03 149.36	7.39 7.45	2,966 2,980	242 242	21.53 22.23	20.02 20.54	20.78 21.39	22.1 22.2	188 189	185.2 185.8	167.22 167.40	18.19 18.04	1.02 1.04	17.17 17.00	282 285
DA-32	150		1,500			20		20	150						
	149.25 149.19	7.43 7.42	1,557 1,547	228 215	24.34 24.34	21.01 21.03	22.68 22.69	22.5 22.4	189 192	186.9 190.2	163.75 163.67	14.50 14.48	1.10 1.10	13.40 13.38	364 371
DA-35	100		1,500			20		20	150						
	100.30 100.13	1.95 1.94	1,502 1,494	191 189	21.73 21.56	18.98 18.80	20.36 20.18	20.5 21.7	160 163	164.5 168.3	127.75 128.01	27.45 27.88	0.86 0.85	26.59 27.03	162 163
DA-36	100		3,000			20		20	150						
	100.97 99.61	1.99 1.91	3,081 3,095	205 212	20.13 20.34	18.98 18.85	19.56 19.60	18.6 19.4	149 157	152.7 161.0	132.37 132.68	31.40 33.07	0.84 0.84	30.56 32.23	130 130
DA-38	100		1,500			40		20	250						
	101.80 101.47	2.04 2.02	1,609 1,617	233 229	38.68 37.93	32.11 32.31	35.40 35.12	16.1 14.8	217 212	223.2 222.5	139.79 138.92	37.99 37.45	1.48 1.47	36.51 35.98	160 161

APPENDIX E

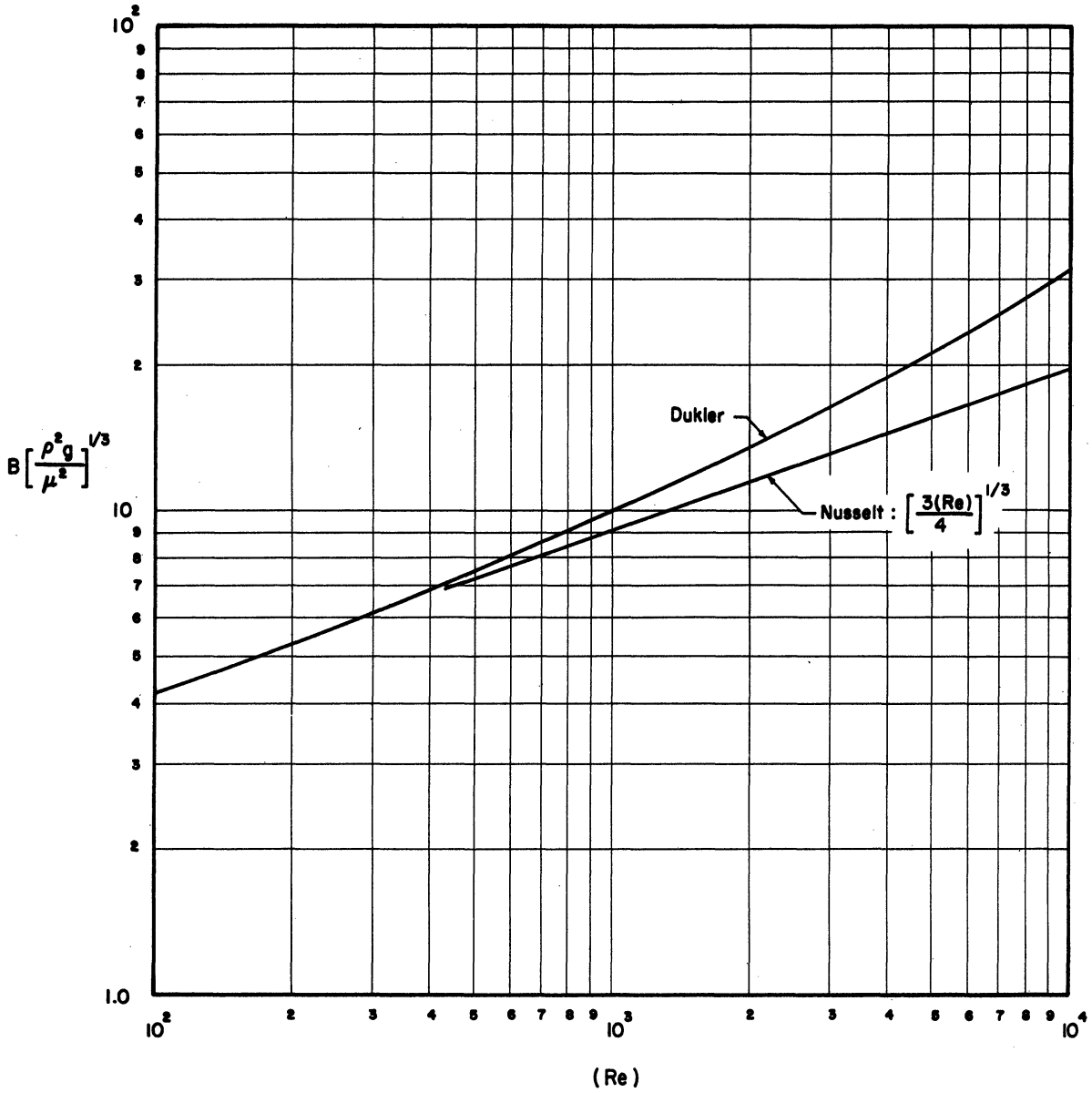
GRAPHS USED TO CORRELATE EXPERIMENTAL DATA

BOILING POINT RISE OF SEA WATER CONCENTRATES



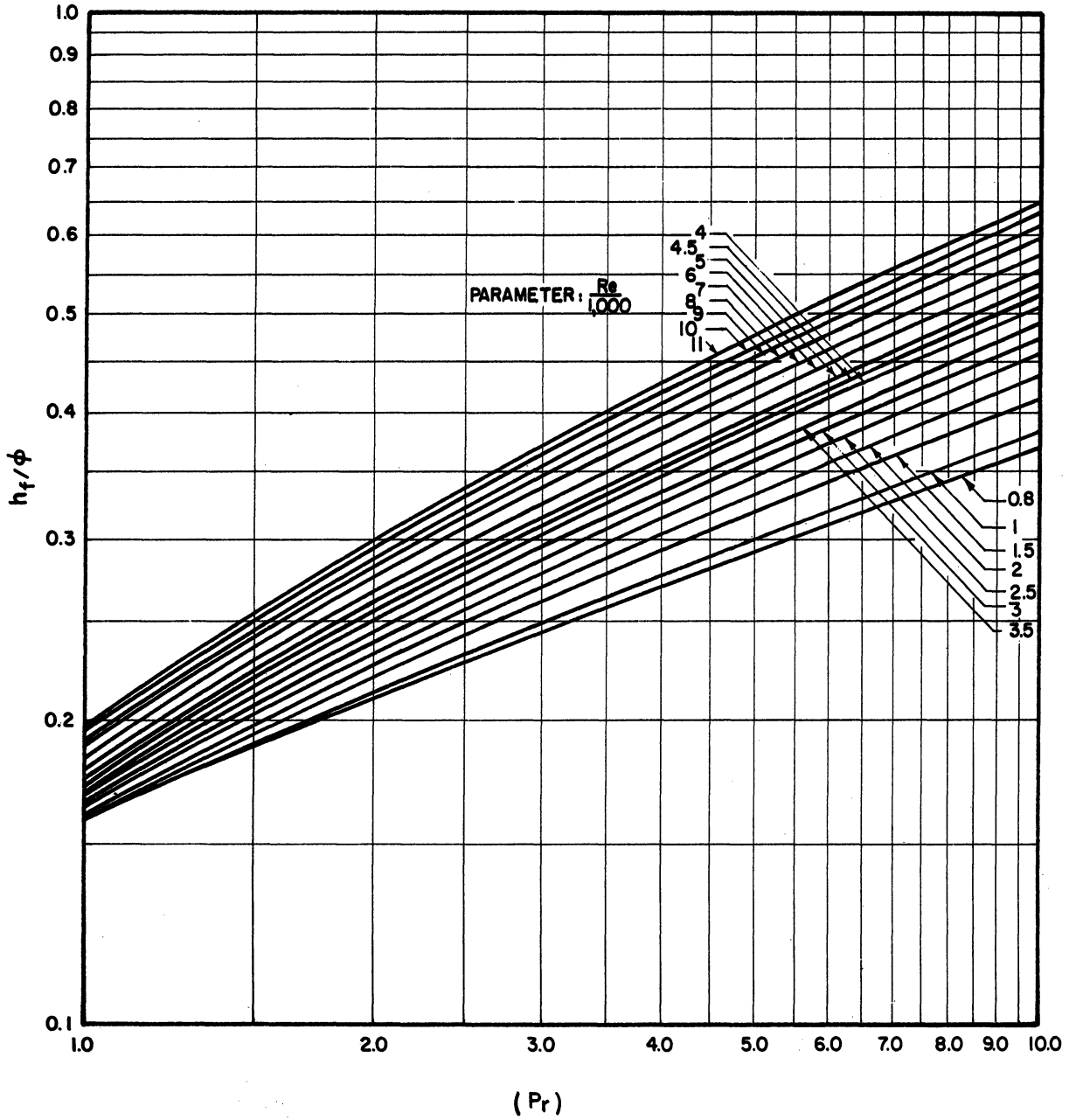
CHLOROSITY - gpl
Graph 1

DUKLER'S FILM THICKNESS CORRELATION



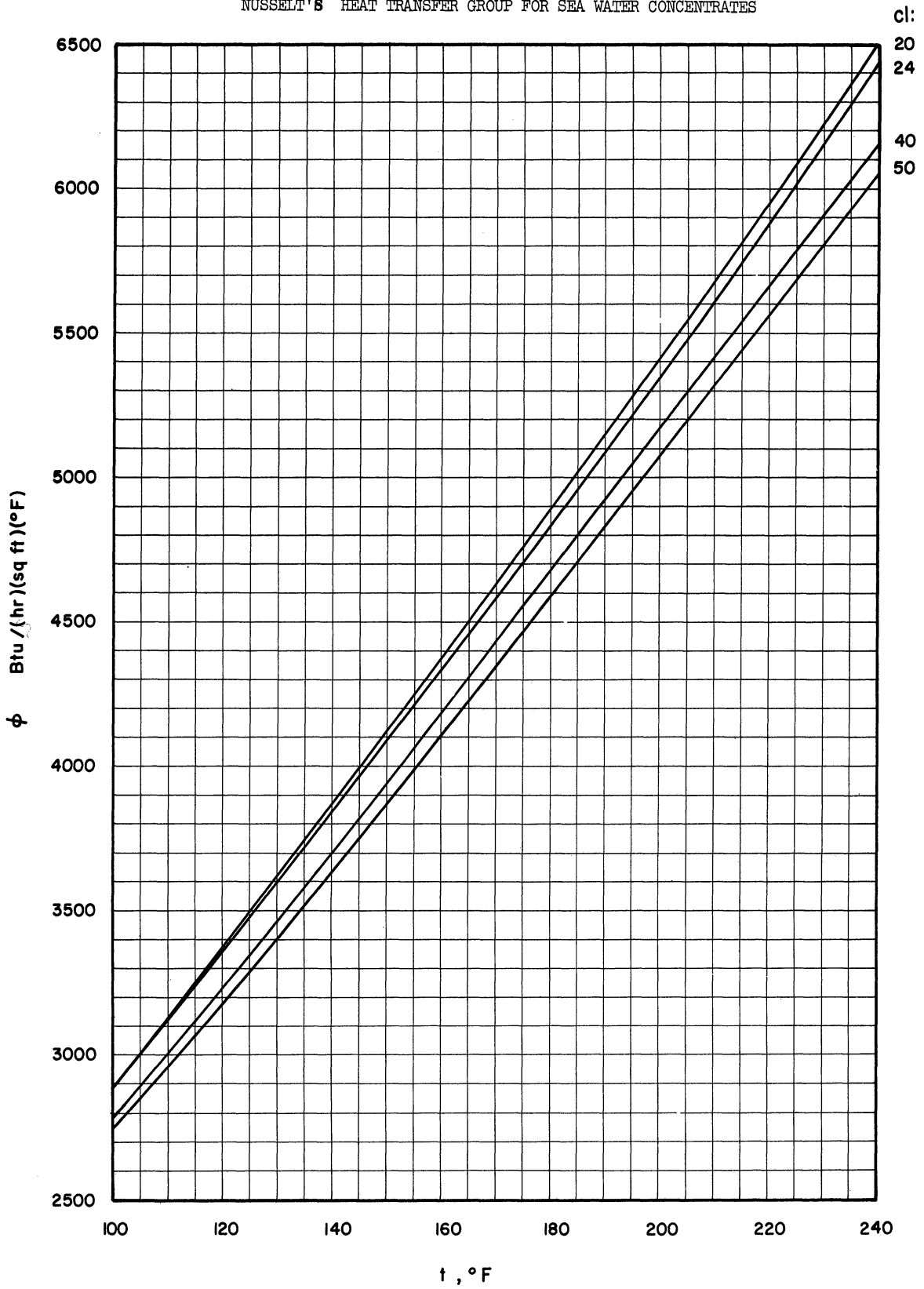
Graph 2

DUKLER'S HEAT TRANSFER CORRELATION



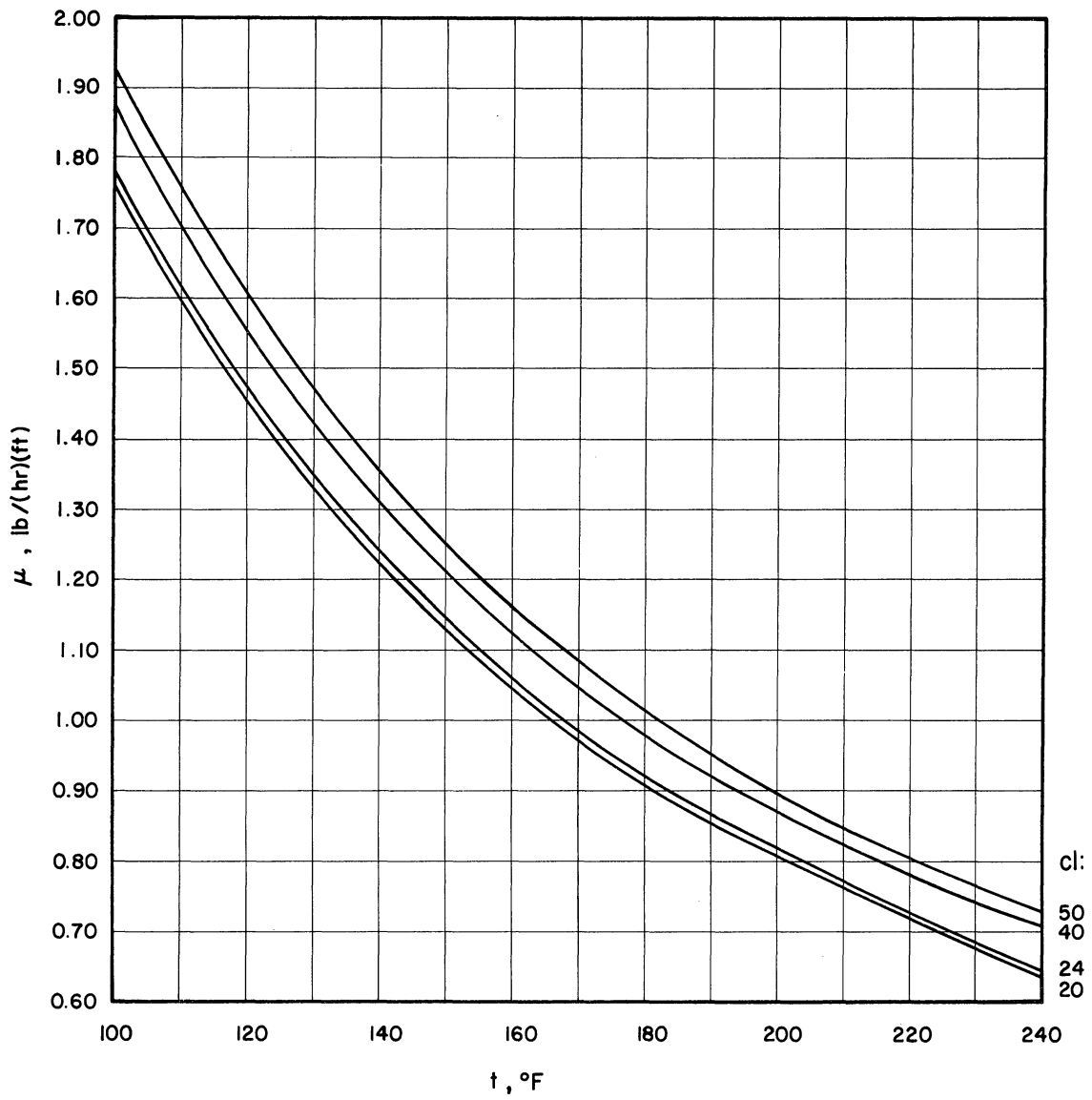
Graph 3

NUSSELT'S HEAT TRANSFER GROUP FOR SEA WATER CONCENTRATES



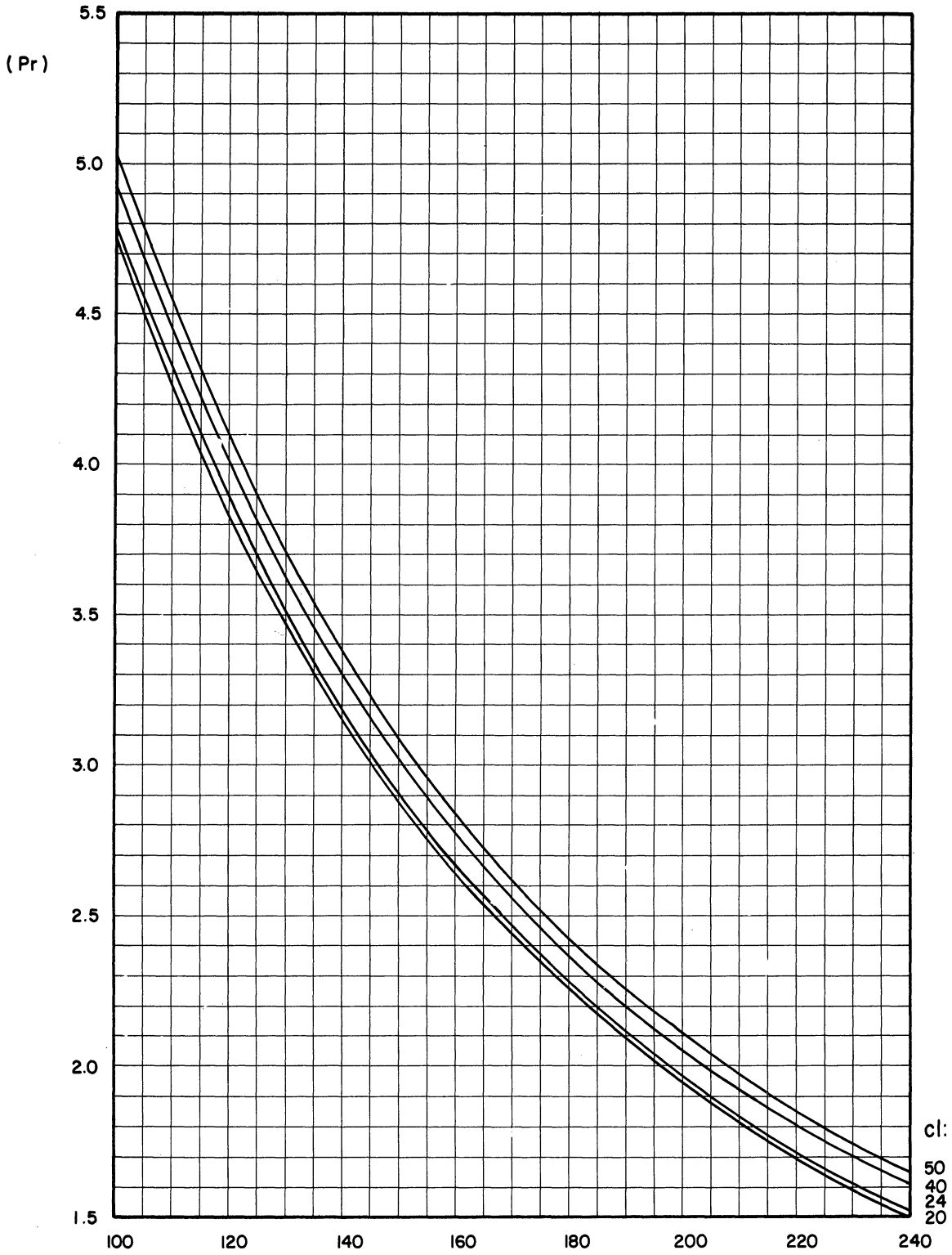
Graph 4

VISCOSITY OF SEA WATER CONCENTRATES



Graph 5

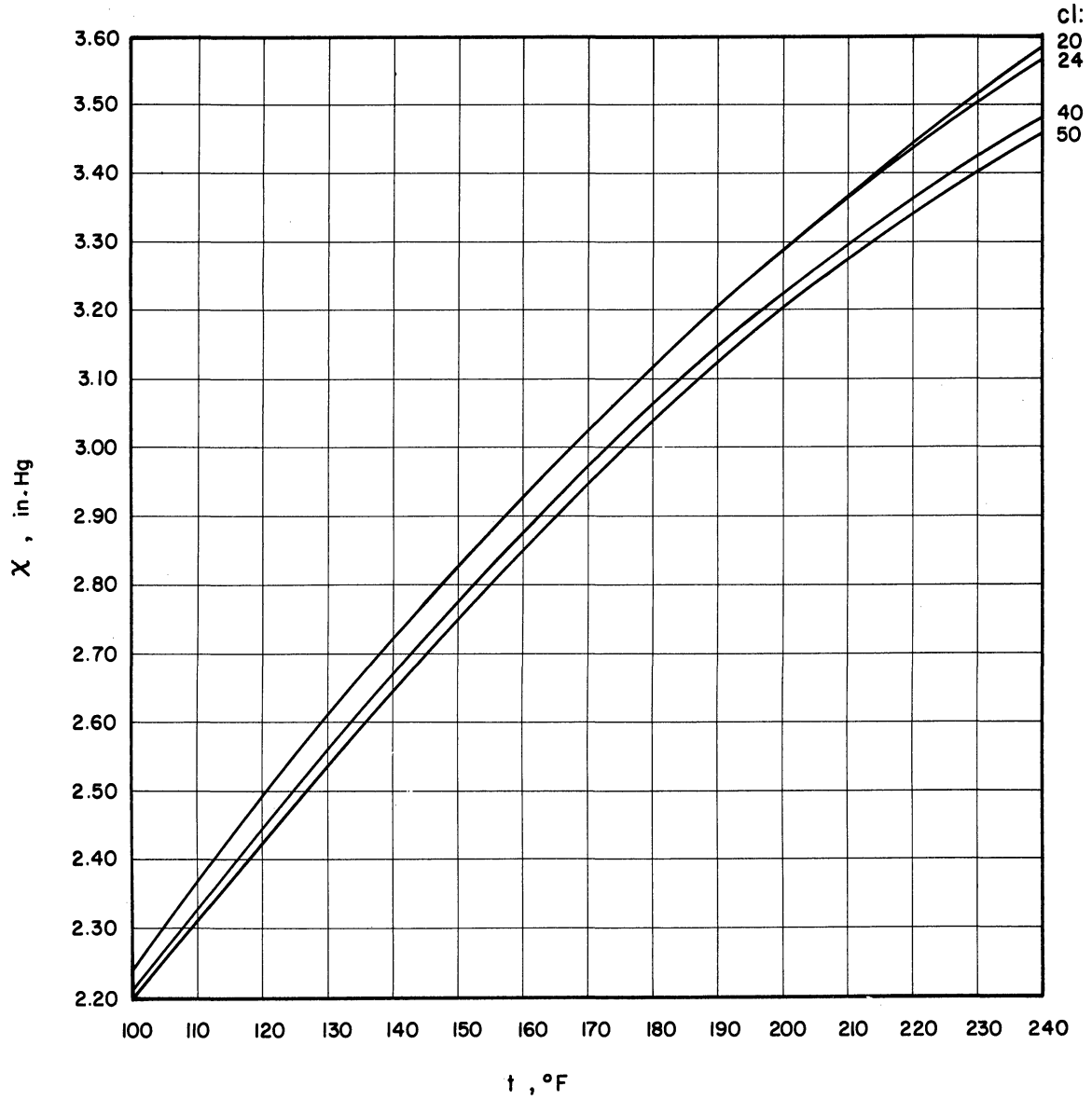
PRANDTL NUMBER OF SEA WATER CONCENTRATES



t, °F

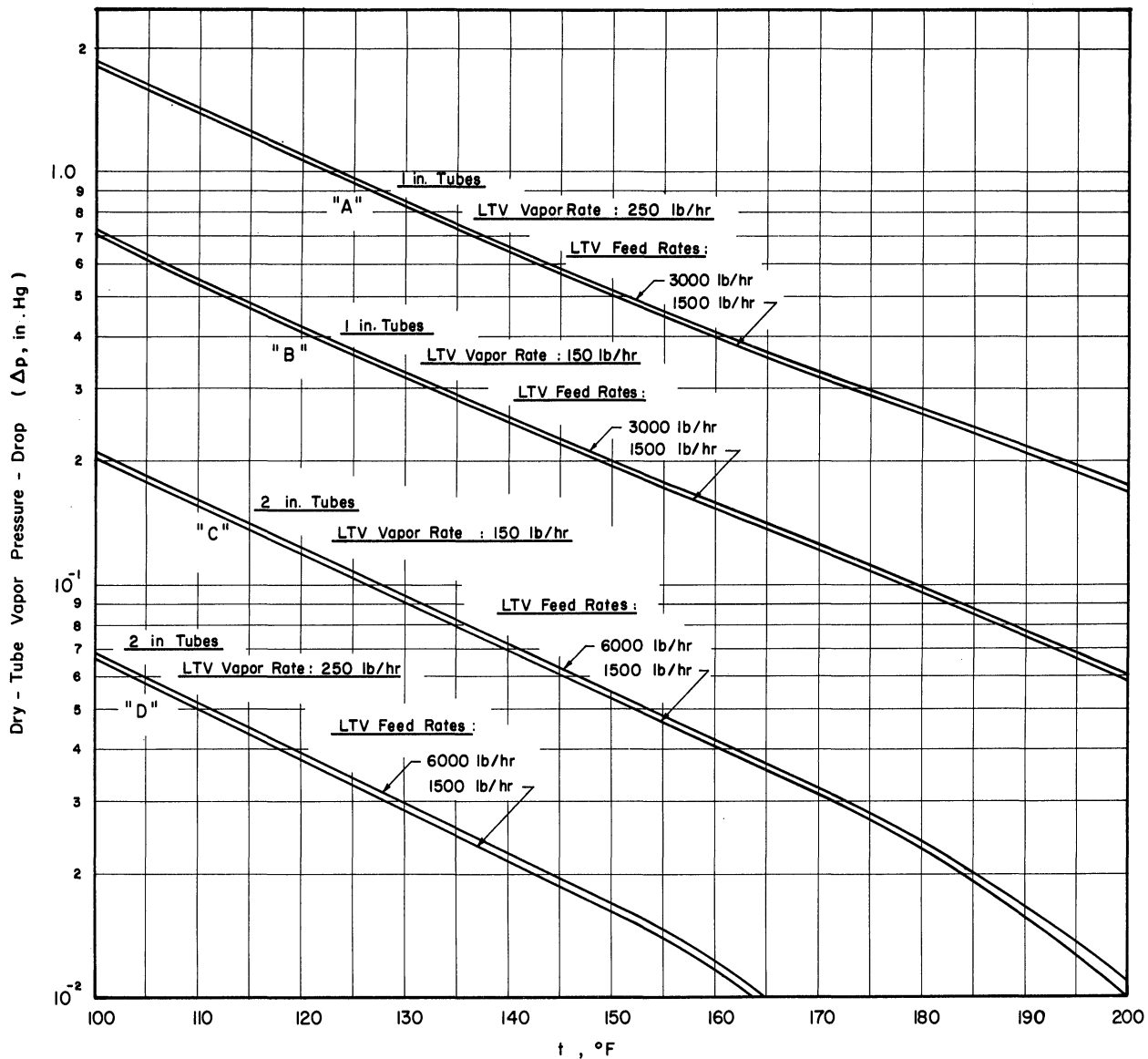
Graph 6

FALLING-FILM BUBBLE SUPERHEAT MAGNITUDE X



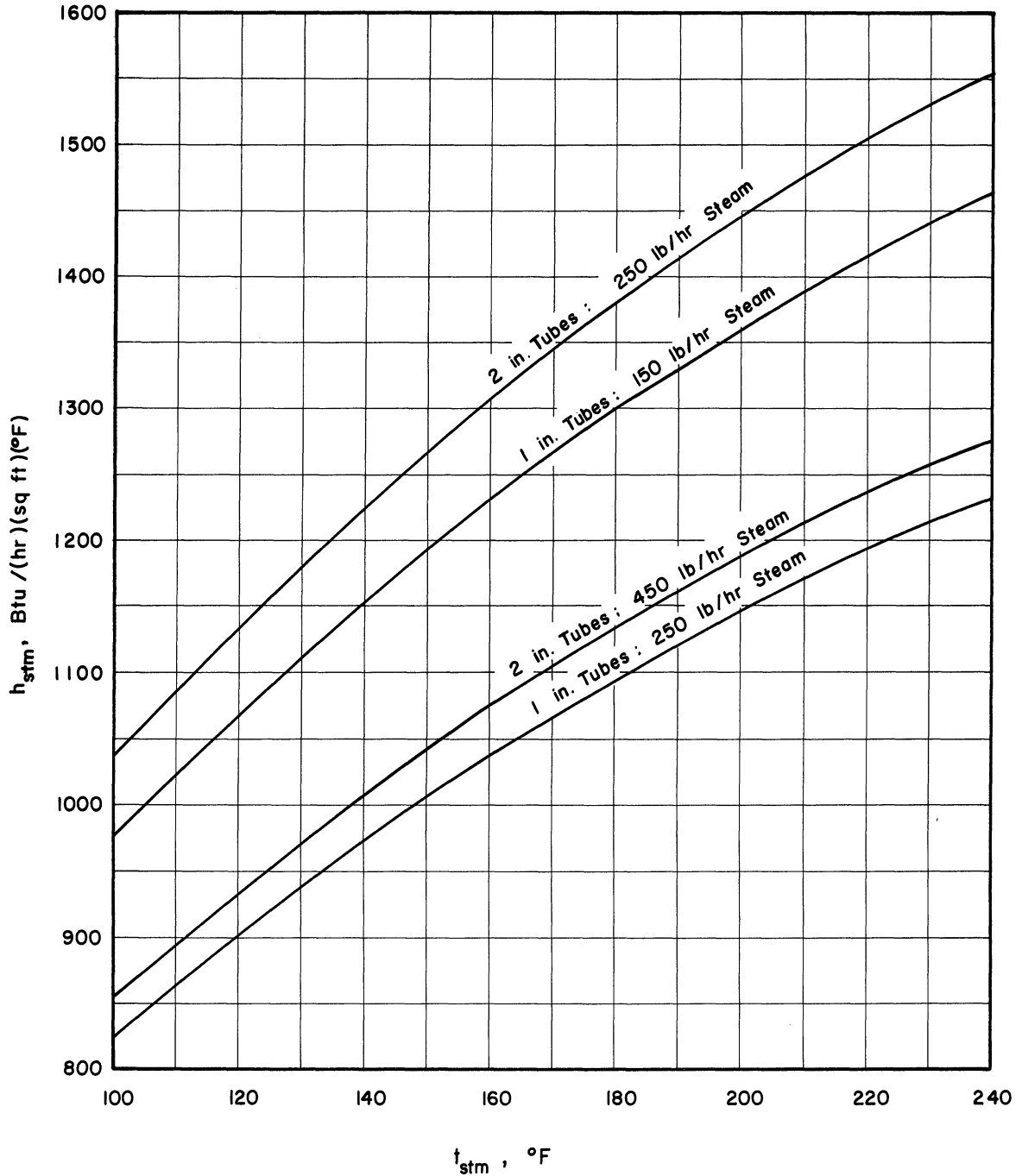
Graph 7

DRY-TUBE VAPOR PRESSURE-DROP



Graph 8

STEAM-SIDE HEAT TRANSFER COEFFICIENTS, PILOT PLANT



Graph 9

APPENDIX F

DISCUSSION OF ACCURACY AND EVENTUAL
MODIFICATION OF THEORETICAL CORRELATION
OF HEAT TRANSFER COEFFICIENTS

Our correlation contains a degree of inaccuracy because steam-side film heat transfer coefficients were not measured but estimated. We have therefore calculated the effect on U_{VH} of the maximum expected scatter in h_{stm} . The result, as presented below, is that agreement between theory and experiment generally falls well within the $\pm 20\%$ deviation boundaries despite the scatter in h_{stm} .

Two simplifications of our theoretical heat transfer model are also discussed below. One is the assumption that sea water physical properties should be taken at feed chlorosity instead of at average chlorosity. The use of the average chlorosity implies complete mixing; we have no proof of the presence or absence of mixing, nor do we postulate either. It turns out that it makes very little difference whether the feed or average chlorosity is used. - Another simplifying modification consists of neglecting $\frac{4\sigma}{B}$, the bubble superheat. It is shown below that the resulting deviation between theory and experiment makes this simplification inadmissible.

a) Effect of Scatter in h_{stm}

In order to predict U_{VH} , we have used our theoretical model to calculate the liquor-side temperature drop, and McAdams' recommendation to estimate the steam-side temperature drop. The question arises as to how accurate this latter estimate is, and to what degree a scatter in h_{stm} will cause U_{VH} to scatter.

Baker, Kazmark and Stroebe⁽¹⁾ used a single-tube LTV consisting of a 2-in. tube 20 ft long in their experimental work. They measured h_{stm} by

means of thermocouples embedded in the tube at 1-ft intervals. Their results are thus seen to be particularly pertinent to our study.

In our region of interest, namely, for steam-side Reynolds numbers below 900, their coefficients averaged roughly 1.28 times the Nusselt-predicted values; hence our use of McAdams' recommendation. Furthermore, practically all their points scattered between 1.00 and 1.56 times the Nusselt-predicted values.

We have used this same degree of scatter in h_{stm} in order to calculate the scatter in U_{VH} . The result is graphically illustrated in Figure 9, which is identical to Figure 8 except that the region of scatter is indicated for each point by means of a vertical line joining the upper and lower limit. It can be seen that agreement between theory and experiment generally falls well within the $\pm 20\%$ deviation boundaries. In other words, the use of McAdams' recommendation is not essential to our theory; h_{stm} does not have to be taken as 1.28 times, but at any value between 1.00 and 1.56 times, the Nusselt-predicted value. We used 1.28.

b) Effect of Using Feed Chlorosity to Calculate U_{VH}

In our runs, the increase in chlorosity from feed to blowdown was relatively low. Run LWCI-14 is the run in which the value of U_{VH} is most affected according to whether feed or average chlorosity is used in order to evaluate physical properties and hence U_{VH} . On recalculating U_{VH} using the feed chlorosity, the only noticeable change is in BPR, which for the average chlorosity is 2.89°F, but which for the feed chlorosity is 2.58°F. The net change in the overall heat transfer

CORRELATION OF U_{VH}

SHOWING OVERALL EFFECT OF UNCERTAINTY IN h_{stm}

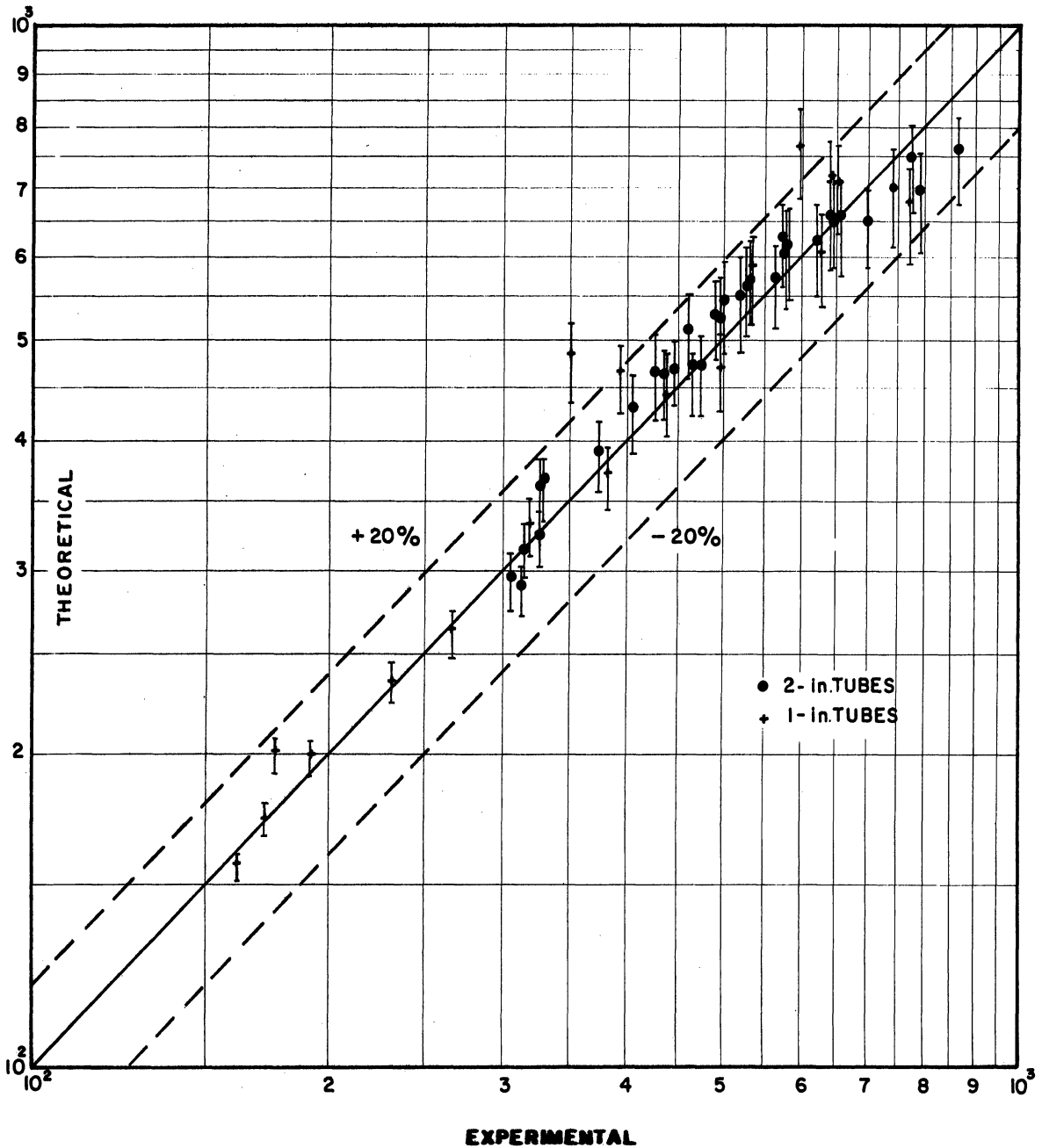


Figure 11.

coefficient is 4%. It can therefore be said that within the region of variables used in our work, it is for all practical purposes indifferent whether the feed or the average chlorosity is used.

c) Effect of Neglecting Bubble Superheat

We have recalculated all points neglecting bubble superheat, and plotted the results on Figure 12. The difference between Figures 12 and 10* is, therefore, the effect of neglecting bubble superheat; the change is quite apparent when the figures are compared.

The scatter is no longer uniform about the 45° ideal straight line but is biased toward the plus side. Furthermore, correlation is quite poor for many points; the only runs that seem to correlate well are

- 1) runs at the high end of the temperature range, where the pressure difference $\frac{4\sigma}{B}$ causes only a very small temperature difference due to the slope of the steam pressure-temperature curve;
- 2) those runs with 1-in. tubes where the large longitudinal pressure-drop overshadows $\frac{4\sigma}{B}$.

Neglect of bubble superheat is clearly inadmissible.

* See page 117.

CORRELATION OF U_{VH}
NEGLECTING BUBBLE SUPERHEAT

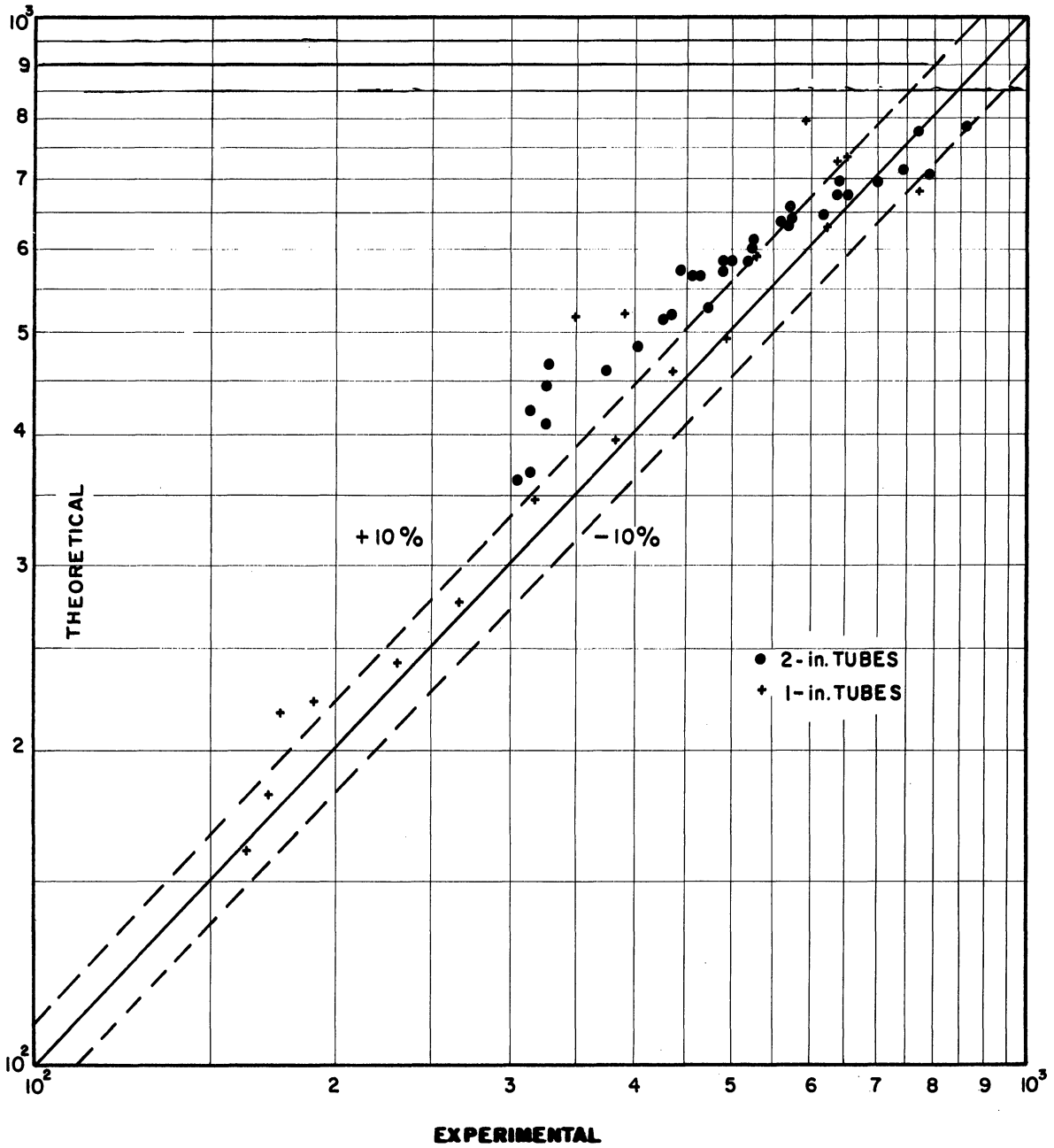


Figure 12.

BIBLIOGRAPHY ON FALLING-FILM

FLUID FLOW AND (NON-BOILING) HEAT TRANSFER

- (1) Anderson, G.H., Mantzouranis, B. G., "Two-phase (gas-liquid) flow phenomena - I", Chem. Eng. Sci., 12, 109 (1960)
- (2) Badger, W. L., "Evaporation of caustic soda to high concentration by means of diphenyl vapor", Ind. Eng. Chem., 22, 700 (1930)
- (3) Badger, W. L., "Heat transfer coefficients for condensing Dowtherm films", Trans. AIChE, 33, 441 (1937), and Ind. Eng. Chem., 29, 910 (1937)
- (4) Baker, E. M., Kazmark, E. W., Stroebe, G.W., "Steam heat transfer coefficients for vertical tubes", Ind. Eng. Chem., 31, 214 (1939)
- (5) Bays, G. S., McAdams, W.H., "Heat transfer coefficients in falling-film heaters - streamline flow", Ind. Eng. Chem., 29, 1240 (1937)
- (6) Brauer, H., "Strömung und Wärmeübergang bei Rieselfilmen", VDI Forsch. - Heft 457, 1956
- (7) Brauer, H., "Wärmeübergang bei der Filmkondensation", Kältetechnik, 9, 274 (1957)
- (8) Brauer, H., "Wärmeübergang bei der Filmkondensation reiner Dämpfe an lotrechten Wänden", Forsch. Ing.-Wes., 24, 105 (1958)
- (9) Brauer, H., "Stoffaustausch beim Rieselfilm", Chem.-Ing. Tech., 30, 75 (1958)
- (10) Brötz, W., "Über die Vorausberechnung der Absorptionsgeschwindigkeit von Gasen in strömenden Flüssigkeitsschichten", Chem.-Ing. Tech., 26, 470 (1954)
- (11) Carpenter, F. G., "Heat transfer and pressure drop by condensing pure vapors inside vertical tubes at high vapor velocities", Ph.D. thesis, Univ. of Delaware, 1948.
- (12) Carpenter, F. G., Colburn, A. P., p. 20, Proceedings of General Discussion on Heat Transfer, Inst. Mech. Engrs. (London) and ASME, 1951.
- (13) Chwang, C. T., S. M. Thesis, Mass. Inst. of Tech., 1926

- (14) Claassen, H., "Versuch zur Bestimmung der Dicke der fließenden und anhaftenden Flüssigkeitsteilchen bei der Berieselung an senkrechten Verdampferrohren", Zentr. Zuckerind., 26, (41), 497 (1918)
- (15) Colburn, A. P., "Calculation of condensation with a portion of condensate layer in turbulent motion", Trans. AIChE, 30, 187 (1934) and Ind. Eng. Chem., 26, 432 (1934)
- (16) Colburn, A.P., "Problems in design and research on condensers of vapors and vapor mixtures", Proc. Inst. Mech. Engrs. (London), 164, 448 (1951)
- (17) Cooper, C. M., Drew, T. B., McAdams, W. H., "Isothermal flow of liquid layers", Ind. Eng. Chem., 26, 428 (1934)
- (18) Cooper, C. M., Willey, G. S., unpublished memo. to W. H. McAdams, 1930 (see ref. 17)
- (19) Deissler, R. G., "Analytical and experimental investigation of adiabatic turbulent flow in smooth tubes", NACA Tech. Note 2138 (1950)
- (20) Deissler, R. G., "Analysis of turbulent heat transfer, mass transfer, and friction in smooth tubes at high Prandtl and Schmidt numbers", NACA Tech. Note 3145 (1954)
- (21) Drew, T. B., personal communication to W. H. McAdams, 1938 (see McAdams, W. H., "Heat Transmission", McGraw-Hill, 3rd ed., 1954, p. 245)
- (22) Dukler, A. E., Bergelin, O. P., "Characteristics of flow in falling liquid films", Chem. Eng. Progr., 48, 557 (1952)
- (23) Dukler, A. E., "Fluid mechanics and heat transfer in vertical falling-film systems", Chem. Eng. Progr. Symp. Series, 56, (30), 1 (1960)
- (24) Fage, A., Townend, H. C. H., "An examination of turbulent flow with an ultramicroscope", Proc. Roy. Soc. (London), A 135, 656 (1932)
- (25) Fallah, R., Hunter, T. G., Nash, A. W., "The application of physico-chemical principles to the design of liquid-liquid contact equipment - III - Isothermal flow in liquid wetted-wall systems", J. Soc. Chem. Ind. (London), 53, 369 T (1934)
- (26) Friedman, S. J., Miller, C. O., "Liquid films in the viscous flow region", Ind. Eng. Chem., 33, 885 (1941)

- (27) Garwin, L., Kelly, E. W., "Inclined falling films", Ind. Eng. Chem., 47, 392 (1955)
- (28) Grigull, U., "Wärmeübergang bei der Kondensation mit turbulenter Wasserhaut", Forsch. Ing.-Wes., 13, 49 (1942)
- (29) Grigull, U., "Wärmeübergang bei Filmkondensation", Forsch. Ing.-Wes., 18, 10 (1952)
- (30) Grimley, S. S., "Liquid flow conditions in packed towers", Trans. Inst. Chem. Engrs. (London), 23, 228 (1945)
- (31) Hopf, L., Ann. Physik, 32, 777 (1910)
- (32) Kamei, S., Oishi, J., Mem. Fac. Engrg. Kyoto Univ., 18, 1 (1956)
- (33) Kirkbride, C. G., "Heat transfer by condensing vapor on vertical tubes", Trans. AIChE, 30, 170 (1933) and Ind. Eng. Chem., 26, 425 (1934)
- (34) McAdams, W. H., "Heat Transmission", McGraw-Hill, 3rd ed., 1954, p. 337
- (35) McAdams, W. H., Drew, T. B., Bays, G. S., Jr., "Heat transfer to falling-water films", Trans. ASME, 62, 627 (1940)
- (36) Misra, B., Bonilla, C. F., "Heat transfer in the condensation of metal vapors: mercury and sodium up to atmospheric pressure", Chem. Eng. Progr. Symp. Series, 52, (18), 7 (1956)
- (37) Nusselt, W., "Die Oberflächenkondensation des Wasserdampfes", Z. VDI, 60, 541 (1916)
- (38) Nusselt, W., "Der Wärmeaustausch am Berieselungskühler", Z. VDI, 67, 206 (1923)
- (39) Pennie, A. M., Belanger, J. Y., "A new method for liquid film thickness measurement", Can. J. Technol., 30, 9 (1952)
- (40) Rohsenow, W., Webber, J.H., Ling, A. T., "Effect of vapor velocity on laminar and turbulent film condensation", Trans. ASME, 78, 1637 (1956)
- (41) Schoklitsch, A., "Über die Bewegungsweise des Wassers in offenen Gerinnen", Akad. Wiss. Wien, Math.-Naturw. Abt. IIa, 129 (1920)
- (42) Seban, R. A., "Remarks on film condensation with turbulent flow", Trans. ASME, 76, 299 (1954)
- (43) Sexauer, Th., "Der Wärmeübergang am senkrechten berieselten Rohr", Forsch. Ing.-Wes., 10, 286 (1939)
- (44) Warden, C. P., S. M. thesis, Mass. Inst. Tech., 1930

BIBLIOGRAPHY ON NUCLEATE BOILING FUNDAMENTALS

- (1) Addoms, J. N., Sc. D. thesis, Mass. Inst. of Techn., 1948
- (2) Averin, E. K., Otdel. Tekh. Nauk Izvestiia, Akad. Nauk SSSR, No. 3, p. 116 (1954), quoted by (7).
- (3) Bankoff, S. G., AIChE Journ., 4, 1 (1958)
- (4) Bankoff, S. G., "The prediction of surface temperatures at incipient boiling". Chem. Eng. Progr. Symp. Series, 55, (29), 87 (1959)
- (5) Bankoff, S. G., Hajjar, A. J., McGlothlin, B. B., Jr., "On the nature and location of bubble nuclei in boiling from surfaces", J. Appl. Phys., 29, 1739 (1958)
- (6) Bankoff, S. G., Mikesell, R. D., "Bubble growth rates in highly subcooled nucleate boiling", Chem. Eng. Progr. Symp. Series, 55, (29), 95 (1959)
- (7) Bernath, L., Begell, W., "Forced-convection, local-boiling heat transfer in narrow annuli", Chem. Eng. Progr. Symp. Series, 55, (29), 59 (1959)
- (8) Clark, H. B., Strenge, P. S., Westwater, J. W., "Active sites for nucleate boiling", Chem. Eng. Progr. Symp. Series, 55, (29), 103 (1959)
- (9) Clark, J. A., Rohsenow, W. M., "Local boiling heat transfer to water at low Reynolds numbers and high pressures", Trans. ASME, 76, 553 (1954)
- (10) Corty, C., Foust, A. S., "Surface variables in nucleate boiling", Chem. Eng. Progr. Symp. Series, 51, (17), 1 (1955)
- (11) Dean, R. B., "The formation of bubbles", J. Appl. Phys., 15, 446 (1944)
- (12) Dergarabedian, P., "The rate of growth of vapor bubbles in superheated water", J. Appl. Mech., Trans. ASME, 75, 537 (1953)
- (13) Engelberg-Foster, K., Greif, R., "Heat transfer to a boiling liquid-mechanism and correlations", J. Heat Transfer, Trans. ASME, p. 43 (1959)
- (14) Faneuff, C. E., McLean, E. A., Scherrer, V. E., "Some aspects of surface boiling", J. Appl. Phys., 29, 80 (1958)

- (15) Forster, H. K., Zuber, N., "Growth of a vapor bubble on a superheated liquid", J. Appl. Phys., 25, 474 (1954)
- (16) Fritz, W., "Berechnung des Maximalvolumens von Dampfblasen", Phys. Z., 36, 379 (1935)
- (17) Gibbs, J. W., "Collected Works", vol. I, p. 254, Yale Univ. Press, New Haven Conn., 1948
- (18) Griffith, P., "Bubble growth rates in boiling", Trans. ASME, 80, 721 (1958)
- (19) Griffith, P., Wallis, J. D., "The role of surface conditions in nucleate boiling", Chem. Eng. Progr. Symp. Series, 56, (30), 49 (1960)
- (20) Grohse, E. W., Mueller, G. O., Findlay, J. A., "Fundamental investigation of boiling heat transfer and two-phase flow", KAPL-M-EWG-1, 1958
- (21) Gunther, F. C., "Photographic study of surface-boiling heat transfer to water with forced convection", Trans. ASME, 73, 115 (1951)
- (22) Gunther, F. C., Kreith, F., "Photographic study of bubble formation in heat transfer to subcooled water", Heat Transf. & Fluid Mech. Inst., p. 113 (1949)
- (23) Jakob, M., "Kondensation und Verdampfung: Neuere Anschauungen und Versuche", Z. VDI, 76, 1161 (1932)
- (24) Jakob, M., Fritz, W., Forsch. Ing.-Wes., 2, 435 (1931)
- (25) Jens., W. H., Lottes, P. A., Report ANL-4627 (1951)
- (26) Kreith, F., Summerfield, N., "Heat transfer to water at high flux densities with and without surface boiling", Trans. ASME, 71, 805 (1949)
- (27) Kreith, F., Summerfield, M., "Pressure drop and convective heat transfer with surface boiling at high heat flux; data for aniline and n-butyl alcohol", Trans. ASME, 72, 869 (1950)
- (28) Levy, S., "Generalized correlation of boiling heat transfer", J. Heat Transfer, Trans. ASME, p. 37 (1959)
- (29) Lowery, A. J., Jr., Westwater, J. W., "Heat transfer to boiling methanol - effect of added agents", Ind. Eng. Chem., 49, 1445 (1957)
- (30) McAdams, W. H., Addoms, J. N., Rinaldo, P. N., Day, R. S., "Heat transfer from single horizontal wires to boiling water", Chem. Eng. Progr., 44, (8), 639 (1948)

- (31) McAdams, W. H., Kennel, W. E., Minden, C. S., Carl, R., Picornell, P. M., Dew, J. E., "Heat transfer at high rates to water with surface boiling", Ind. Eng. Chem., 41, 1945 (1949)
- (32) McNelly, M. J., J. Imp. Coll. Chem. Eng. Soc., 7, 18 (1953)
- (33) Morgan, A. I., Bromley, L. A., Wilke, C. R., "Effect of surface tension on heat transfer in boiling", Ind. Eng. Chem., 41, 2767 (1949)
- (34) Pike, F. P., Miller, P. D., Jr., Beatty, K. O., Jr., "Effect of gas evolution on surface boiling at wire coils", Chem. Eng. Progr. Symp. Series, 51, (17), 13 (1955)
- (35) Plesset, M. S., "The dynamics of bubble cavitation", J. Appl. Mech., Trans. ASME, 16, 277 (1949)
- (36) Plesset, M. S., Zwick, S. A., "The growth of vapor bubbles in superheated liquids", J. Appl. Phys., 25, 493 (1954)
- (37) Rinaldo, R. N., M. S. thesis, Mass. Inst. Techn., 1948
- (38) Rohsenow, W. M., "A method of correlating heat transfer data for surface-boiling of liquids", Trans. ASME, 74, 969 (1952)
- (39) Rohsenow, W. M., Clark, J. A., "A study of the mechanism of boiling heat transfer", Trans. ASME, 73, 609 (1951)
- (40) Rohsenow, W. M., Clark, J. A., "Heat transfer and pressure drop data for high heat flux densities to water at high sub-critical pressures", Heat Transf. & Fluid Mech. Inst., p. 193 (1951)
- (41) Rohsenow, W. M., Griffith, P., "Correlation of maximum-heat-flux data for boiling of saturated liquids", Chem. Eng. Progr. Symp. Series, 52, (18), 47 (1955)
- (42) Vos, A. S., van Stralen, S. J. D., "Heat transfer to boiling water-methylethylketone mixtures", Chem. Eng. Sci., 5, 50 (1956)
- (43) Yamagata, K., Hirano, F., Nishikawa, K., Matsuoka, H., "Nucleate boiling on a horizontal heating surface", Jap. Sci. Rev., 2, 409 (1952)

BIBLIOGRAPHY ON GAS-LIQUID FLOW

- (1) Baker, O., "Design of pipe lines for the simultaneous flow of oil and gas", Oil & Gas J., July 26 (1954)
- (2) Benjamin, M. W., Miller, J. G., "The flow of saturated water through throttling orifices", Trans. ASME, 63, 419 (1941)
- (3) Benjamin, M. W., Miller, J. G., "The flow of a flashing mixture of water and steam through pipes", Trans. ASME, 64, 657 (1942)
- (4) Bergelin, O. P., Kegel, P. K., Carpenter, F. G., Gazley, C., Jr., "Co-current gas-liquid flow - II. Flow in vertical tubes", Heat Trans. & Fluid Mech. Inst., p. 19 (1949)
- (5) Boelter, L. M. K., Kepner, R. H., "Pressure drop accompanying two-component flow through pipes", Ind. Eng. Chem., 31, 426 (1939)
- (6) Bottomley, W. T., "The flow of saturated water through throttling orifices", Trans. North-East Coast Inst. Engrs. & Shipbuilders, 53, 65 (1937)
- (7) Calvert, S., "Vertical upward annular two-phase flow in smooth tubes", Ph. D. thesis, Univ. of Mich., 1952
- (8) Carpenter, F. G., "Heat transfer and pressure drop for condensing pure vapors inside vertical tubes at high vapor velocities", Ph. D. thesis, Univ. of Del., 1948
- (9) Chenoweth, J. M., Martin, H. W., Petr. Ref., 34, 151 (1955)
- (10) Davidson, W. F., Hardie, P. H., Humphreys, C. G. R., Markson, A. A., Mumford, A. R., Ravese, T., Trans. ASME, 65, 553 (1943)
- (11) Dengler, C. E., "Heat transfer and pressure drop for evaporation of water in a vertical tube", D. Sc. thesis, Mass. Inst. Techn., 1952
- (12) Dittus, F. W., Hildebrand, A., "A method of determining the pressure drop for oil-vapor mixtures flowing through furnace coils", Trans. ASME, 64, 185 (1942)
- (13) Gazley, C., Jr., "Co-current gas-liquid flow - III. Interfacial shear and stability", Heat Transf. & Fluid Mech. Inst., p. 29 (1949)
- (14) Jakob, M., Leppert, G., Reynolds, J. B., "Pressure drop during forced-circulation boiling", Chem. Eng. Progr. Symp. Series, 52, (18), 29 (1956)

- (15) Johnson, H. A., Abou-Sabe, A. H., "Heat transfer and pressure drop for turbulent flow of air-water mixtures in a horizontal pipe", Trans. ASME, 74, 977 (1952)
- (16) Levy, S., "Theory of pressure drop and heat transfer for two-phase two-component annular flow in pipes", Ohio State Univ. Engrg. Exptl. Station Bull. No. 149, Proc. 2nd Midwestern Conf. Fluid Mech., p. 337, 1952
- (17) Lieberson, N. G., "Two-phase flow in vertical pipes", M. S. thesis, Mass. Inst. Techn., 1952
- (18) Linning, D. L., "The adiabatic flow of evaporating fluids in pipes of uniform bore", Inst. Mech. Engrs. (London), Proc. (B), 1 B, 2 (1952)
- (19) Lockhart, R. W., Martinelli, R. C., "Proposed correlation of data for isothermal two-phase, two-component flow in pipes", Chem. Eng. Progr., 45, 39 (1948)
- (20) Marcy, G. P., "Pressure drop with change of phase in a capillary tube", Refriger. Eng., 57, 53 (1949)
- (21) Martinelli, R. C., Boelter, L. M. K., Taylor, T. H. M., Thomsen, E. G., Morrin, E. H., "Isothermal pressure drop for two-phase two-component flow in a horizontal pipe", Trans. ASME, 64, 275 (1942)
- (22) Martinelli, R. C., Nelson, D. B., "Prediction of pressure drop during forced-circulation boiling of water", Trans. ASME, 70, 695 (1948)
- (23) Martinelli, R. C., Putnam, J. A., Lockhart, R. W., "Two-phase, two-component flow in the viscous region", Trans. AIChE, 42, 681 (1946)
- (24) McAdams, W. H., Woods, W. K., Heroman, L. C., Jr., "Vaporization inside horizontal tubes - II. Benzene-oil mixtures", Trans. ASME, 64, 193 (1942)
- (25) Radford, B. A., "Gas-liquid flow in vertical pipes - a preliminary investigation", M. S. thesis, Univ. of Alberta, 1949
- (26) Schmidt, E., "Ähnlichkeitstheorie der Bewegung von Flüssigkeitsgemischen", VDI Forsch. - Heft 365, 1934
- (27) Shugaeff, V., Sorokin, S., "The hydraulic resistance of a two-phase mixture", Zhur. Tekhn. Fiziki, IX, (20), 1854 (1939)

- (28) Stein, R. P., Hoopes, J. W., Jr., Markels, M., Jr., Selke, W. A., Bendler, A. J., Bonilla, C. F., "Pressure drop and heat transfer to nonboiling and boiling water in turbulent flow in an internally heated annulus", Chem. Eng. Progr. Symp. Series, 50, (11), 115 (1954)
- (29) Styrikovich, M. A., Miropolski, Z. L., "Flow lamination of a high-pressure steam-water mixture in a heated horizontal pipe", Dokl. Akad. Nauk SSSR, 71, (2), (1950)
- (30) Untermeyer, S., "Boiling reactors: direct steam generation for power", Nucleonics, 12, 43 (1954)
- (31) Van Wingen, N., "Pressure drop for oil-gas mixtures in horizontal flow lines", World Oil, 129, (7), 156 (1949)

BIBLIOGRAPHY ON EVAPORATOR STUDIES

- (1) Billet, R., "Trennung von Flüssigkeitsgemischen durch teilweise Destillation", Chem.-Ing.-Tech., 29, 733 (1957)
- (2) Chambers, F. S., Peterson, R. F., "Sulfuric acid concentration - DuPont Falling-Film Process", Chem. Eng. Progr., 43, (5), 219 (1947)
- (3) Dengler, C. E., "Heat transfer and pressure drop for evaporation of water in a vertical tube", Sc. D. thesis, Mass. Inst. Techn., 1952
- (4) Guerrieri, S. A., Talty, R. D., "A study of heat transfer to organic liquids in single-tube, natural-circulation, vertical-tube boilers", Chem. Eng. Progr. Symp. Series, 52, (18), 69 (1956)
- (5) Hadley, G. F., Thomas, A. L., "A mathematical and experimental study of a climbing film evaporator", Ind. Eng. Chem., 52, 71 (1960)
- (6) Harvey, B. F., Foust, A. S., "Two-phase one-dimensional flow equations and their application to flow in evaporator tubes", Chem. Eng. Progr. Symp. Series, 49, (5), 93 (1953)
- (7) Hausschild, W., "Leistung von Dünnschichtverdampfern mit zwangsläufig ausgebildeten Filmen", Chem.-Ing.-Tech., 25, 573 (1953)
- (8) Karetnikov, U. P., "Investigation of heat transfer in a boiling liquid film", Zhur. Tekhn. Fiziki, XXIV, (2), 193 (1954)
- (9) Kern, D. Q., Karakas, H. J., "Mechanically aided heat transfer", Chem. Eng. Progr. Symp. Series, 55, (29), 141 (1959)
- (10) Kerry, F. G., "Safe design and operation of low temperature air separation plants", Chem. Eng. Progr., 52, (11), 441 (1956)
- (11) Keville, J. K., "Heat transfer aspects of concentrated milk in a falling film evaporator", preprint 18, Second National Heat Transfer Conference AIChE-ASME, Chicago, Ill., Aug. 18-21, 1958
- (12) Kirschbaum, E., Dieter, K., "Wärmeübergang und Teildestillation in Dünnschichtverdampfern", Chem.-Ing.-Tech., 30, 715 (1958)
- (13) Lustenader, E. L., Richter, R., Neugebauer, F. J., "The use of thin films for increasing evaporation and condensation rates in process equipment", paper 59-SA-30, Semi-Annual Meeting ASME, St. Louis, Mo., June 14-18, 1959
- (14) Mueller, A. C., "Discrepancies between theory and practice", Chem. Eng. Progr., 57, 76 (1961)

- (15) Poocha, A., "Beitrag zur Theorie des Dunnschichtverdampfers", Chem.-Ing.-Tech., 30, 648 (1958)
- (16) Richkov, A. I., Pospelov, V. K., "Study of heat transfer in the boiling of caustic soda solutions in a thin film", Khim. Prom., (5), 426 (1959)
- (17) Schneider, R., "Ein neuer Dunnschichtverdampfer", Chem.-Ing.-Tech., 27, 257 (1955)
- (18) Schweppe, J. L., Foust, A. S., "Effect of forced circulation rate on boiling heat transfer and pressure drop in a short vertical tube", Chem. Eng. Progr. Symp. Series, 49, (5), 77 (1953)

For a recently published literature review on evaporation for 1959 and 1960, see also:

Dedert, W. G., "Evaporation", Ind. Eng. Chem., 53, 669 (Aug. 1961)

This article does not contain mention of any significant development on falling-film evaporation not quoted in our dissertation.



ADDITIONAL BIBLIOGRAPHY USED

IN DESIGN, RESULTS AND ANALYSIS OF EXPERIMENTS

- (1) Baker, E. M., Kazmark, E. W., Stroebe, G. W., "Steam-film heat transfer coefficients for vertical tubes", Trans. AIChE., 35, 127 (1939); Ind. Eng. Chem., 31, 214 (1939)
- (2) Keenan, J. H., Keyes, F. G., "Thermodynamic Properties of Steam", John Wiley & Sons, 1st ed., 1936
- (3) Sverdrup, H. U., Johnson, M. W., Fleming, R. H., "The Oceans", Prentice-Hall, 1st ed., 1942, p. 70
- (4) Volk, W., "Applied Statistics for Engineers", McGraw-Hill, 1st ed., 1958, p. 207
- (5) W. L. Badger and Associates, Inc., Ann Arbor, Mich., Report No. 438, "Properties of Sea Water and Its Concentrates", 1957, and supplement, 1960, to U. S. Department of Interior, Office of Saline Water